The Experimental Status of Glueballs

V. Crede[1] and C. A. Meyer[2]
[1]Florida State University, Tallahassee, FL 32306 USA
[2]Carnegie Mellon University, Pittsburgh, PA 15213 USA

November 13, 2008

Abstract

Glueballs and other resonances with large gluonic components are predicted as bound states by Quantum Chromodynamics (QCD). The lightest (scalar) glueball is estimated to have a mass in the range from 1 to 2 GeV/c^2; a pseudoscalar and tensor glueball are expected at higher masses. Many different experiments exploiting a large variety of production mechanisms have presented results in recent years on light mesons with $J^{PC} = 0^{++}$, 0^{-+}, and 2^{++} quantum numbers. This review looks at the experimental status of glueballs. Good evidence exists for a scalar glueball which is mixed with nearby mesons, but a full understanding is still missing. Theoretical expectations of phenomenological models and QCD on the lattice are briefly discussed.

1 Introduction

While we believe that Quantum Chromodynamics (QCD) is the correct description of the interactions of quarks and gluons, it is a theory that is very difficult to solve in the low-energy regime—that which describes the particles of which the universe is made. This is changing with advances that have been made in Lattice QCD, and the access to ever faster computers. Within QCD, one of the perplexing issues has been the existence of gluonic excitations. In the meson sector, nearly all the observed states can be explained as simple $q\bar{q}$ systems, with the naive quark model both providing a very good explanations for these particles, as well as providing a nice framework in which they can be described.

However, both phenomenological models and lattice calculations predict that there should exist additional particles in which the gluons themselves can contribute to the quantum numbers of the states. These include the pure-glue objects known as glueballs as well as $q\bar{q}$ states with explicit glue, known as hybrid mesons. Some of these latter states are expected to have quantum numbers which are forbidden to $q\bar{q}$ systems—exotic quantum numbers which can provide a unique signature for the existence of such particles.

Over the last decade, a great deal of new experimental data on mesons has been collected. This new information bears directly on both the search for, and our current understanding

of gluonic excitations of mesons, in particular glueballs and hybrids. In this review, we will focus on glueballs, rather than gluonic excitations in general. This paper will review the new data, and present a sampling of the phenomenological work that has been developed based on this.

In order to be able to discuss glueballs, it is necessary to understand conventional quark-antiquark systems (mesons). Over the last decade, there have been several relevant reviews on this subject, all of which touch upon gluonic excitations at some level. A very nice review by Close [1] looked at *gluonic hadrons* and summarized much of the criteria used to classify glueballs. Much of the new data on mesons came from the Crystal Barrel experiment. An excellent review by Amsler [2] covers the results of that experiment. A later review by Godfrey and Napolitano [3] reviewed the status of meson spectroscopy in light of many of the new results at the time. A more recent review by Amsler and Tornqvist [4] covers the status of the mesons beyond the naive quark model. Most recently, an encyclopedic review by Klempt and Zaitsev [5] covers in great detail both meson spectroscopy and gluonic excitations. Finally, many useful mini-reviews can be found in the *Review of Particle Physics* [6].

2 Meson Spectroscopy

Before discussing the expectations for gluonic excitations, we will briefly discuss the simple quark model picture for mesons. A meson consists of a $q\bar{q}$ system, which because it contains both a particle and an antiparticle, has intrinsics negative parity, $P = -1$. The total parity of such a system is given as $P = -(-1)^L$, where L is the orbital angular momentum in the $q\bar{q}$ system. Because quarks have spin $\frac{1}{2}$, the total spin of such a system can be either $S = 0$ or $S = 1$, which leads to a total angular momentum $J = L + S$, where the sum is made according to the rules of addition for angular momentum. In addition the parity, there is also C-parity, or charge conjugation, which for a $q\bar{q}$ system is $C = (-1)^{(L+S)}$.

The two lightest quarks also carry an additional quantum number: isospin. Each has total isospin $\frac{1}{2}$, with the u quark being the $+\frac{1}{2}$ part and the d quark being the $-\frac{1}{2}$ part of the doublet. If we form a meson out of only these, we can have $I = 0$ or $I = 1$. If one of the quarks is a strange quark, then $I = \frac{1}{2}$ and if both are strange, then $I = 0$. For a $q\bar{q}$ system, we can define an additional conserved quantum number, G-parity: $G = (-1)^{L+S+I}$. Using these relationships to build up possible $\mathbf{J^{PC}}$'s for $\bar{q}q$ mesons, we find the following quantum numbers are allowed:

$$0^{-+}, 0^{++}, 1^{--}, 1^{+-}, 1^{--}, 2^{--}, 2^{-+}, 2^{++}, 3^{--}, 3^{+-}, 3^{--}, \cdots \tag{1}$$

and looking carefully at these, we find that there is a sequence of $\mathbf{J^{PC}}$'s which are not allowed for a simple $q\bar{q}$ system.

$$0^{--}, 0^{+-}, 1^{-+}, 2^{+-}, 3^{-+}, \cdots \tag{2}$$

These latter quantum numbers are known as *explicitly exotic* quantum numbers and, if observed, would correspond to something beyond the simple $q\bar{q}$ states of the quark model.

If we consider only the three lightest quarks, u, d and s then we can form nine $q\bar{q}$ combinations, all of which can have the same S, L and J. We can represent these in spectroscopic notation, $^{2S+1}L_J$, or as states of total spin, parity and for the neutral states, charge conjugation: J^{PC}. Naively, these $q\bar{q}$ combinations would simply be a quark and an antiquark. However, those states consisting of the same quark and antiquark ($u\bar{u}$, $d\bar{d}$ and $s\bar{s}$) are rotated into three other states based on Isospin and SU(3) symmetries. The combinations shown in equation 3 correspond the the non-zero isospin states, while those in equation 4 correspond to a pair of isospin zero states. The latter two states are also mixed by SU(3) to yield a singlet ($|\ 1>$) and and octet ($|\ 8>$) state.

$$\begin{array}{ccc} & (d\bar{s}) & \\ (d\bar{u}) & \frac{1}{\sqrt{2}}(u\bar{u}-d\bar{d}) & (u\bar{d}) \\ & (s\bar{d}) & \end{array} \qquad \begin{array}{ccc} & (u\bar{s}) & \\ & & \\ & (s\bar{u}) & \end{array} \tag{3}$$

$$|\ 8> = \frac{1}{\sqrt{6}}(u\bar{u}+d\bar{d}-2s\bar{s}) \quad |\ 1> = \frac{1}{\sqrt{3}}(u\bar{u}+d\bar{d}+s\bar{s}) \tag{4}$$

The nominal mapping of these states onto the familiar pseudoscalar mesons is shown in 5 and 6.

$$\begin{array}{ccc} & K^\circ & K^+ \\ \pi^- & \pi^\circ & \pi^+ \\ & \bar{K}^\circ & K^- \end{array} \tag{5}$$

$$\eta \quad \eta\prime \tag{6}$$

However, because SU(3) is broken, the two $I = 0$ mesons in a given nonet are usually admixtures of the singlet ($|1> = \frac{1}{\sqrt{3}}\left(u\bar{u}+d\bar{d}+s\bar{s}\right)$) and octet ($|8> = \frac{1}{\sqrt{6}}\left(u\bar{u}+d\bar{d}-2s\bar{s}\right)$) states. In nature, the physical states (f and $f\prime$) are mixtures, where the degree of mixing is given by an angle θ.

$$f = \cos\theta|1> + \sin\theta|8> \tag{7}$$

$$f' = \cos\theta|8> - \sin\theta|1> \tag{8}$$

For the vector mesons, ω and ϕ, one state is nearly pure light-quark ($n\bar{n}$) and the other is nearly pure $s\bar{s}$. This is known as ideal mixing and occurs when $\tan\theta = \frac{1}{\sqrt{2}}$ ($\theta = 35.3^\circ$). In Table 1 are listed our current picture of the ground state mesons for several different L's. The last two columns list the linear (equation 9) and quadratic (equation 10) calculations of the mixing angle for the nonets.

$$\tan\theta = \frac{4m_K - m_a - 3m_{f\prime}}{2\sqrt{2}(m_a - m_K)} \tag{9}$$

$$\tan^2\theta = \frac{4m_K - m_a - 3m_{f\prime}}{-4m_K + m_a + 3m_f} \tag{10}$$

The mixing angle θ can also be used to compute relative decay rates to final states such as pairs of pseudoscalar mesons, or two-photon widths, for the f and $f\prime$ in a given nonet.

$n^{2s+1}l_J$	J^{PC}	$I=1$ $u\bar{d}\cdots$	$I=\frac{1}{2}$ $u\bar{s}\cdots$	$I=0$ f	$I=0$ $f\prime$	θ_q	θ_l
1^1S_0	0^{-+}	π	K	η	$\eta\prime$	$-11.5°$	$-24.6°$
1^3S_1	1^{--}	ρ	K^*	ω	ϕ	$38.7°$	$36.0°$
1^1P_1	1^{+-}	$b_1(1235)$	K_{1B}	$h_1(1170)$	$h_1(1380)$		
1^3P_0	0^{++}	$a_0(1450)$	$K_0^*(1430)$	$f_0(1370)$	$f_0(1710)$		
1^3P_1	1^{++}	$a_1(1260)$	K_{1A}	$f_1(1285)$	$f_1(1420)$		
1^3P_2	2^{++}	$a_2(1320)$	$K_2^*(1430)$	$f_2(1270)$	$f_2\prime(1525)$	$29.6°$	$28.0°$
1^1D_2	2^{-+}	$\pi_2(1670)$	$K_2(1770)$	$\eta_2(1645)$	$\eta_2(1870)$		
1^3D_1	1^{--}	$\rho(1700)$	$K^*(1680)$	$\omega(1650)$			
1^3D_2	2^{--}		$K_2(1820)$				
1^3D_3	3^{--}	$\rho_3(1690)$	$K_3^*(1780)$	$\omega_3(1670)$	$\phi_3\prime(1850)$	$32.0°$	$31.0°$
1^1F_4	4^{++}	$a_4(2040)$	$K_4^*(2045)$	$f_4(2050)$			
1^3G_5	5^{--}	$\rho_5(2350)$					
1^3H_6	6^{++}	$a_6(2450)$		$f_6(2510)$			
2^1S_0	0^{-+}	$\pi(1300)$	$K(1460)$	$\eta(1295)$	$\eta(1475)$	$-22.4°$	$-22.6°$
2^3S_1	1^{--}	$\rho(1450)$	$K^*(1410)$	$\omega(1420)$	$\phi(1680)$		

Table 1: A modified reproduction of the table from the 2006 Particle Data Book [7] showing the current assignment of known mesons to quark-model states. When sufficient states are know, the nonet mixing angle is computed using both the quadratic and linear forms.

Examples of this can be found in reference [7] and reference there in. The key feature is that for a given nonet, the f and $f\prime$ states can be identified by looking at the relative decay rates to pairs of particles.

As an example of a decay calculation, we consider the decay of the tensor ($J^{PC} = 2^{++}$) mesons to pairs of pseudoscalar mesons ($\pi\pi$, $K\bar{K}$ and $\eta\eta$). Following the work in references [7–9] and using the decay rates in reference [6], we can compute a decay constant γ from the SU(3) algebra corresponding to the decays. This can then be turned into a decay rate, Γ as in equation 11

$$\Gamma \;=\; \gamma^2 \cdot f_L(q) \cdot q \tag{11}$$

where q is the break-up momentum of the meson into the pair of daughter mesons. amplitude γ depends on the nonet mixing angle and the pseudoscalar mixing angle, θ_P. A typical

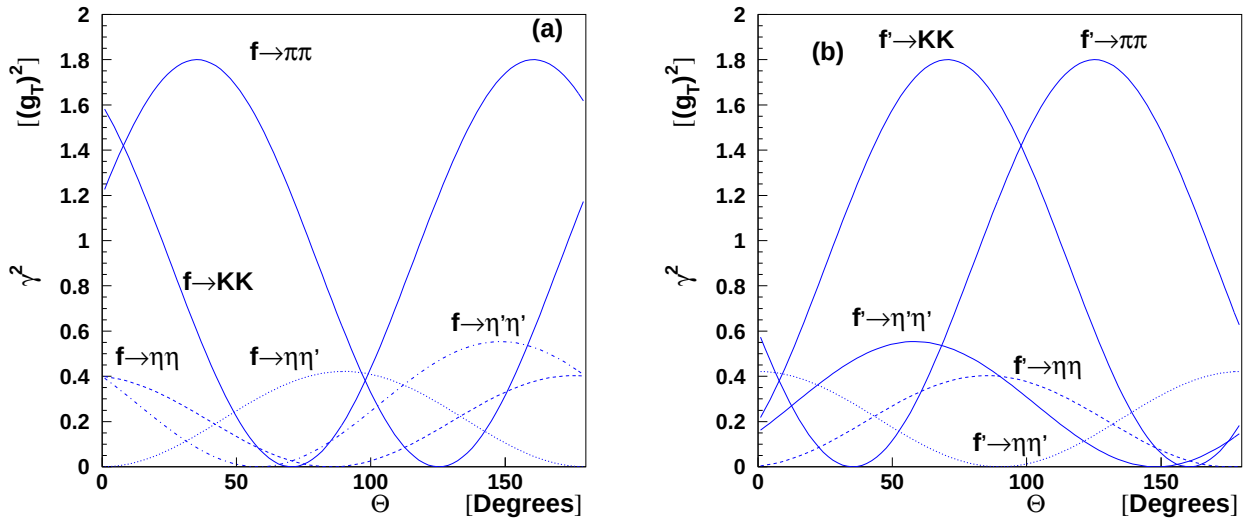

Figure 1: The decay amplitude, γ^2, as a function of the nonet mixing angle, θ. (a) is for f decays while (b) is for $f\prime$ decays. In this particular example, the pseudoscalar mixing angle is taken as $\theta_P = -17°$.

example is shown in Figure 1 which is shown in terms of an arbitrary scale factor. The quantity f_L is a form factor that depends on the angular momentum, L, between the pair of daughter mesons. A typical form is given as in equation 12

$$f_L(q) \quad = \quad q^{2L} e^{-\frac{q^2}{8\beta^2}} \tag{12}$$

where β is a constant that is in the range of 0.4 to 0.5 GeV/c. One can fit the ratio of decay rates to pairs of mesons for both the $f_2(1270)$ and the $f_2\prime(1525)$ and fit to the best value of the nonet mixing angle. We can compute a χ^2 between the measured and predicted decay rates to determine what the optimal choice of the mixing angle is. This is shown in Figure 2, where the optimal value is at about 32.5°. The location of the optimum does not depend strongly on either θ_P or β and is in good agreement with the values from the mass formulas for the tensors in Table 1.

Measuring the masses and decay rates of mesons can be used to identify the quark contents of a particular meson. The lightest glueballs have J^{PC} quantum numbers of normal mesons and would appear as an SU(3) singlet state. If they are near a nonet of the same J^{PC} quantum numbers, than they will appear as an extra f-like state. While the fact that there is an extra state is suggestive, the decay rates and production mechanisms are also needed to unravel the quark content of the observed mesons.

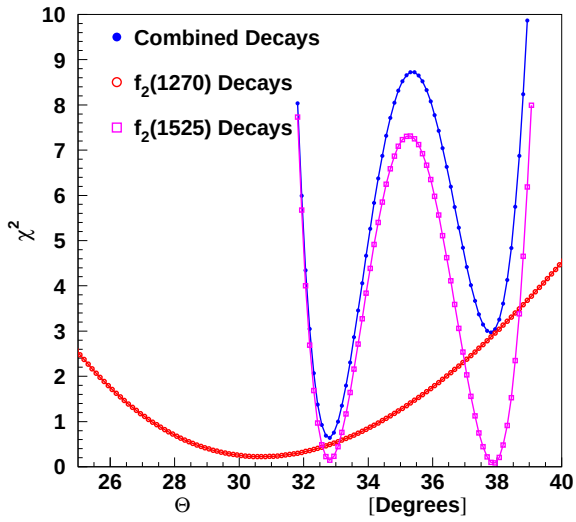

Figure 2: (color online) The χ^2 computed between the measured and predicted decay rates for the isoscalar tensor mesons. The open red circles are for the $f_2(1270)$ alone. The open purple squares are for the $f_2\prime(1525)$ alone and the solid blue circles are for the combined fit. The former two are for one degree of freedom, while the latter is for three.

3 Theoretical Expectations for Glueballs

3.1 *Historical*

One of the earliest models in which glueball masses were computed is the bag model [10]. In these early calculations, boundary conditions were placed on gluons confined inside the bag [11]. The gluon fields could be in transverse electric (TE) or transverse magnetic modes (TM). For a total angular momentum (J), the TE modes had parity of $(-1)^{(J+1)}$, while the TM modes had parity $(-1)^J$. The gluons then had to populate the bag to yield a color singlet state. This led to predictions for two- and three-gluon glueballs as given in Table 2.

Because glueballs contain no quarks, the expectation is that they would couple to all flavors of quarks equally. In a simple SU(3) calculation, the γ^2 from equation 11 are given

Gluons	J^{PC} Quantum Numbers	Mass
$(TE)^2$	0^{++}, 2^{++}	0.96 GeV/c^2
(TE)(TM)	0^{-+}, 1^{-+}, 2^{-+}	1.29 GeV/c^2
$(TE)^3$	0^{+-}, 1^{++}, 2^{+-}, 3^{++}	1.46 GeV/c^2
$(TM)^2$	0^{++}, 2^{++}	1.59 GeV/c^2

Table 2: Masses of glueballs in the bag model [11].

Decay	$\pi\pi$	$K\bar{K}$	$\eta\eta$	$\eta\eta'$	$\eta'\eta'$
γ^2	3	4	1	0	1

Table 3: The expected decay amplitudes for a glueball normalized to the rate to $\eta\eta$.

in Table 3. In addition to the decay predictions, there are reactions which are expected to be *glue rich*. The first of these is radiative decays of the J/ψ. Because the $c\bar{c}$ quarks have to decay via annihilation, the intermediate state must have gluons in it. This same argument can be applied to other $q\bar{q}$ reactions such as proton-antiproton annihilation and Υ decays. In the J/ψ decays, Chanowitz [12] proposed a variable known as *stickiness* which is the relative rate of production of some hadron h in radiative J/ψ decays to its two-photon width (photons only couple to electric charge, hence to quarks). The stickiness, S can be defined as in equation 13 for a hadron h of mass $M(h)$. l is the lowest orbital angular momentum needed to couple to two vector particles and the photon energy k_γ is that from the radiative decay in the ψ rest frame. The overall constant C is chosen such that $S\left[f_2(1270)\right] = 1$.

$$S \;=\; C\left(\frac{M(h)}{k_\gamma}\right)^{2l+1}\frac{\Gamma(\psi\to\gamma h)}{\Gamma(h\to\gamma\gamma)} \tag{13}$$

While this quantity has been computed for many of the glueball candidates, it appears to be most limited by our detailed knowledge of the two-photon width of the states [13]. A recent analysis by Pennington [14] has looked closely at the world data for this and still finds sizeable uncertainties in these widths.

Related to stickiness, Farrar [15] proposed a method of extracting decay rate of hadrons to gluons based on the radiative decay rate of vector quarkonium to the state. The was later applied to several mesons by Close [16] to try and distinguish glueball candidates.

There has also been questions raised about the validity of the flavor-blind decay assumption of glueballs. Lee and Weingarten [17] looked at decays of glueballs and proposed that the decay rates should scale with the mass of the mesons, thus favoring the heaviest possible meson pairs.

3.2 *Model Calculations*

The first glueball mass calculation within the flux-tube model was carried out by Isgur and Paton [18, 19]. In this model, the glueball is treated as a closed flux tube. Isgur and Paton found that the lightest glueball has $J^{PC} = 0^{++}$ and a mass of 1.52 GeV/c^2. In later flux-tube calculations [20], predictions were made for lightest three glueball masses. These were found to be consistent with the lattice calculations in reference [21]. Table 4 summarizes several flux-tube calculations of the scalar, tensor and pseudoscalar glueball. Finally, a recent article speculates that within the flux tube model, the scalar and pseudoscalar glueball should be degenerate in mass [22].

Another tool that has been used to predict glueball masses are QCD sum rules. This method looks at a two-point correlator of appropriate field operators form QCD and pro-

$J^{PC} = 0^{++}$	$J^{PC} = 2^{++}$	$J^{PC} = 0^{-+}$
1.52 GeV/c^2 [18, 19]	2.84 GeV/c^2 [18, 19]	2.79 GeV/c^2 [18, 19]
1.68 GeV/c^2 [20]	2.69 GeV/c^2 [20]	2.57 GeV/c^2 [20]
1.6 GeV/c^2 [23]		

Table 4: Flux-tube predictions for masses of the lowest lying glueballs.

duces a sum rule by equating a dispersion relation for the correlator to an operator product expansion. One of the first such calculations for glueballs was carried out by Novikov [24], and since then by many other authors. Kisslinger [25] points out that most of these calculations find the lightest scalar glueball with a mass in the range of 0.3 to 0.6 GeV/c^2. A more recent article by Narison [26] looks at all the known scalar mesons and finds a scalar meson state at about 1 GeV/c^2 and the scalar glueball at 1.5 ± 0.2 GeV/c^2.

Swanson and Szczepaniak compute the glueball spectrum using Hamiltonian QCD in the Coulomb Gauge [27] by constructing a quasiparticle gluon basis. They also find results which are in good agreement with lattice calculations. The lightest glueball is a scalar with mass of 1.98 GeV/c^2, followed by a pseudoscalar at 2.22 GeV/c^2 and then a tensor at 2.42 GeV/c^2.

3.3 *Lattice Calculations*

Lattice QCD discretizes space and time on a four-dimensional Euclidean lattice, and use this to solve QCD numerically. This is done by looking at path integrals of the action on the discrete lattice. Quarks and antiquarks live on the discrete points of the lattice, while gluons span the links between the points. Depending on the problem being solved, and the availability of computing resources, the size of the lattice may vary. In addition, there are many different choices for the action, each of which has its own advantages and disadvantages. In specifying the calculation, the grid and action are specified and a damping factor, β, is chosen. After the calculation has been completed, the physical quantities of interest as well as the lattice spacing can be determined. For a given choice of action, a larger β maps into a smaller lattice spacing. However, the same β with different actions can lead to quite different lattice spacings.

To date, most lattice calculations have been carried out in the quenched approximations, where the fluctuation of a gluon into a quark-antiquark pair is left out. As computer power continues to increase, and more efficient ways of carrying out calculations evolve, this is starting to change.

There is also a lattice artifact that can affect the mass calculations of the scalar glueball [28]. A singularity not related to QCD can cause the mass of the scalar glueball to be artificially small. This effect is particularly apparent when Wilson fermions are used with too-large a lattice spacing. Other choices are less sensitive to this, and when the lattice spacing is small enough, the effect does go away. However, for Wilson fermions, the critical value of β is 5.7, which is very close to the values used in many glueball calculations.

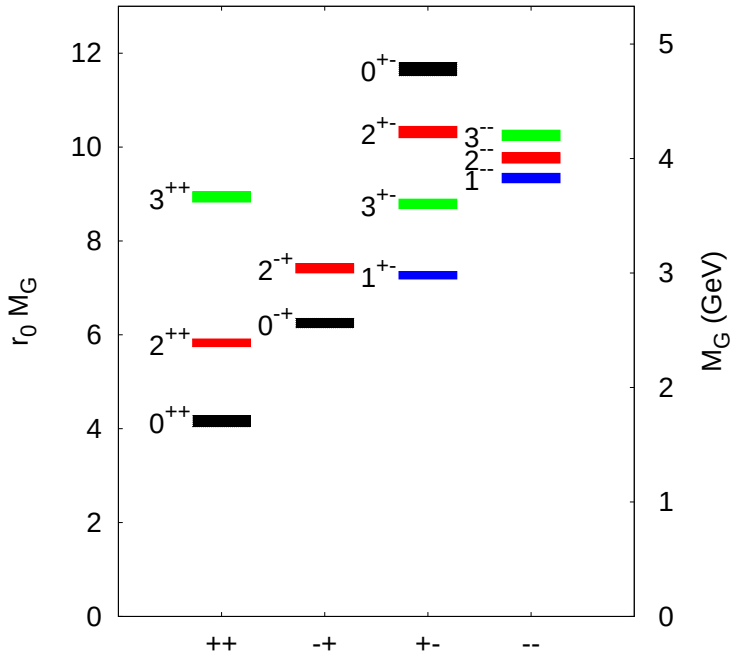

Figure 3: (color online) The mass spectrum of glueballs. The height of each box indicates the statistical uncertainty. Figure used with permission from reference [32].

Some of the earliest lattice calculations of the glueball spectrum were carried out in the quenched approximation on relatively small lattices [29], [30]. These calculations indicated that the mass of the lightest glueball spectrum started at about 1.5 GeV/c^2. As both computational resources increased and the lattice actions and methods improved, calculations on larger were carried out, and the spectrum of the states began to emerge [31]. After extrapolating to the continuum limit, the lightest three states emerge as the scalar ($J^{PC} = 0^{++}$), tensor ($J^{PC} = 2^{++}$) and the pseudoscalar ($J^{PC} = 0^{-+}$), with the scalar around 1.55 ± 0.05 GeV/c^2, the tensor at 2.27 ± 0.1 GeV/c^2 and the pseudoscalar at about the same mass. It was also possible to identify a number of other states with the first exotic (non-$q\bar{q}$) quantum number state above 3 GeV/c^2.

A later calculation using a larger lattice and smaller lattice parameters yielded a mass for the scalar glueball 1.625 ± 0.094 GeV/c^2 [33, 34]. The authors also calculated the decay of the scalar glueball to pairs of pseudoscalar mesons and estimated that the total width of the glueball would be under 0.2 GeV/c^2. They also found that the decay width of the scalar glueball depended on the mass of the daughter mesons, with coupling increasing with mass. This was in contradiction to the lore that glueballs should decay in a flavor-blind fashion with the coupling to pairs of pseudoscalar mesons being independent of flavor or mass. Other work has followed this in discussions of violations of flavor-blind decays [35, 36]. This breaking is (effectively) accomplished by introducing a parameter r in the matrix that mixes quarkonium with glueballs. For flavor blind decays, $r = 1$. Values that are close to 1 are

J^{PC}	M_G (GeV/c^2)
0^{++}	1.710(.050)(.080)
2^{++}	2.390(.030)(.120)
0^{-+}	2.560(.035)(.120)
1^{+-}	2.980(.030)(.140)
2^{-+}	3.040(.040)(.150)
3^{+-}	3.600(.040)(.170)
3^{++}	3.670(.050)(.180)
1^{--}	3.830(.040)(.190)
2^{--}	4.010(.045)(.200)
3^{--}	4.200(.045)(.200)
2^{+-}	4.230(.050)(.200)
0^{+-}	4.780(.060)(.230)

Table 5: The glueball mass spectrum in physical units. For the mass of the glueballs (M_G), the first error comes from the combined uncertainty of $r_0 M_G$, the second from the uncertainty of $r_0^{-1} = 410(20)\,\mathrm{MeV}$. Data are taken from [32].

typically found. On the lattice [33,34], it is found that $r = 1.2 \pm 0.07$, while a fit to data [35] finds $r = 1 \pm 0.3$. Finally, in a microscopic quark/gluon model [36], $r = 1.1 - 1.2$. Taken together, one should probably expect small violations of flavor-blind decays for glueballs, but not large.

Using an improved action, detailed calculations for the spectrum of glueballs was carried out by Morningstar and colleagues [32,37]. This is shown in Figure 3 and the corresponding masses reported in Table 5. These calculations are currently the state of the art in lattice glueball mass predictions.

Hart and Tepper [38] carried out an unquenched calculation of the scalar and tensor glueballs using Wilson fermions. They found that the tensor mass did not move, while the scalar mass came out at about 85% of the unquenched mass. McNeile [39] speculates that this may be a result of the lattice artifact mentioned above. In another unquenched calculation, Gregory [40]. find that unquenching the lattice calculations for glueballs appears not to significantly alter the results from unquenched calculations.

4 The Known Mesons

4.1 Experimental Methods and Major Experiments

Results on meson spectroscopy have come from a large variety of experiments using different experimental techniques. Production of glueballs has mainly been predicted for glue-rich

environments [41]. The most promising examples are proton-antiproton annihilation, central pp collisions through double-Pomeron exchange [] or radiative decays of quarkonia, where one of the three gluons arising from the quark-antiquark annihilation is replaced by a photon leaving two gluons to form bound states. The most prominent example is the radiative decay $J/\psi \to \gamma G$ [15, 16]. The following sections describe the main experimental methods and major experiments devoted to the study of meson resonances and the search for glueballs.

Proton-Antiproton Annihilation

In $p\bar{p}$ annihilations, glueballs may be formed when quark-antiquark pairs annihilate into gluons. Though not very likely, this may proceed via *formation* (as opposed to *production*) without a recoil particle; in this case, exotic quantum numbers are forbidden and the properties of the glueball candidate can be determined from the initial state. Instead, production of a heavier resonance recoiling against another meson is normally expected, but interaction of gluons forming glueballs sounds likely. However, the usually observed final states consisting of light u- and d-quarks can be just as effectively produced by quark rearrangements, i.e. without glueballs in the intermediate state. In $p\bar{p}$ annihilations at rest, mesons with masses up to 1.7 GeV/c^2 can be produced. Feynman Graphs of $p\bar{p}$ formation, production, etc.?

The $p\bar{p}$ annihilation at rest offers a natural way of limiting the number of partial waves involved in the process facilitating spin-parity analyses. At the Low-Energy Antiproton Ring (LEAR) at CERN, slow antiprotons of about 200 MeV/c were decelerated in liquid or gaseous hydrogen (or deuterium) by ionizing hydrogen molecules and eventually stopped and captured by protons forming hydrogen-like atoms called *protonium*. A highly excited $p\bar{p}$ state is formed by ejecting an electron via *Auger effect*:

$$\bar{p} + \mathrm{H}_2 \to \boxed{p\bar{p}} + \mathrm{H} + \mathrm{e}^-$$

Annihilation takes place from atomic orbits. The capture of the $\bar{p}$ typically occurs at a principal quantum number of $n \approx 30$ and at a high angular momentum between the proton and the antiproton of $L \approx n/2$. For $n \approx 30$, the radius of the protonium atom matches the size of hydrogen atoms in their ground state. For lower n values, the protonium radius becomes much smaller; the first Bohr radius of the $p\bar{p}$ atom is 57 fm. Due to this small size and due to the fact that protonium carries no charge, it can diffuse through hydrogen molecules. The $\bar{p}$ reaches an atomic state with angular momentum $L = 0$ or $L = 1$ when annihilation takes place. In media of high density like liquid H_2, the protonium is exposed to extremely large electromagnetic fields so that rotation invariance is broken. Transitions between different nearly mass-degenerate angular momentum states at the same high principal quantum number n occur (*Stark mixing*). The effect is proportional to the target density and for liquid targets the rate is very high, such that about 90 % of all annihilations appear to be S-wave annihilations. For gaseous hydrogen targets, the P-wave contribution is much larger. The incoherent superposition of the $L = 0$ or $L = 1$ angular momentum eigenstates of the $p\bar{p}$ atom corresponds to six different partial waves: ${}^1S_0, {}^3S_1, {}^1P_1, {}^3P_0, {}^3P_1, {}^3P_2$.

Proton and antiproton both carry isospin $|I, I_3\rangle = |\frac{1}{2}, \pm\frac{1}{2}\rangle$ and can couple to either $|I = 0, I_3 = 0\rangle$ or $|I = 1, I_3 = 0\rangle$. Given that initial state interactions due to $p\bar{p} \to n\bar{n}$ are

small [42], we have

$$p\bar{p} = \sqrt{\frac{1}{2}}(|I = 1, I_3 = 0\rangle + |I = 0, I_3 = 0\rangle). \tag{14}$$

A large number of meson resonances was studied in $\bar{p}N$ annihilations at rest and in flight. The most recent experiments were carried out at LEAR at CERN; the accelerator was turned off in 1996. The OBELIX Collaboration at LEAR had a dedicated program on light-meson spectroscopy. The detector system allowed operation of a variety of hydrogen targets: liquid H_2, gaseous H_2 at normal temperature and pressure, and also a target at very low pressures. A special feature of the detector was the possibility to study antineutron interactions, where the $\bar{n}$ beam was produced by charge exchange in a liquid H_2 target. The Open Axial-Field Magnet of the experimental setup provided a magnetic field of 0.5 T. Particle detection proceeded via a Spiral Projection Chamber acting as vertex detector, a time-of-flight (TOF) system, a Jet Drift Chamber (JDC) for tracking and identification of charged particles by means of $\mathrm{d}E/\mathrm{d}x$, and a High-Angular Resolution Gamma Detector (HARGD), a system of four supermodules for the identification and measurement of neutral annihilation products. A detailed description of the experimental setup is given in [43]. The resolution of pions in the reaction $p\bar{p} \to \pi^+\pi^-$ was determined to 3.5 % at 928 MeV/c and the mass resolution of π^0 mesons given by $\sigma = 10$ MeV/c^2. Results are summarized in [43–50].

Adjacent to OBELIX in the experimental hall, the Crystal Barrel spectrometer was operational from 1989-1996. The apparatus is described in [51] and shown in Fig. 4. It could measure multi-meson final states including charged particles and photons from the decay of neutral mesons. The detector consisted of two concentric cylindrical multi-wire proportional chambers (PWC), a jet drift chamber (JDC), and a barrel-shaped, modular electromagnetic CsI(Tl) calorimeter giving the detector system its name. The PWC was replaced by a silicon vertex detector in September 1995. The JDC had 30 sectors with each sector having 23 sense wires and allowed the detection and identification of charged particles with a momentum resolution for pions of less than 2 % at 200 MeV/c. Separation of π/K below 500 MeV/c proceeded via ionisation sampling. The magnetic field of up to 1.5 T with a relative homogeneity of 2 % in the region of the drift chamber was created by a conventional solenoid ($B_r \approx B_\phi \approx 0$, $B_z \neq 0$) which was encased in a box-shaped flux return yoke. Data were taken on hydrogen and deuterium at rest [52–70] and at different incident beam momenta [71–75].

The basic idea of the ASTERIX Experiment was to measure $p\bar{p}$ annihilations with and without X-rays from the $p\bar{p}$ cascade in coincidence. Antiprotons were stopped in a cylindrical H_2 gas target at room temperature and pressure (45m in length, 14 cm in diameter). The detector consisted of a X-ray drift chamber and seven multi-wire proportional chambers. Two end-cap detectors with three wire planes and cathode readout on both sides gave large solid-angle coverage. The detection volume was situated in a homogeneous axial magnet field of up to 0.82 T. Pion and kaon separation was possible up to 400 MeV/c. The solid angle for charged particles was 50 % of 4π with a momentum resolution of $\sigma = 4.2$ % at 1 GeV/c. The detector is fully described in [76]. Since the ASTERIX Experiment was designed to

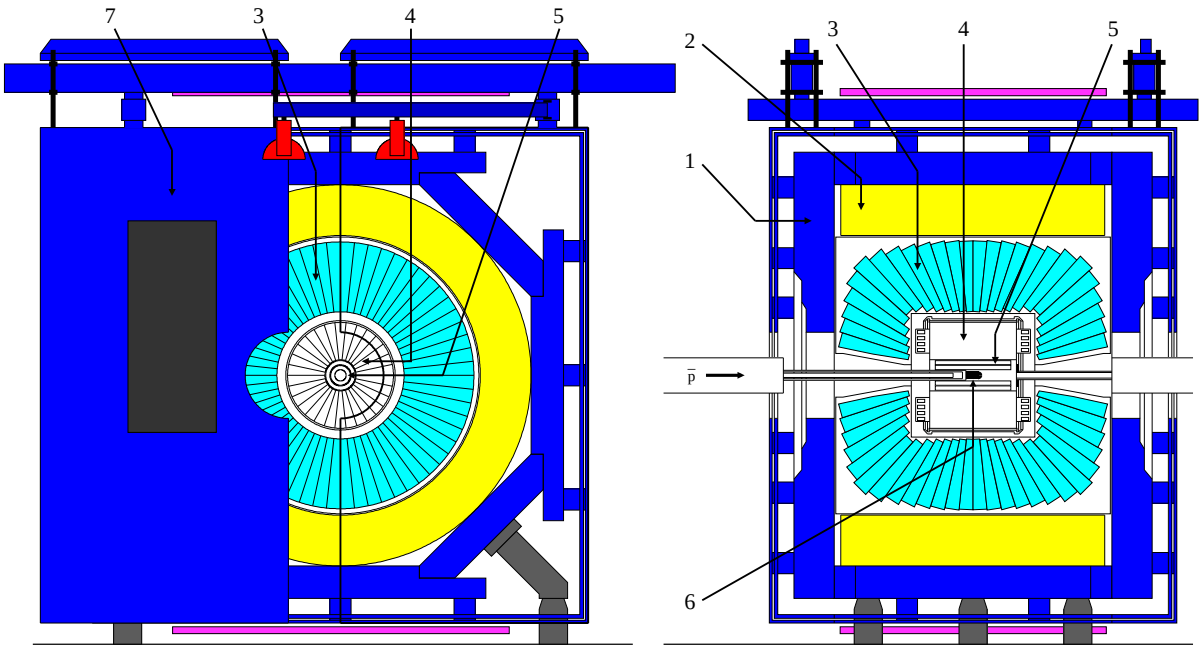

Figure 4: Cross section of the Crystal-Barrel Detector at LEAR. From the outside: (1) magnet yoke, (2) magnet coils, (3) CsI(Tl) barrel calorimeter, (4) jet drift chamber, (5) proportional wire chamber, (6) target, (7) one half of the endplate

stop antiprotons in a H_2 gas target, data were taken at the lowest available beam momenta: 300 MeV/c in 1983, 200 MeV/c in 1984, and 105 MeV/c in 1985 and 1986. Typical intensities used for data taking were $10^4 - 10^5$ antiprotons per second. The experiment was dismantled and removed from the floor in 1986. The physics program on meson spectroscopy was then extended by the Crystal-Barrel and OBELIX experiments.

e^+e^- Annihilation Experiments and Radiative Decays of Quarkonia

The study of radiative decays of quarkonia is considered most suggestive in the glueball search. Most of the information in this field has centered on J/ψ decays; after photon emission, the $c\bar{c}$ annihilation can go through C-even gg states, and hence may have a strong coupling to the low-lying glueballs. Study of J/ψ decays facilitates the search because the $D\bar{D}$ threshold is above the J/ψ mass of 3097 MeV/c^2 and the OZI rule[1] suppresses decays of the $c\bar{c}$ system into light quarks. Radiative $\Upsilon(1S)$ decays are also supposed to be glue-rich and a corresponding list of two-body decay branching ratios for $\Upsilon(1S)$ is desirable. Results have been recently reported by the CLEO Collaboration [77, 78]. The search for glueballs in

[1]The OZI rule states that decays corresponding to disconnected quark diagrams are forbidden.

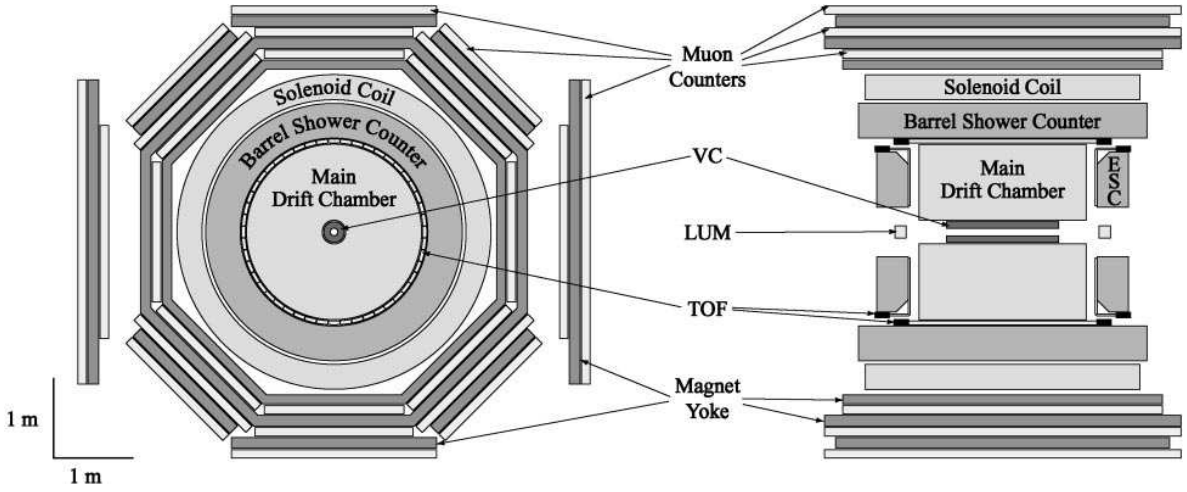

Figure 5: End view (left) and side view (right) of the BES-II detector at IHEP, Beijing

$\Upsilon(1S)$ decays is however challenging because the ratio

$$\frac{\Gamma^{\rm rad}_{\Upsilon}}{\Gamma^{\rm tot}_{\Upsilon}} = \left(\frac{\alpha_s(\Upsilon)}{\alpha_s(J/\psi)}\right)^4 \left(\frac{\Gamma_{\Upsilon\to e^+e^-}}{\Gamma^{\rm tot}_{\Upsilon}} \cdot \frac{\Gamma^{\rm tot}_{J/\psi}}{\Gamma_{J/\psi\to e^+e^-}} \cdot \frac{\Gamma^{\rm rad}_{J/\psi}}{\Gamma^{\rm tot}_{J/\psi}}\right) \approx 0.013 \tag{15}$$

is much smaller than for J/ψ mesons and a naive suppression factor of ~ 6 is expected. Moreover, information on any possible χ_{cJ} hadronic decays provides valuable insight into possible glueball dynamics.

J/ψ decays can also be used to study the flavor content of mesons in the so-called *flavor-tagging* approach. The reaction $J/\psi \to V\,X$ may serve as an example, where V is one of the light vector mesons (ω, ϕ, ρ^0) and X is the exclusive final state of interest. The flavor of X can now be tagged as the structure of the light vector is known. If the $\phi(1020)$ is produced, for instance, then the reaction $J/\psi \to \phi\,X$ indicates those recoiling mesons X, which are produced through their $s\bar{s}$ component. For this reason, J/ψ decays to $\omega f_2(1270)$ and $\phi f_2'(1525)$ are clearly observed, but decays to $\omega f_2'(1525)$ and $\phi f_2(1270)$ are missing. High-statistics flavor-tagging is a promising tool and has helped determine mixing angles as discussed in section 2. Similar decays of the $\psi'(3770)$, the first radial excitation of the J/ψ, provides access to mesons with even higher masses.

Radiative decays of $c\bar{c}$ states can best be studied in *formation* at $\rm e^+e^-$ colliders via a virtual photon in the process

$$e^+e^- \to \gamma^* \to c\bar{c}. \tag{16}$$

Only states with the quantum numbers of the photon ($J^P = 1^-$) can be created and the lowest-mass candidate is the $1^3S_{1^-}$ J/ψ state.

Several reactions have been studied in the BES experiment at the e^+e^- collider BEPC at IHEP, Beijing. Operation started in 1989 with a maximum collider energy of $2E = 4.4$ GeV and a luminosity of up to $10^{31}/\mathrm{cm}^2/\mathrm{s}$. A layout of the BES-II detector is shown in Fig. 5. The detector is a large solid-angle magnetic spectrometer based on a conventional 0.4 T solenoidal magnet [79]. It identifies charged particles using $\mathrm{d}E/\mathrm{d}x$ measurements in the drift chambers and time-of-flight measurements in a barrel-like array of 48 scintillation counters. The barrel shower counter measures the energy of photons with a resolution of $\sigma_E/E = 28\,\%/\sqrt{E}$ (E in GeV). More than 10^7 J/ψ events and more than 10^6 $\psi\,'(3770)$ events have been accumulated. The BES-III detector is a major upgrade aiming at $L = 10^{33}/\mathrm{cm}^2/\mathrm{s}$ luminosity and recorded its first hadronic event in July 2008. Results relevant to this review are summarized in [80–86].

Radiative decays of $c\bar{c}$ and Υ ($b\bar{b}$) states have been studied with the CLEO detector at the e^+e^- collider CESR at Cornell University. Based on the CLEO-II detector, the CLEO-III detector started operation in 1999 [87]. CLEO consisted of drift chambers for tracking and $\mathrm{d}E/\mathrm{d}x$ measurements and a CsI electromagnetic calorimeter based on 7800 modules inside a 1.5 T magnetic field. For CLEO-III, a silicon-strip vertex detector and a ring-imaging Čerenkov detector for particle identification were added. The integrated luminosity accumulated by the CLEO-III detector in 1999-2003 was 16 fb^{-1}. In 2003, CLEO was upgraded to CLEO-c in order to study charm physics at high luminosities. The CLEO-c operations ended in Spring 2008. The anticipated program of collecting data at $\sqrt{s} \sim 3.10$ GeV for the J/ψ was given up due to technical difficulties in favor of a total of 572 pb^{-1} on the $\psi'(3770)$. Selected results of the CLEO Collaboration can be found in [77, 78, 88–95].

The KLOE Collaboration has studied radiative $\phi(1020)$ decays to $f_0(980)$ and $a_0(980)$ at the Frascati ϕ factory DAPHNE. These decays play an important role in the study of the controversial structure of the light scalar mesons. In particular, the ratio $\mathcal{B}(\phi \to f_0(980)\gamma)/\mathcal{B}(\phi \to a_0(980)\gamma)$ depends strongly on the structure of the scalars [96]. The KLOE detector consists of a cylindrical drift chamber, which is surrounded by an electromagnetic calorimeter and a superconducting solenoid providing a 0.52 T magnetic field. The energy resolution of the calorimeter is $\sigma_E/E = 5.7\,\%/\sqrt{E}$ (E in GeV). The detector accumulated 1.4×10^9 ϕ decays in 2 years (2001-2002) with a maximum luminosity of up to $7.5 \times 10^{32}/\mathrm{cm}^2/\mathrm{s}$. KLOE resumed data taking in 2004 with an upgraded machine. Relevant results are summarized in [97–99].

Production Experiments: Central Production

In contrast to *formation* experiments like e^+e^- and $p\bar{p}$ annihilation discussed in the previous sections, the total energy in *production* experiments is shared among the recoiling particle(s) and the multi-meson final state. The mass and quantum numbers of the final state cannot be determined from the initial state and thus, many resonant waves with different angular momenta can contribute.

In central production, glueballs were suggested long time ago to be produced copiously

in the process [100]:

$$\text{hadron}_{\text{beam}}\, p \to \text{hadron}_{\text{f}}\, X\, p_s\,, \tag{17}$$

where the final-state hadrons carry large fractions of the initial-state hadron momenta and are scattered diffractively into the forward direction. To fulfill this requirement in a (proton) fixed-target experiment, a slow proton and a fast hadron needs to be observed in the final state. Mostly proton beams were used for these kinds of experiments, but some also involved pions or even kaons. The triggers in these experiments enhanced double-exchange processes – Reggeon-Reggeon, Reggeon-Pomeron, or Pomeron-Pomeron – relative to single-exchange and elastic processes. Early theoretical predictions suggested that the cross section for double-Pomeron exchange is constant with center-of-mass energy $\sqrt{s}$, whereas a falling cross section is expected for the other exchange mechanisms [41]:

$$\sigma\ (\text{Reggeon} - \text{Reggeon}) \sim 1/s \tag{18}$$

$$\sigma\ (\text{Reggeon} - \text{Pomeron}) \sim 1/\sqrt{s} \tag{19}$$

$$\sigma\ (\text{Pomeron} - \text{Pomeron}) \sim \text{constant} \tag{20}$$

At sufficiently high center-of-mass energies, reaction (17) is expected to be dominated by double-Pomeron exchange. The pomeron carries no charges – neither electric nor color charges – and is expected to have positive parity and charge conjugation. Thus, double-Pomeron exchange should favor production of isoscalar particles with positive G-parity in a glue-rich environment as no valence quarks are exchanged.

The observation in central production of a significant enhancement of glueball candidates over the production of conventional $q\bar{q}$ mesons at small transverse momenta led to the idea of a *glueball filter* [101]. No dynamical explanation has been given for this empirical finding, yet. In fact, the data show a strong kinematical dependence at small transverse momenta for all mesons. Just a momentum filter?

Several experiments, especially at CERN, made remarkable contributions. The WA76 Collaboration recorded data, mainly at 300 GeV/c, using a 60 cm long H_2 target. Multi-wire proportional chambers triggered on exactly one "fast" particle in the forward direction. Some results from WA76 can be found in [102].

The electromagnetic multiphoton spectrometer GAMS-2000 originally took data at the IHEP proton synchrotron, Protvino, in a 38 GeV/c negative-pion beam [103]. The detector was later upgraded for experiments at the CERN SPS [104]. GAMS-4000 used a 50 cm long liquid H_2 target and comprised a matrix of 64×64 lead glass cells covering almost 6 m^2.

Both the WA91 and WA102 Collaborations reported strong kinematical dependences of central meson production. The layout of the WA102 experiment is shown in Fig. 6. The experiment was a continuation of the WA76, WA91 and NA12/2 experiments at CERN aiming at a more complete study of the mass region from 1.2 to 2.5 GeV/c^2. The experimental setup was a combination of the WA76 setup serving as a charged-particle tracker and the GAMS-4000 detector in the forward region providing the opportunity to detect and study events with charged and neutral particles. Results from WA102 are summarized in [105–122].

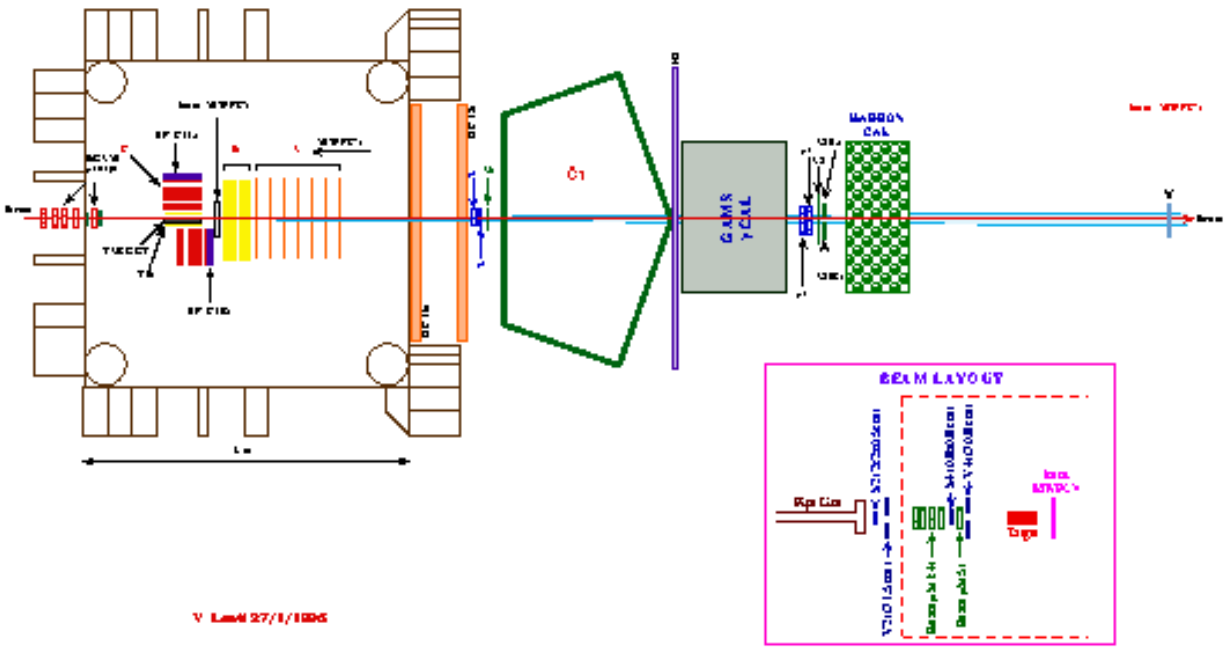

Figure 6: Layout of the WA102 experiment using the CERN Ω spectrometer and GAMS-4000 (1996 run) Better picture?

Two-Photon Fusion at e^+e^- Colliders

In contrast to direct glueball signals, the corresponding absence of states or glueball candidates in certain reactions can be as informative. Models predict for example that the $\gamma\gamma$ coupling of non-$q\bar{q}$ mesons is small. In particular, glueball production should be strongly suppressed in two-photon fusion because there is no valence charge to couple to photons. The collision of two photons can best be studied in *inelastic Bhabha scattering* at e^+e^- colliders via the the reaction $e^+e^- \to e^+e^-\,\gamma\gamma \to e^+e^-\,X$ [123]. This is analogous to the central production process in which the photons replace the less-well-understood Pomeron. In e^+e^- annihilations, only final states with $J^{PC} = 1^{--}$ can be formed, whereas two-photon collisions provide access to most of the $C = +1$ mesons.

In the two-photon process, each photon can be almost massless, though both can combine to form a massive state X. The square of the mass of each photon is determined by the scattering angle θ and the initial and final energies E and E' of its scattered lepton:

$$m_\gamma^2 \equiv q^2 \approx -2EE'(1 - cos\,\theta)\,. \tag{21}$$

Spectroscopic data from two-photon collisions are generally separated into *tagged* and *untagged* event samples. If both leptons scatter at very small angles, $\theta \approx 0$, then they remain within the beam pipe and most likely escape undetected. In such a *no-tag* experiment, the

two-photon invariant mass W comes from the electron-positron energy losses:

$$W \approx \sqrt{(E_1 - E_1')(E_2 - E_2')}\,, \tag{22}$$

and one can safely assume that the exchanged photons are essentially "real" with $q^2 \approx 0$. The allowed quantum numbers for a system formed by two quasi-real photons can be found by considering gauge invariance and symmetry principles. Since photons are identical bosons, two of them must be in a $C = +1$ state. Moreover, Yang's theorem forbids any spin-1 state and odd-spin states with negative parity [124], leaving $J^{PC} = 0^{\pm+}, 2^{\pm+}, 3^{++}$, etc. for *untagged* events. However, if the incident e^+e^- pair is scattered through a large angle sufficient to be *tagged* by the experimental setup, the exchanged photons will be virtual and will also have a significant component of longitudinal polarization. A factor $1/M^3$ in the cross section indicates that the formation of lighter mesons is favored over heavier ones with the same $\Gamma_{\gamma\gamma}$.

In addition to the *stickiness* (as defined in Eq. 13), a further quantitative test was proposed whether a meson state is a glueball or a conventional $q\bar{q}$ meson. In [16], the normalized quantity *gluiness* denotes the ratio of the two-gluon to the two-photon coupling of a particle and is expected to be near unity for a $q\bar{q}$ meson within the accuracy of the approximations made in [16]:

$$G \;=\; \frac{9e_Q^4}{2}\left(\frac{\alpha}{\alpha_s}\right)^2 \frac{\Gamma_{R\to gg}}{\Gamma_{R\to\gamma\gamma}} \tag{23}$$

Two-photon fusion has been studied in *production* with the CLEO II and upgraded CLEO II.V detectors at CESR using 13.3 fb^{-1} of e^+e^- data. The hadron is produced in the fusion of two space-like photons emitted by the beam electron and positron. Results of two-photon fusion studies from CLEO can be found in [90, 125].

Further results on the $\gamma\gamma$-width of mesons have been reported by the LEP program at CERN. Though mainly focussing on electroweak physics, significant results on meson spectroscopy were achieved. The 4π detector ALEPH was designed to give as much detailed information as possible about complex events in high-energy e^+e^- collisions [126]. A superconducting coil produced a uniform 1.5-T field in the beam direction. Inside the coil, in order of increasing radius, there was a microstrip solid-state device, an Inner Tracking Chamber (ITC) using drift wires, a 3.6×4.4 m Time Projection Chamber (TPC), and an electromagnetic calorimeter of 2 mm lead sheets with proportional wire sampling. A hadron calorimeter and a double layer of drift tubes aiding in good electron/muon identification were located outside the magnet coil. ALEPH data-taking ended on November 2000. The L3 detector was designed to measure the energy and position of leptons with the highest obtainable precision allowing a mass resolution of $\delta m/m$ smaller than 2 % in dilepton final states [127]. Hadronic energy flux was detected by a fine-grained calorimeter, which also served as a muon filter and a tracking device. The outer boundary of the detector was given by the iron return-yoke of a conventional magnet. The field was 0.5 T over a length of 12 m. Radially inwards was a combined hadron calorimeter and muon absorber. The electromagnetic energy flow was determined by approximately 11,000 BGO crystals. Full

electromagnetic shower containment over nearly 4π solid angle coverage was achieved. L3 data-taking ended on November 2000. Important ALEPH and L3 results on the $\gamma\gamma$-width of mesons are given in [128–130].

Other Experiments

Many more experiments have significantly contributed to meson spectroscopy though these were not particularly devoted to the glueball search. Pion- and kaon beams were exploited in charge-exchange reactions:

$$\pi^-(K^-) + \text{proton} \rightarrow \text{neutron} + \text{meson} \tag{24}$$

In case of an kaon-induced reaction, the baryon in the final state can also be a Λ baryon. Reactions with positively-charged beams on proton targets are also possible. These peripheral processes are viewed as exciting the "beam" particles by means of an exchange with the "target" particle, leaving the target essentially unchanged. This is in contrast to "central production", which refers to the case in which there is a collision between exchange particles. Peripheral reactions are characterized by the square of the exchanged 4-momentum, $t^2 \equiv (p_{\text{beam}} - p_X)^2 < 0$. These meson-nucleon reactions are strongly forward peaked at high energies since the cross section is approximately exponentially falling with t. The fairly-well understood $\pi^- p$ charge-exchange reaction at small values of $-t$ provides access only to states with $J^{PC} = \text{even}^{++}$ and odd^{--} states, so-called "natural-parity" states. Other states such as $J^{PC} = 0^{-+}$ can for example be produced by neutral $J^{PC} = 0^{++}$ Pomeron exchange, which is not as well understood.

The LASS facility at SLAC was developed for strangeonium spectroscopy [131]. This spectrometer was designed for charged-particle final states and based on a superconducting solenoid producing a 2.24 T field along the beam axis and a subsequent 3 Tm dipole magnet with a vertical field. Particles under large scattering angles at low momenta and high-energy secondaries could be detected, respectively, with very good angular and momentum resolution. The LASS Collaboration recorded over $135 \cdot 10^6$ kaon-induced events.

The VErtex Spectrometer (VES) setup at Protvino was a large-aperture magnetic spectrometer including systems of proportional and drift chambers, a multi-channel threshold Čerenkov counter, beam-line Čerenkov counters, a lead-glass γ-detector (LGD) and a trigger hodoscope. This arrangement permits full identification of multi-particle final states. A negative particle beam (π^-, K^-) with momenta between 20-40 GeV/c was provided by the 70 GeV/c proton synchrotron. A description of the setup can be found in [132].

Experiment E852 at Brookhaven National Laboratory was an experiment in meson spectroscopy configured to detect both neutral and charged final states of 18 GeV/c $\pi^- p$ collisions in a search for meson states incompatible with the constituent quark model. The E852 apparatus was located at the Multi-Particle Spectrometer facility (MPS) of Brookhaven's Alternating Gradient Synchrotron (AGS). The apparatus consisted of a fully instrumented beamline, a hydrogen target, a recoil particle spectrometer, forward charged particle tracking, a large, segmented lead glass calorimeter and a nearly hermetic photon detection system.

A flexible, programmable trigger allowed multiple final-state topologies to be collected simultaneously. A detailed description of the E852 apparatus is given in Reference [133].

Light-Meson Spectroscopy at Heavy-Flavor Experiments

Decays of B mesons offer a wide phase space at the expense of small event numbers per MeV/c^2. Among many other things, they provide interesting and surprising insight into the nature of lighter mesons. In 1999, two so-called $B\bar{B}$ factories started data-taking with the main goal to study time-dependent CP asymmetries in the decay of these mesons: BaBar at the Stanford Linear Accelerator Center (SLAC) and Belle at the KEKB e^+e^- collider in Tsucuba, Japan. The very high luminosities of the electron-positron colliders and the general-purpose character of the detectors makes them suitable places also for the study of lighter mesons.

BaBar is a cylindrically-shaped detector [134] with the interaction region at its center. The 9 GeV electron beam of the PEP-II facility collides with a 3.1 GeV positron beam to produce a center-of-mass energy of 10.58 GeV, corresponding to the $\Upsilon(4S)$ resonance. This highly unstable state decays almost instantly into two B mesons; about 10^9 B mesons have been recorded. The momenta of charged particles are measured with a combination of a five-layer silicon vertex tracker and a 40-layer drift chamber in a solenoidal magnetic field of 1.5 T. The momentum resolution is about $\sigma_{p_t} \approx 0.5\,\%$ at $p_t = 1.0$ GeV/c. A detector of internally reflected Čerenkov radiation is used for charged particle identification. The electromagnetic calorimeter is a finely segmented array of CsI(Tl) crystals with energy resolution of $\sigma_E/E \approx 2.3\,\% \times E^{-1/4} + 1.9\,\%$, where the energy is in GeV. The instrumented flux return contains resistive plate chambers for muon and long-lived neutral hadron identification. Some results are given in [135].

The Belle experiment operates at the KEKB e^+e^- accelerator, the world's highest luminosity machine with a world record in luminosity of 1.7×10^{34} cm^{-2}s^{-1} and with an integrated luminosity exceeding 700 fb^{-1}. The Belle detector [136] is a large-solid-angle magnetic spectrometer based on a 1.5 T superconducting solenoid. Charged particle tracking is provided by a three-layer silicon vertex detector and a 50-layer central drift chamber (CDC) surrounding the interaction point. The charged particle acceptance covers laboratory polar angles between $\theta = 17°$ and 150°, corresponding to about 92 % of the total solid angle in the center-of-mass system. The momentum resolution is determined from cosmic rays and $e^+e^- \to \mu^+\mu^-$ events to be $\sigma_{p_t}/p_t = (0.30/\beta \oplus 0.1\,p_t)\,\%$, where p_t is the transverse momentum in GeV/c. Charged hadron identification and pion/kaon separation is provided by dE/dx measurements in the CDC, an array of 1188 aerogel Čerenkov counters (ACC), and a barrel-like array of 128 time-of-flight scintillation counters with rms resolution of 0.95 ps. Electromagnetic showering particles are detected in an array of 8736 CsI(Tl) crystals of projective geometry that covers the same solid angle as the charged particle system. The energy resolution of electromagnetic showers is $\sigma_E/E = (1.3 \oplus 0.07/E \oplus 0.8/E^{1/4})\,\%$ with E in GeV. Results on light-meson spectroscopy relevant to this review are summarized in [137, 138].

Name	Mass [MeV/c^2]	Width [MeV/c^2]	Decays
$f_0(600)$ $*$	$400-1200$	$600-1000$	$\pi\pi$, $\gamma\gamma$
$f_0(980)$ $*$	980 ± 10	$40-100$	$\pi\pi$, $K\bar{K}$, $\gamma\gamma$
$f_0(1370)$ $*$	$1200-1500$	$200-500$	$\pi\pi$, $\rho\rho$, $\sigma\sigma$, $\pi(1300)\pi$, $a_1\pi$, $\eta\eta$, $K\bar{K}$
$f_0(1500)$ $*$	1507 ± 5	109 ± 7	$\pi\pi$, $\sigma\sigma$, $\rho\rho$, $\pi(1300)\pi$, $a_1\pi$, $\eta\eta$, $\eta\eta'$ $K\bar{K}$, $\gamma\gamma$
$f_0(1710)$ $*$	1718 ± 6	137 ± 8	$\pi\pi$, $K\bar{K}$, $\eta\eta$, $\omega\omega$, $\gamma\gamma$
$f_0(1790)$			
$f_0(2020)$	1992 ± 16	442 ± 60	$\rho\pi\pi$, $\pi\pi$, $\rho\rho$, $\omega\omega$, $\eta\eta$
$f_0(2100)$	2103 ± 7	206 ± 15	$\eta\pi\pi$, $\pi\pi$, $\pi\pi\pi\pi$, $\eta\eta$, $\eta\eta'$
$f_0(2200)$	2189 ± 13	238 ± 50	$\pi\pi$, $K\bar{K}$, $\eta\eta$

Table 6: The $I=0$, $J^{PC}=0^{++}$ mesons as listed by the particle data group [6]. Resonances marked with $*$ are listed in the Meson Summary Table.

4.2 *The scalar, pseudoscalar and tensor mesons*

If we focus on the expected three lightest mass glueballs, $J^{PC}=0^{++}$, 2^{++}, and 0^{-+}, we note that these are all quantum numbers of normal $q\bar{q}$ mesons. As such, it is important to understand what the known spectra and multiplet assignments of these states are. As a starting point, we take the point of view of the Particle Data Group (PDG) [139]. The $I=0$ mesons are listed for $J^{PC}=0^{++}$ in Table 6, $J^{PC}=2^{++}$ in Table 7 and $J^{PC}=0^{-+}$ in Table 8. In additions to the listings, the Particle Data Group also has minireviews on the three sectors: the scalar mesons [140,141], the pseudoscalars [142] and the tensors [143]. The following sections describe the main experimental findings in the search for the lightest-mass glueballs.

Results from $p\bar{p}$ Annihilation: The Crystal Barrel Experiment

The Crystal Barrel experiment [51] studied $p\bar{p}$ annihilation both at rest and in flight and observed final states with multiple charged particles and photons. In particular, many all-neutral final states were observed for the first time. The experiment accumulated about 10^8 $p\bar{p}$ annihilation at rest in liquid hydrogen and thus, exceeded statistics collected in bubble-chamber experiments by about three orders of magnitude. At the beginning of the Crystal-Barrel data taking in late 1989, only three scalar states were well established: $a_0(980)$, $f_0(980)$, and the $K_0^*(1430)$. The high-statistics data sets collected at rest provided firm evidence for new states, among others the $f_0(1500)$ scalar state.

For annihilations at rest into three-pseudoscalar final states, Crystal Barrel studied the following reactions: $p\bar{p}\to\pi^0\pi^0\pi^0$ [52,53], $p\bar{p}\to\pi^0\pi^0\eta$ [52], $p\bar{p}\to\pi^0\eta\eta$ [52,54,55], $p\bar{p}\to\pi^0\eta\eta'$ [56], $p\bar{p}\to K_L^0K_S^0\pi^0$ [57], $p\bar{p}\to K_L^0K_S^0\eta$ [57], $p\bar{p}\to K^+K^-\pi^0$ [58], $p\bar{p}\to K_LK_L\pi^0$ [59], $p\bar{p}\to\pi^0\pi^0\eta'$ [60], $p\bar{p}\to\eta\pi\pi$ [61], $n\bar{p}\to\pi^-\pi^0\pi^0$ [67], $n\bar{p}\to\pi^+\pi^-\pi^-$ [68]. Studies were also

Name	Mass [MeV/c^2]	Width [MeV/c^2]	Decays
$f_2(1270)$ $*$	1275.4 ± 1.1	$185.2^{+3.1}_{-2.5}$	$\pi\pi$, $\pi\pi\pi\pi$, $K\bar{K}$, $\eta\eta$, $\gamma\gamma$
$f_2(1430)$	1430	$13 - 150$	$K\bar{K}$, $\pi\pi$
$f_2'(1525)$ $*$	1525 ± 5	73^{+6}_{-5}	$K\bar{K}$, $\eta\eta$, $\pi\pi$, $K\bar{K}^* + cc$
$f_2(1565)$	1546 ± 12	126 ± 12	$\pi\pi$, $\rho\rho$, $\eta\eta$, $a_2\pi$, $\omega\omega$, $K\bar{K}$, $\gamma\gamma$
$f_2(1640)$	1638 ± 6	99^{+28}_{-24}	$\omega\omega$, 4π,$K\bar{K}$
$f_2(1810)$	1815 ± 12	197 ± 22	$\pi\pi$, $\eta\eta$, 4π, $K\bar{K}$
$f_2(1910)$	1915 ± 7	163 ± 50	$\pi\pi$,$K\bar{K}$, $\eta\eta$, $\omega\omega$, $\eta\eta\prime$, $\eta\prime\eta\prime$, $\rho\rho$
$f_2(1950)$ $*$	1944 ± 12	472 ± 18	$K^*\bar{K}^*$, $\pi\pi$, 4π, $a_2\pi$, $f_2\pi\pi$, $\eta\eta$,$K\bar{K}$, $\gamma\gamma$
$f_2(2010)$ $*$	2011^{+60}_{-80}	202 ± 60	$\phi\phi$,$K\bar{K}$
$f_2(2150)$	2156 ± 11	167 ± 30	$\pi\pi$, $\eta\eta$, $K\bar{K}$, $f_2\eta$, $a_2\pi$
$f_2(2300)$ $*$	2297 ± 28	149 ± 40	$\phi\phi$, $K\bar{K}$, $\gamma\gamma$
$f_2(2340)$ $*$	2339 ± 60	319^{+80}_{-70}	$\phi\phi$, $\eta\eta$

Table 7: The $I = 0$, $J^{PC} = 2^{++}$ mesons as listed by the particle data group [6]. Resonances marked with $*$ are listed in the Meson Summary Table. A mini-review in the 2004 edition of the PDG discusses more solid evidence for the $f_2(1565)$.

Name	Mass [MeV/c^2]	Width [MeV/c^2]	Decays
$\eta(548)$ $*$	547.51 ± 0.18	$1.30 \pm .07$ keV	$\gamma\gamma$, 3π
$\eta\,'(958)$ $*$	957.78 ± 0.14	0.203 ± 0.016	$\eta\pi\pi$, $\rho\gamma$, $\omega\gamma$, $\gamma\gamma$
$\eta(1295)$ $*$	1294 ± 4	55 ± 5	$\eta\pi\pi$, $a_0\pi$, $\gamma\gamma$, $\eta\sigma$, $K\bar{K}\pi$
$\eta(1405)$ $*$	1409.8 ± 2.5	51.1 ± 3.4	$K\bar{K}\pi$, $\eta\pi\pi$, $a_0\pi$, $f_0\eta$, 4π
$\eta(1475)$ $*$	1476 ± 4	87 ± 9	$K\bar{K}\pi$, $K\bar{K}^* + cc$, $a_0\pi$, $\gamma\gamma$
$\eta(1760)$	1760 ± 11	60 ± 16	$\omega\omega$, 4π
$\eta(2225)$	2220 ± 18	$150^{+300}_{-60} \pm 60$	$K\bar{K}K\bar{K}$

Table 8: The $I = 0$, $J^{PC} = 0^{-+}$ mesons as listed by the particle data group [6]. Resonances marked with $*$ are listed in the Meson Summary Table.

carried out for several four-pseudoscalar-meson final states where $p\bar{p} \to \eta\pi^0\pi^0\pi^0$ [62] was studied. In addition a number of five-pions final states were analyzed, $p\bar{p} \to 5\pi$ [63–66]. In addition, the reactions $p\bar{p} \to \omega\pi^0\pi^0$ [69], $n\bar{p} \to \omega\pi^-\pi^0$ [70], were analyzed. Measurements were also made in flight at several different incident $\bar{p}$ momenta: $p\bar{p} \to K\bar{K}\pi^\circ$ [71], $p\bar{p} \to \eta\pi^0\pi^0$ [72], $p\bar{p} \to \eta\pi^0\pi^0\pi^0$ [73], $p\bar{p} \to \omega\pi^\circ$ [74], $p\bar{p} \to \omega\eta$ [74], $p\bar{p} \to \omega\eta\,'$ [74], $p\bar{p} \to \pi^0\pi^0\pi^0$ [75], $p\bar{p} \to \pi^0\pi^0\eta$ [75], $p\bar{p} \to \pi^0\eta\eta$ [75], $p\bar{p} \to K^+K^-\pi^0$ [75].

Results on Scalar States

The first experimental hint for an isoscalar state around 1500 MeV/c^2 came in 1973 from a low-statistics analysis of $p\bar{p}$ annihilations at rest into three pions [144]. The state was later confirmed with a mass of 1527 MeV/c^2 suggesting a spin-0 assignment and also reporting a missing $K\bar{K}$ decay mode [145]. A very broad, somewhat higher-mass S-wave state called G(1590) was reported in 38 GeV/c pion-induced reactions by the GAMS-2000 Collaboration decaying to $\eta\eta$ [146] and $\eta\eta'$ [147]. The group reported that the decay rate into two neutral pions is at least three times lower than the rate into $\eta\eta$.

Crystal Barrel provided high-statistics for final states with three light pseudoscalar mesons. In summary, a consistent description of all these data was achieved in a coupled-channel analysis by using four (isoscalar) scalar $\pi^0\pi^0$ waves: $f_0(980)$, $f_0(1370)$, $f_0(1500)$, and a broad structure $f_0(400-1200)$ – listed as $f_0(600)$ by the PDG. In particular, the $3\pi^0$ and $\pi^0\eta\eta$ channels need the two scalar states, $f_0(1370)$ and $f_0(1500)$, decaying to $\pi^0\pi^0$ and $\eta\eta$. Consistency in the description of the data sets further requires two poles for the $\eta\pi^0$ S-wave in annihilation into $\pi^0\pi^0\eta$, $a_0(980)$ and $a_0(1450)$, in addition to a tensor meson in the $\pi\pi$ P-wave, $f_2(1565)$ [52].

Dalitz plots from various Crystal Barrel analyses are shown in Fig. 7 for $p\bar{p}$ annihilation into $\pi^0\eta\eta$ (a), $\pi^0\pi^0\eta$ (b), $3\pi^0$ (c), and $\pi^0K_LK_L$ (d). The most prominent features are labeled in the figure. The Dalitz plot for proton-antiproton annihilation into $\pi^0\eta\eta$ is dominated by the crossing vertical and horizontal bands for the isovector state $a_0(980)$ decaying into $\pi\eta$ (Fig. 7 (a)). A good description of the data requires two isoscalar states, labeled $f_0(1370)$ and $f_0(1500)$, decaying to $\eta\eta$ in the 6γ final state [55]. In fact, an earlier analysis based on a reduced $\pi^0\eta\eta$ data set provided the first evidence for the $f_0(1370)$ [54]. The observation of two necessary scalar states decaying to $\eta\eta$ is confirmed in an analysis of the $\pi^0\eta\eta \to 10\gamma$ final state, which exhibits entirely different systematics. It is now widely accepted that the $f_0(1500)$ observed by Crystal Barrel is identical to the G(1590) observed by the GAMS Collaboration [146]. In the Crystal Barrel coupled-channel analysis, the K-matrix mass and width of the $f_0(1500)$ come out to be $M \sim 1569$ MeV/c^2 and $\Gamma \sim 191$ MeV/c^2 which are quite similar to the reported $G(1590)$.

A narrow band of about constant intensity is observed in the $3\pi^0$ Dalitz plot (Fig. 7 (c)) indicating the presence of the $f_0(1500)$. Further visible features include an increased population at the edges of the Dalitz plot along the $\pi\pi$ band marked $f_2(1270)$. This indicates that one decay π^0 is preferentially emitted along the flight direction of the resonance, which is typical of a spin-2 resonance decaying with an angular distribution of $(3\cos^2\theta - 1)^2$ from the $^1S_0$ initial state. Striking are the corner blobs, which follow a $\sin^2\theta$ angular distribution and correspond to the $f_2'(1525)$ interfering constructively with the two $\pi\pi$ S-waves. The fit also requires a small contribution from the $f_2(1565)$. An important piece of information to clarify the internal structure of the $f_0(1500)$ is to study its $K\bar{K}$ decay mode. In fact, no strange decay was reported by a previous bubble-chamber experiment [145], which had very limited statistics and no partial wave analysis was performed. The Dalitz plot for the $\pi^0K_LK_L$ channel at rest from Crystal Barrel is shown in Fig. 7 (d). One K_L was missing in the analysis and the other K_L interacted hadronically in the CsI calorimeter. Events

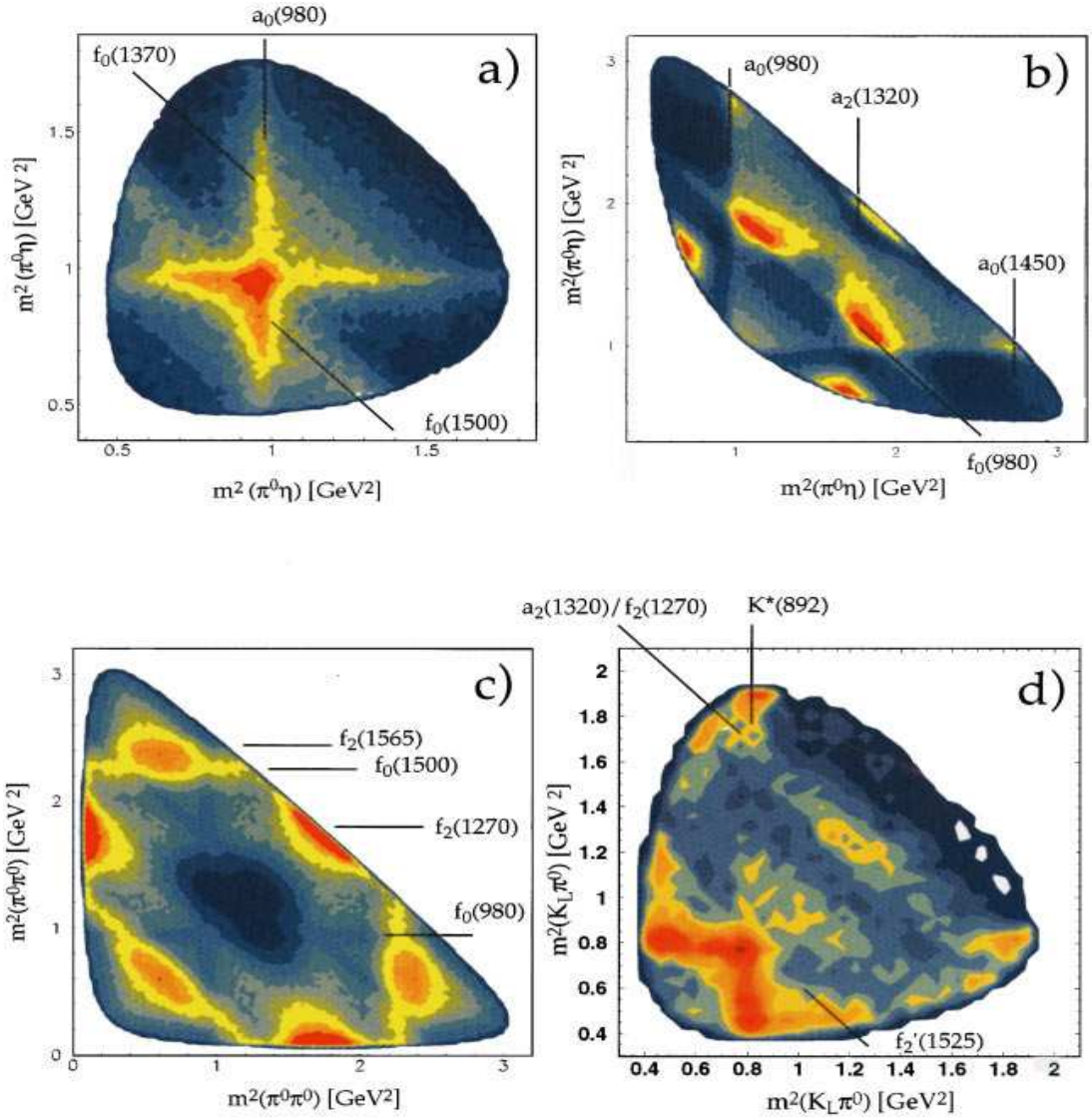

Figure 7: Dalitz plots for $p\bar{p}$ annihilation at rest from Crystal Barrel into (a) $\pi^0\eta\eta$ ($\sim 2\times10^5$ events), (b) $\pi^0\pi^0\eta$ ($\sim 2.8\times10^5$ events), (c) $3\pi^0$ ($\sim 700,000$ events), (d) $\pi^0K_LK_L$ ($\sim 37,000$ events). All events are entered more than once for symmetry reasons. Figure taken from [2].

with three clusters in the barrel were used for the analysis [59]. The contributions from the $f_0(1370)$ and $f_0(1500)$ were found to be small. The precise determination is however challenging because the isovector state $a_0(1450)$ also decays to K_LK_L, which can form both an $I = 0$ and $I = 1$ system. Contributions from $a_0(1450)$ were thus determined from the $K_LK^{\pm}\pi^{\mp}$ final state by using isospin conservation and the fact that no isoscalar S-wave contributes.

The 4π decay modes of scalar mesons were studied at rest in proton-antiproton anni-

Ratio	$f_0(1370)$	$f_0(1500)$
$\Gamma(K\bar{K})\,/\,\Gamma(\pi\pi)$	(0.37 ± 0.16) to (0.98 ± 0.42) [66]	[a] 0.186 ± 0.066 [53, 59]
		[b] 0.119 ± 0.032 [52]
$\Gamma(\eta\eta)\,/\,\Gamma(\pi\pi)$	0.020 ± 0.010 [66]	[a] 0.226 ± 0.095 [53, 55]
		[b] 0.157 ± 0.062 [52]
$\Gamma(\eta\eta')\,/\,\Gamma(\pi\pi)$		[a] 0.066 ± 0.028 [53, 56]
		[b] 0.042 ± 0.015 [52]
$\Gamma(\rho\rho)\,/\,\Gamma(4\pi)$	0.260 ± 0.070 [65]	0.130 ± 0.080 [65, 66]
$\Gamma(\sigma\sigma)\,/\,\Gamma(4\pi)$	0.510 ± 0.090 [65]	0.260 ± 0.070 [65]
$\Gamma(\rho\rho)/\Gamma(2[\pi\pi]_S)$		0.500 ± 0.340 [65]
$\Gamma(4\pi)\,/\,\Gamma_{\rm tot}$	0.800 ± 0.050 [148]	0.760 ± 0.080 [65]

Table 9: A summary of Crystal-Barrel results on the decay of scalar mesons. Branching ratios for decays into 4π are determined from $\bar{p}n$ annihilation. Results labeled [a] are from single channel analyses and [b] from a coupled channel analysis including $3\pi^0$, $2\pi^0\eta$, and $\pi^0\eta\eta$.

hilation into $5\pi^0$ [64] and $3\pi^0\pi^+\pi^-$ [63] as well as in antiproton-neutron annihilation into $4\pi^0\pi^-$ [65, 66] and $2\pi^0 2\pi^-\pi^+$ [66]. All data sets are dominated by 4π scalar isoscalar interactions and at least the two states, $f_0(1370)$ and $f_0(1500)$, are required in the analysis. It is observed that the 4π-decay width of the $f_0(1370)$ is more than 6 times larger than the sum of all observed partial decay widths to two pseudoscalar mesons. This may indicate a dominant $n\bar{n}$ component over a $s\bar{s}$ structure. The 4π-decays of the $f_0(1500)$ represent about half of its total width. The analyses also yield important couplings to $(\pi\pi)_S(\pi\pi)_S$ and to $\rho\rho$ (Table 9). It was pointed out in [149] that the $\rho\rho$ decay should dominate $2[\pi\pi]_S$ if the $f_0(1500)$ was a mixture of the ground state glueball with nearby $q\bar{q}$ states, at least in the framework of the $^3P_0$ $Q\bar{Q}$ pair creation model. In leading order of this scheme, the decay mechanism of the $f_0(1500)$ proceeds dominantly via its quarkonia components. Unfortunately, results from Crystal Barrel and WA102 entirely disagree leaving the experimental situation unsettled (Tables 9 and 11). A possible source of this disagreement may be due to the different ways of treating the decay to a pair of broad resonaces, $\rho\rho$ or $(\pi\pi)_S(\pi\pi)_S$ where the mass of the scalars are close to the "nominal" thresholds for $\rho\rho$. Additional work is required to develop a consistent way to handle this problem.

In the limit of no s-quark admixture in the proton wave function, the OZI rule does not support production of pure $s\bar{s}$ states in $p\bar{p}$ annihilation. For this reason, observation of the $f_0(1710)$ scalar state should be strongly suppressed, which is assumed to have a dominant $s\bar{s}$ component. The state was discovered by the Crystal-Ball Collaboration in radiative J/ψ decays into $\eta\eta$ [150], but the spin ($J = 0$ or 2) remained controversial for a long time. The WA102 Collaboration later determined the spin in favor of 0^{++} in central production at 450 GeV/c. Crystal Barrel data for the reactions $p\bar{p} \to \pi^0\pi^0\pi^0$, $p\bar{p} \to \pi^0\pi^0\eta$, and $p\bar{p} \to \pi^0\eta\eta$ in flight at 900 MeV/c were used to search for isoscalar 0^{++} and 2^{++} states in the 1000-

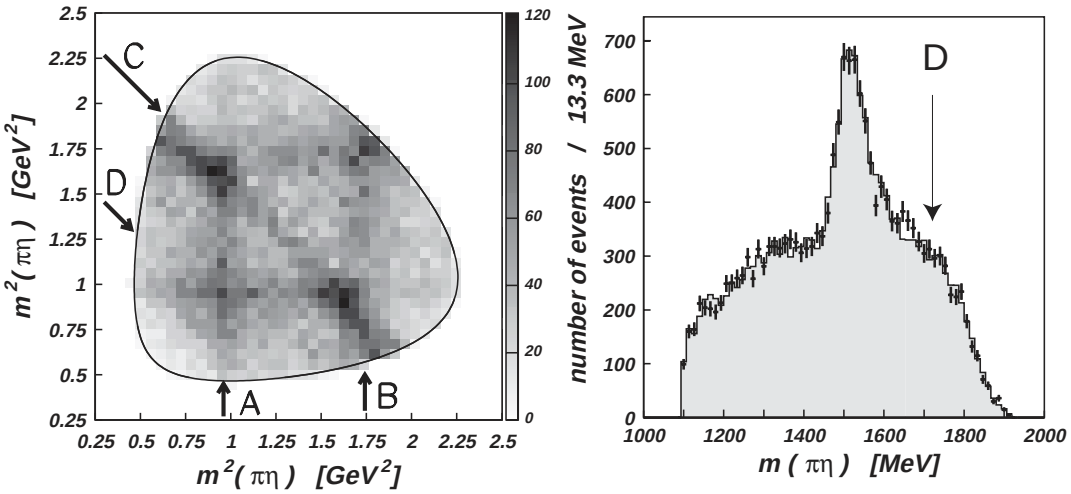

Figure 8: Dalitz plot for $p\bar{p} \to \pi^0\eta\eta$ in flight at 900 MeV/c (left). The arrows indicate $a_0(980)$ (A), $a_2(1320)$ (B), $f_0(1500)/f_2'(1525)$ (C), whereas (D) shows the expected location of the $f_0(1710)$. The $\eta\eta$ mass projection (right) is dominated by the $f_0(1500)/f_2'(1525)$ peak; the shaded area represents the fit [75]. Figure taken from [4].

2000 MeV/c^2 mass range, in particular for the $f_0(1710)$ [75]. A satisfactory signal around 1700 MeV/c^2 was neither observed for a scalar nor for a tensor state in the partial wave analyses of both the $\pi^0\pi^0\pi^0$ and $\pi^0\eta\eta$ channels. The $\pi^0\eta\eta$ Dalitz plot and the corresponding $\eta\eta$ mass projection are shown in Fig. 8. The (D) arrow indicates the expected location of the $f_0(1710)$. None of the fits using the PDG mass and width for the $f_0(1710)$ had a stable solution and the log-likelihood improvement was not significant even in the best fit. The state does not seem to be produced in proton-antiproton annihilations in flight at 900 MeV/c and upper limits at the 90 % confidence level were derived using PDG mass and width of $M = 1715$ MeV/c^2 and $\Gamma = 125$ MeV/c^2 [151]:

$$\frac{\mathcal{B}(p\bar{p} \to \pi^0 f_0(1710) \to \pi^0\pi^0\pi^0)}{\mathcal{B}(p\bar{p} \to \pi^0 f_0(1500) \to \pi^0\pi^0\pi^0)} < 0.31 \tag{25}$$

$$\frac{\mathcal{B}(p\bar{p} \to \pi^0 f_0(1710) \to \pi^0\eta\eta)}{\mathcal{B}(p\bar{p} \to \pi^0 f_0(1500) \to \pi^0\eta\eta)} < 0.25 \tag{26}$$

For this reason, the non-observation of the $f_0(1710)$ scalar state in $p\bar{p}$ reactions is consistent with a dominant $s\bar{s}$ assignment to this state assuming it has a $q\bar{q}$ structure. Though the WA102 Collaboration supported this conclusion by reporting a much stronger $K\bar{K}$ coupling of the $f_0(1710)$ than $\pi\pi$ coupling, it was not directly observed in the amplitude analysis of the reaction $K^-p \to K_SK_S\Lambda$ [152]. As mentioned before, the spin assignment was controversial for a long time and much later settled in favor of 0^{++}. In fact, the assumption in the analysis of K^--induced data was $J = 2$ and may explain the absence.

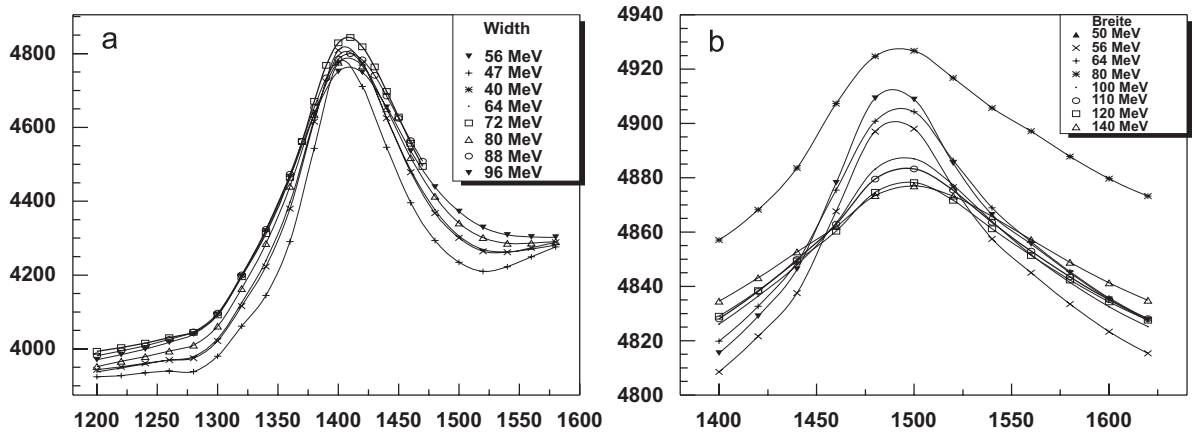

Figure 9: Analysis of the annihilation reaction $p\bar{p} \to \pi^+\pi^-\pi^+\pi^-\eta$: mass scans for $0^+\,0^\pm$ resonances assuming different widths [153]. (a) The left side shows a clear peak identified as $\eta(1405$ with the likelihood fit optimizing at $M = 1407 \pm 5,\ \Gamma = 57 \pm 9$ MeV/c^2. (b) The right side shows the search for a second pseudoscalar state indicating the presence of the $\eta(1475)$ with $M = 1490 \pm 15,\ \Gamma = 74 \pm 10$ MeV/c^2.

Results on Pseudoscalar States

In addition to the familiar η and η' mesons, Crystal Barrel observed a pseudoscalar state identified with the $\eta(1405)$ in the reactions $\bar{p}p \to \eta\pi^+\pi^-\pi^0\pi^0$ [61] and $\bar{p}p \to \eta\pi^+\pi^-\pi^+\pi^-$ [153] with masses:

$$M_{\eta(1405)} = 1409 \pm 3 \text{ MeV}/c^2 \qquad \Gamma = 86 \pm 10 \text{ MeV}/c^2$$
$$M_{\eta(1405)} = 1407 \pm 5 \text{ MeV}/c^2 \qquad \Gamma = 57 \pm 9 \text{ MeV}/c^2\,,$$

respectively. The state was observed to decay to both $\eta\pi^0\pi^0$ and $\eta\pi^+\pi^-$. Partial wave analysis indicated that the decays were via two reactions, $\eta(1405) \to a_0(980)\pi$ and $\eta(\pi\pi)_S$ with [61]:

$$\frac{B(\eta \to \eta(\pi\pi)_S)}{B(\eta \to a_0\pi)} \quad = \quad 0.78 \pm 0.12 \pm 0.10\,.$$

It was reported by the MarkIII Collaboration [154] that in radiative J/ψ decays in the 1400 mass region, there were actually two pseudoscalar states. The lighter decaying via $a_0\pi$ and the heavier via K^*K. This is not inconsistent with the Crystal Barrel observation of a single state [61] which is likely the lighter of the two MarkIII states. In fact, the later Crystal Barrel analysis [153] on the $\eta\pi^+\pi^-\pi^+\pi^-$ confirmed the lighter pseudoscalar state (see Fig. 9, left side) and also searched for an additional $0^+\,0^\pm$ resonance. A scan shown in Fig. 9 (b) provides evidence for the heavier $\eta(1475)$ state with a mass of $M = 1490 \pm 15$ MeV/c^2.

Oddly, the expected lighter pseudoscalar state, the $\eta(1295)$, was not observed by Crystal Barrel [155], even though its dominant decays are expected to be the same final states as the $\eta(1405)$. In [155], a peak at 1285 MeV/c^2 could be described best with the $f_1(1285)$.

	Reaction	Mass	Width	Reference
$\eta(1405)$	$\bar{p}p \to K^{\pm}K^0_S\pi^{\mp}\pi^+\pi^-$	1405 ± 5	50 ± 4	[47]
	$\bar{p}p \to K^+K^-\pi^+\pi^-\pi^0$	1413 ± 2	51 ± 4	[48]
$\eta(1460)$	$\bar{p}p \to K^{\pm}K^0_S\pi^{\mp}\pi^+\pi^-$	1500 ± 10	100 ± 20	[47]
	$\bar{p}p \to K^+K^-\pi^+\pi^-\pi^0$	1460 ± 12	120 ± 15	[48]

Table 10: Masses and widths of $\eta(1405)$ and $\eta(1460)$ from OBELIX.

Results from the OBELIX Experiment

The OBELIX detector system was operated at LEAR with a liquid H_2 (D_2) target, a gaseous H_2 target at room temperature and pressure, and a target at low pressures (down to 30 mbar). Among other things, the wide range of target densities provided detailed information about the influence of the atomic cascade on the annihilation process.

Results on Pseudoscalar States

The collaboration has performed several studies looking at the $\eta(1405)$ and $\eta(1460)$ in the $K\bar{K}\pi$ final states. The first study looked at $\bar{p}p \to K^{\pm}K^0_{miss}\pi^{\mp}\pi^+\pi^-$ at rest [45] where they confirmed two pseudoscalar states previously announced by the MarkIII Collaboration. The lighter decayed mainly to $K\bar{K}\pi$ (via $a_0(980)\pi$) while the heavier decayed to K^*K. Further evidence for the two states is provided in references [46] and [47] based on the analyses of the reactions $\bar{p}p \to \eta(1440)(\pi\pi) \to K^{\pm}K^0_Lp^{\mp}(\pi\pi)$ and $\bar{p}p \to K^{\pm}K^0_S\pi^{\mp}\pi^+\pi^-$, respectively. Production rates of $\eta(1440) \to K^{\pm}K^0_L\pi^{\mp}$ were determined for the first time with the same detector setup for three different hydrogen target densities: $f_{\eta(1440)}(\text{liquid } H_2) = (6.0 \pm 0.5) \cdot 10^{-4}$, $f_{\eta(1440)}(NTP) = (2.9 \pm 0.4) \cdot 10^{-4}$, and $f_{\eta(1440)}(5 \text{ mbar}) = (1.0 \pm 0.2) \cdot 10^{-4}$.

A spin-parity analysis of $p\bar{p} \to K^+K^-\pi^+\pi^-\pi^0$ at rest in a gaseous hydrogen target, which included the observation of the axial vector meson $f_1(1420)$ decaying into $K^*\bar{K}$ (produced from $^3P_1$ protonium), provides more information on the $\eta(1405)$ and $\eta(1460)$ [48]. Also hints of the $f_0(1710)$ decaying to $f_0(1370)(\pi\pi)_S$ were found in this analysis. Masses and widths of the two pseudoscalar states from OBELIX are sumarized in Table 10.

OBELIX also observed an isovector scalar state with a mass of about 1.3 GeV/c^2 in its $K\bar{K}$ decay mode [49,50]; the state is relatively narrow, with a 80 MeV width. In formation, the collaboration reported on the 3π decays of the $\pi(1300)$ as well as suggested a 3π decay of the $\pi_1(1400)$ from $p\bar{p} \to 2\pi^+2\pi^-$ [44] at rest and in flight.

Results on Scalar States

The OBELIX Collaboration recently studied the $\pi^+\pi^-\pi^0$, $K^+K^-\pi^0$, and $K^{\pm}K^0\pi^{\mp}$ final states in proton-antiproton annihilation at rest at three different hydrogen target densities in the framework of a coupled-channel analysis together with $\pi\pi$, πK, and $K\bar{K}$ scattering data [50]. One of the main goals of the analysis was to determine branching ratios as well as $\pi\pi$ and $K\bar{K}$ partial widths of all the involved ($J^P = 0^+,\ 1^-,\ 2^+$) resonances. Dalitz-plot

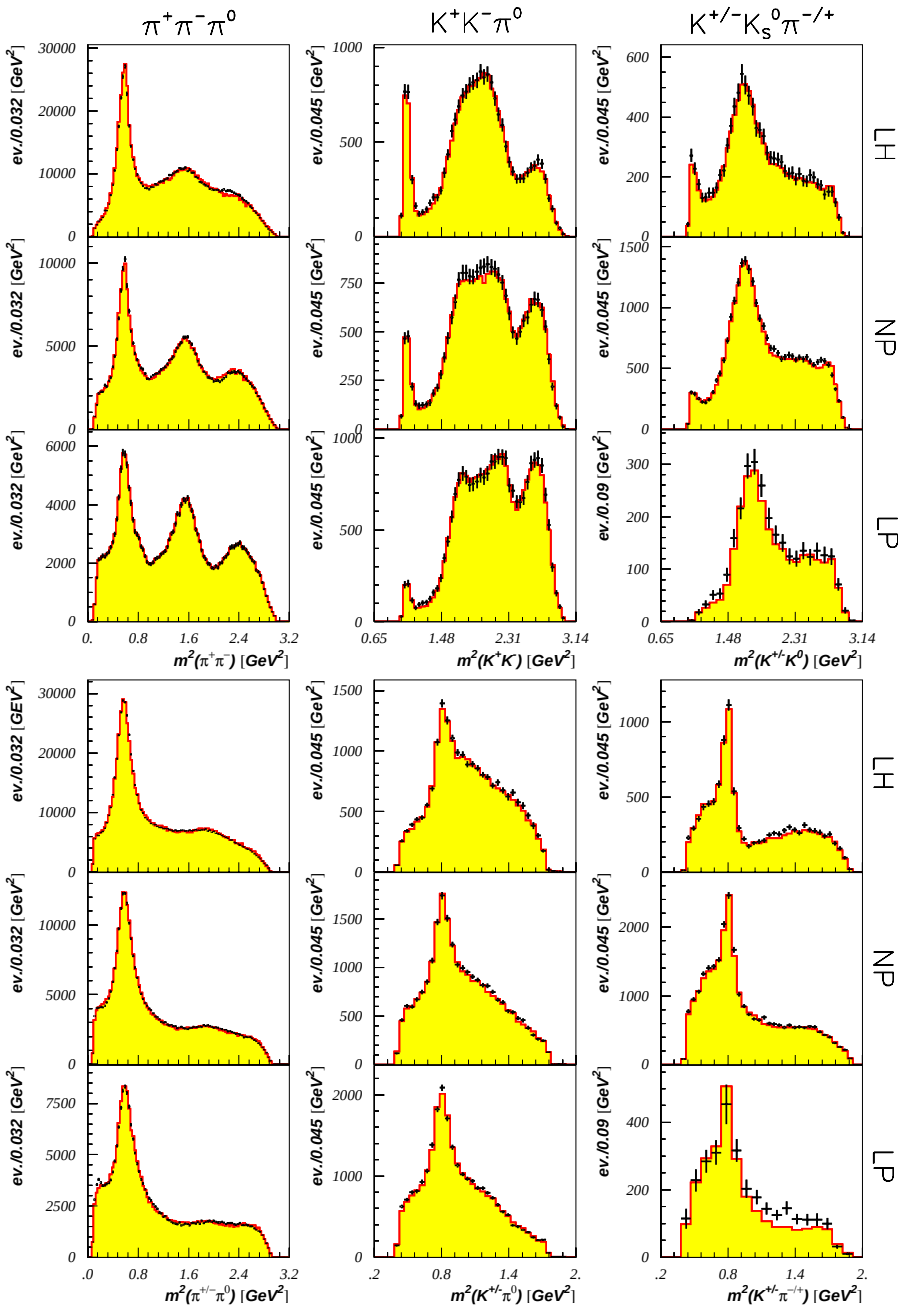

Figure 10: Theoretical (shaded histograms) and experimental (background subtracted) Dalitz-plot projections from the OBELIX experiment of the three annihilation reactions $p\bar{p} \to \pi^+\pi^-\pi^0$, $p\bar{p} \to K^+K^-\pi^0$, and $p\bar{p} \to K^{\pm}K^0_S\pi^{\mp}$ in liquid (LH) hydrogen, H_2 gas at normal pressure and temperature (NP), and low pressure (LP) hydrogen gas. Theoretical and experimental errors are summed. Figure is taken from [50].

projections of the three annihilation reaction are shown in Fig. 10. The scattering data, in particular the $\theta_0(\pi\pi \to \pi\pi)$ phase shift, clearly require contributions from the $f_0(980)$ pole. The authors further report on two additional poles required by annihilation data, a broad $f_0(1370)$ and a relatively narrow $f_0(1500)$. The introduction of a fourth scalar state improves the data and splits the initially broad $f_0(1370)$ into a broad $f_0(400-1200)$ and a relatively narrow $f_0(1370)$. The $f_0(1710)$ does not seem to be needed by the data. In addition, a good description requires the $f_2(1270)$ and $f_2'(1525)$ tensor states. The $f_2(1565)$ pole is needed for the $\pi^+\pi^-\pi^0$ and $K^+K^-\pi^0$ data at low pressure and in hydrogen gas at normal temperature and pressure. The following $\Gamma_{K\bar{K}}/\Gamma_{\pi\pi}$ ratios of branching fractions for $f_0(1370)$, $f_0(1500)$, and $f_2(1270)$ were determined:

$$\frac{\mathcal{B}(p\bar{p} \to f_0(1370)\pi^0,\ f_0 \to K\bar{K})}{\mathcal{B}(p\bar{p} \to f_0(1370)\pi^0,\ f_0 \to \pi\pi)} = \begin{cases} 1.000 \pm 0.200 & {}^1S_0 \\ 0.940 \pm 0.200 & {}^3P_1 \end{cases} \tag{27}$$

$$\frac{\mathcal{B}(p\bar{p} \to f_0(1500)\pi^0,\ f_0 \to K\bar{K})}{\mathcal{B}(p\bar{p} \to f_0(1500)\pi^0,\ f_0 \to \pi\pi)} = \begin{cases} 0.240 \pm 0.040 & {}^1S_0 \\ 0.300 \pm 0.040 & {}^3P_1 \end{cases} \tag{28}$$

$$\frac{\mathcal{B}(p\bar{p} \to f_2(1270)\pi^0,\ f_2 \to K\bar{K})}{\mathcal{B}(p\bar{p} \to f_2(1270)\pi^0,\ f_2 \to \pi\pi)} = \begin{cases} 0.043 \pm 0.010 & {}^1S_0 \\ 0.045 \pm 0.010 & {}^3P_1 \\ 0.048 \pm 0.010 & {}^3P_2 \end{cases} \tag{29}$$

The values for $f_0(1500)$ from OBELIX obtained in a coupled-channel framework are somewhat greater than earlier coupled-channel results from Crystal-Barrel (Table 9) and agree well with results from WA102 [112] (Table 11). The $f_2(1270)$ ratios agree with the PDG values within the experimental errors.

Results from Central Production: The WA102 Experiment

The WA102 experiment looked at 450 GeV/c protons incident on a proton target to study the reaction $pp \to p_{(f)ast}\, X\, p_{(s)low}$ – so-called *central production*. Such reactions are believed to have a significant contribution from double-pomeron exchange – a reaction that is supposed to be glue-rich. Relevant to the search for scalar glueballs, the collaboration carried out partial wave analysis on a large number of final states. $pp \to pp4\pi$ [105–108], $pp \to pp\pi^0\pi^0$ [109], $pp \to pp\pi^+\pi^-$ [105, 110, 112], $pp \to ppK^+K^-$ [111, 112], $pp \to ppK^0_SK^0_S$ [111], $pp \to pp\eta\eta$ [114], $pp \to pp\eta\eta'$ [113], $pp \to pp\eta'\eta'$ [113], $pp \to pp\eta\eta$ [114], $pp \to pp\phi\phi$ [115], $pp \to pp\omega\omega$ [116], $pp \to pp\phi\omega$ [117] and $pp \to ppK^*(892)\bar{K}^*(892)$ [117].

In addition, a number of studies that bear on the search from pseudoscalar states were also performed: $pp \to pp\pi^0\pi^0\pi^0$ [118], $pp \to pp\pi^+\pi^-\pi^0$ [119], $pp \to pp\eta\pi^0$ [120], $pp \to pp\eta\pi^+\pi^-$ [121], and $pp \to ppK\bar{K}\pi$ [122].

Results of measured decay branching ratios into two pseudoscalar mesons are listed in Table 11 [105–111, 113, 122]. Further selected PWA results from the WA102 experiment on central production are presented in Fig. 11 [5, 112–114]. The K^+K^- S-wave from a

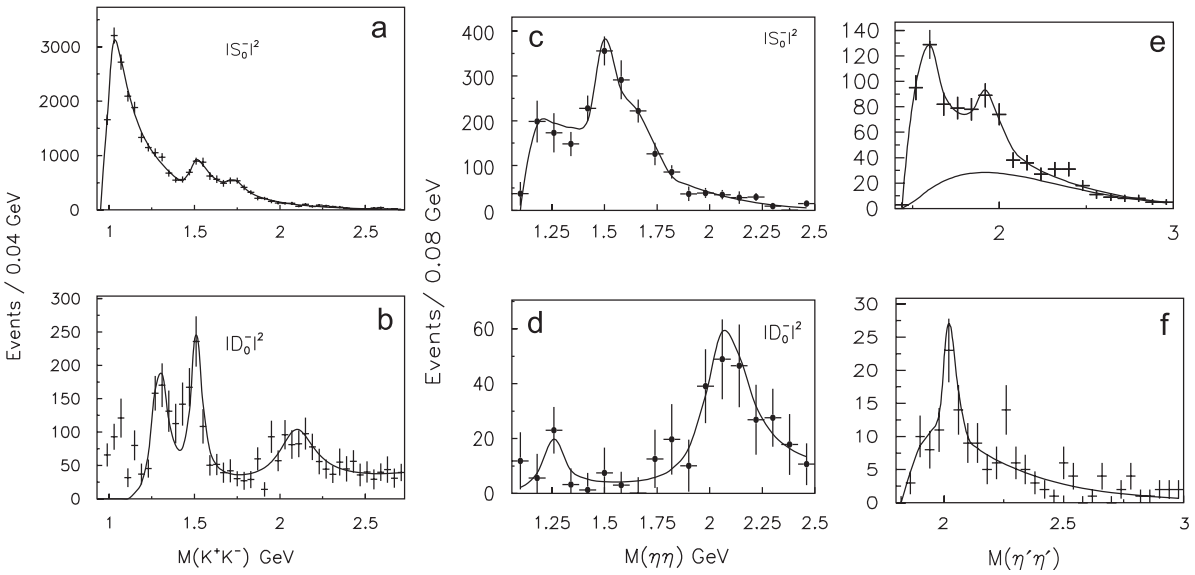

Figure 11: K^+K^- S- (a) and D-wave (b) from a coupled-channel analysis of WA102 $\pi^+\pi^-$ and K^+K^- data [112]. The T-matrix formalism was used for overlapping resonances to account for unitarity. Signals for $f_0(1500)$ and $f_0(1710)$ are clearly observed. Mass distributions for $\eta\eta$ S- and D-wave are shown in (c) and (d). The right panel shows $\eta\eta'$ (e) and $\eta'\eta'$ (f) mass distributions.

coupled-channel analysis of $\pi^+\pi^-$ and K^+K^- data is shown in (a). The long tail beyond the dominant threshold enhancement for the $f_0(980)$ includes signals for the three scalar resonances of Table 11. Only the two higher-mass states are observed as peaks [112]. The corresponding K^+K^- D-wave (b) shows resonant peaks for the two established tensor mesons $f_2(1270)$ and $f_2'(1525)$. A structure at 2.15 GeV/c^2 is also observed in the mass distribution. The pole positions for the $f_0(1370)$ and $f_0(1500)$ are in excellent agreement with results from the Crystal-Barrel experiment. Fig. 11 (c) and (d) present the $\eta\eta$ S- and D-wave [114]. The $f_0(1500)$ is clearly seen in the S-wave $\eta\eta$ mass distribution (c). In addition to a weak $f_2(1270)$ signal, the resonant structure at 2.15 GeV/c^2 is also observed in the $\eta\eta$ D-wave (d).

Scalar	$\pi\pi/K\bar{K}$	$\pi\pi/\eta\eta$	$\eta\eta/K\bar{K}$	$\rho\rho/2[\pi\pi]_S$	$\rho\rho/4\pi$	$\sigma\sigma/4\pi$
$f_0(1370)$	2.17 ± 0.90		0.35 ± 0.21		~ 0.9	~ 0
$f_0(1500)$	3.13 ± 0.68	5.5 ± 0.84		2.6 ± 0.4 [1]	0.74 ± 0.03	0.26 ± 0.03
				3.3 ± 0.5 [2]		
$f_0(1710)$	0.20 ± 0.03		0.48 ± 0.14			

Table 11: A summary of WA102 results on the decay of scalar mesons [105–111, 113, 122]. The result for the decay of the $f_0(1500)$ into 4π is derived [1] from $2\pi^+2\pi^-$ and [2] from $\pi^+\pi^-2\pi^0$.

J^{PC}	Res.	σ [nb]	$dP_T \leq 0.2$ GeV	$0.2 \leq dP_T \leq 0.5$ GeV	$dP_T \geq 0.5$ GeV
0^{-+}	π^0	$22\,011 \pm 3\,267$	12 ± 2	45 ± 2	43 ± 2
	η	$3\,859 \pm 368$	6 ± 2	34 ± 2	60 ± 3
	η'	$1\,717 \pm 184$	3 ± 2	32 ± 2	64 ± 3
0^{++}	$a_0(980)$	638 ± 60	25 ± 4	33 ± 5	42 ± 6
	$f_0(980)$	$5\,711 \pm 450$	23 ± 2	51 ± 3	26 ± 3
	$f_0(1370)$	$1\,753 \pm 580$	18 ± 4	32 ± 2	50 ± 3
	$f_0(1500)$	$2\,914 \pm 301$	24 ± 2	54 ± 3	22 ± 4
	$f_0(1710)$	245 ± 65	26 ± 2	46 ± 2	28 ± 2
	$f_0(2000)$	$3\,139 \pm 480$	12 ± 2	38 ± 3	50 ± 4
1^{++}	$a_1(1260)$	$10\,011 \pm 900$	13 ± 3	51 ± 4	36 ± 3
	$f_1(1285)$	$6\,857 \pm 1\,306$	3 ± 1	35 ± 2	61 ± 4
	$f_1(1420)$	$1\,080 \pm 385$	2 ± 2	38 ± 2	60 ± 4
2^{++}	$a_2(1320)$	$1\,684 \pm 134$	10 ± 2	38 ± 5	52 ± 6
	$f_2(1270)$	$3\,275 \pm 422$	8 ± 1	29 ± 1	63 ± 2
	$f_2'(1520)$	68 ± 9	4 ± 3	36 ± 3	60 ± 4
	$f_2(1910)$	528 ± 40	20 ± 4	62 ± 7	18 ± 4
	$f_2(1950)$	$2\,788 \pm 175$	27 ± 2	46 ± 5	27 ± 2
	$f_2(2150)$	121 ± 12	3 ± 3	53 ± 4	44 ± 3

Table 12: A summary of WA102 results on resonance production at $\sqrt{s} = 29.1$ GeV [156]. The quoted errors are statistical and systematic errors summed in quadrature. Numbers given for resonance production as a function of dP_T are percentages of the total contribution.

The $f_0(1500)$ was also observed in studies of the $\eta\eta'$ decay mode [113], shown in Fig. 11 (e), and in the 4π final state [107]. Beyond the $\eta(548)$ and $\eta\prime(958)$, no pseudoscalar states were reported in central production by WA102.

The small $\Gamma(\pi\pi)/\Gamma(K\bar{K})$ value for the $f_0(1710)$ in Table 11 clearly indicates that this resonance must have a large $s\bar{s}$ component. By contrast, the same ratio is much greater than one for the $f_0(1500)$. If interpreted as $q\bar{q}$ state, the $f_0(1500)$ cannot have a large $s\bar{s}$ component since pure $s\bar{s}$ mesons do not decay to pions. Moreover, we recall that an enhancement of gluonic states is expected in Pomeron-Pomeron fusion (Close-Kirk glueball filter) [101]. Though the $f_0(1710)$ couples more strongly to $K\bar{K}$, the K^+K^- S-wave signal for the $f_0(1500)$ shown in Fig. 11 (a) is larger in agreement with predictions of the glueball filter. As mentioned earlier, there are significant discrepancies with Crystal Barrel results on the decay of these scalars to $\rho\rho$ and $/2[\pi\pi]_S$ final states. This may be due to how the opening of broad thresholds is treated in the individual analyses.

Table 12 shows further results on resonance production from WA102. The cross section

is given at 450 GeV/c for the reaction

$$p\,p \to p_{\,f}\,X\,p_s\,,$$

and the dependence of the production of X on the parameter dP_T, denoting the difference in transverse momentum between the particles exchanged from the fast and slow vertices. Production of $X = \rho^0$ with $I = 1$ cannot proceed via double-Pomeron exchange (DPE). The $\pi^+\pi^-$ mass spectra from the WA76 Collaboration at $\sqrt{s} = 12.7$ GeV and $\sqrt{s} = 23.8$ GeV [102] show a reduction of the ρ^0 yield at higher center-of-mass energies. The Collaboration reports a cross section ratio of 0.44 ± 0.07 indicating that DPE becomes more important with increasing energy.

Table 12 also shows that production of isovector states is strong, e.g. the $a_1(1260)$, which requires Reggeon exchange.

Scalar resonances are consistent with Pomeron-Pomeron fusion. Production of $a_0(980)$ is suppressed by almost a factor of 10 with respect to the $f_0(980)$. The $a_0(1450)$ is not even seen, whereas a large $f_0(1500)$ yield is observed. Interestingly, production of the $f_0(1710)$ is very weak.

Though, scalar meson production indicates dominant (glue-rich) Pomeron-Pomeron exchange, the situation for other resonances is less clear. Elaborate more on validity of double-pomeron exchange

Light Mesons from e^+e^- Experiments: The BES Experiment

Several reactions have been studied in the BES experiment. Partial wave analysis has been performed on several radiative decays of the J/ψ and are reported for the following reactions: $J/\psi \to \gamma\pi^+\pi^-\pi^+\pi^-$ [80], $J/\psi \to \gamma\pi^+\pi^-$ [81], $J/\psi \to \gamma\pi^0\pi^0$ [81], $J/\psi \to \gamma K^+K^-$ [82], $J/\psi \to \gamma K^0_S K^0_S$ [82], and $J/\psi \to \gamma\phi\omega$ [83]. In addition to the radiative decays, BES has also examined decays to associated vector meson decays. Here, analysis has been performed on the reactions: $J/\psi \to \omega\pi^+\pi^-$ [84], $J/\psi \to \phi\pi^+\pi^-$ [85], $J/\psi \to \omega K^+K^-$ [86], and $J/\psi \to \phi K^+K^-$ [85].

Results on Scalar States

BES II results on J/ψ radiative decays to $\pi^+\pi^-$ and $\pi^0\pi^0$ are shown in Fig. 12. A sample of 58 M J/ψ events was used for the PWA [81]. Similar structures are visible in both mass spectra. Three clear peaks are observed in both distributions in the 1.0 to 2.3 GeV/c^2 mass range: a strong $f_2(1270)$ signal exhibiting a shoulder on the high-mass side, an enhancement at $\sim$ 1.7 GeV/c^2 associated with the $f_0(1710)$, and a peak at $\sim$ 2.1 GeV/c^2. The shaded histogram in Fig. 12 (a) corresponds to dominant background from $J/\psi \to \pi^+\pi^-\pi^0$. The estimated background in (b) stems from various reactions; PDG branching ratios have been used in the studies. Three scalar mesons are observed with approximately consistent results from both fits. The lowest 0^{++} state is consistent with the $f_0(1500)$ and associated with the shoulder in Fig. 12. The collaboration reports that spin 0 is strongly preferred over spin 2 in the analysis. Though not favored in the PWA, the presence of the $f_0(1370)$ is not excluded.

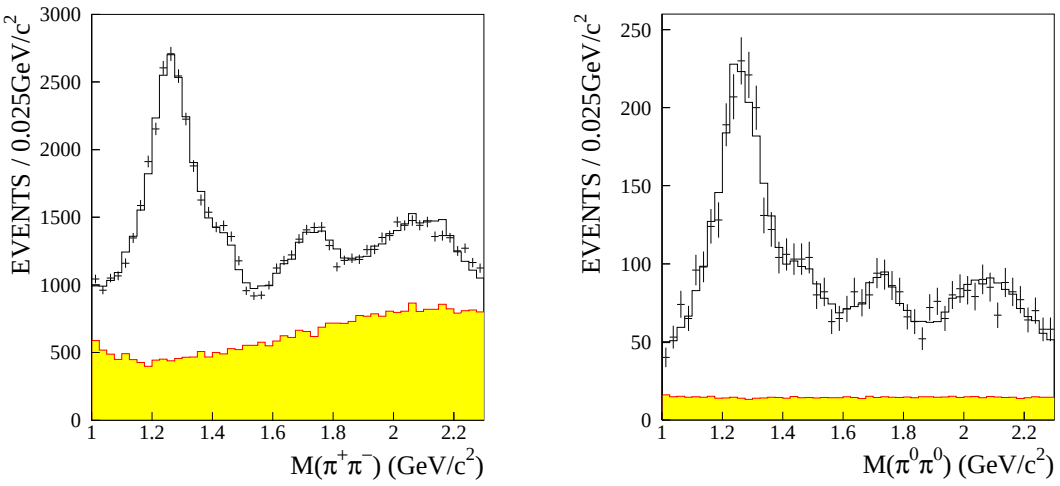

Figure 12: The $\pi^+\pi^-$ invariant mass distribution (a) and the $\pi^0\pi^0$ mass distribution (b) from the reaction $J/\psi \to \gamma\pi\pi$ from BES [81]. The crosses are data, the full histogram shows the maximum likelihood fit, and the shaded area corresponds to the background.

The fitted masses and widths from $J/\psi \to \gamma\pi^+\pi^-$ for the two lowest-mass states are given by:

$$M_{f_0(1500)} = 1466 \pm 6 \pm 20 \text{ MeV}/c^2 \qquad \Gamma = 108^{+14}_{-11} \pm 25 \text{ MeV}/c^2$$
$$M_{f_0(1710)} = 1765^{+4}_{-3} \pm 13 \text{ MeV}/c^2 \qquad \Gamma = 145 \pm 8 \pm 69 \text{ MeV}/c^2 \,,$$

whereas PDG values for the $f_0(2020)$ are used for the structure at $\sim$ 2.1 GeV/c^2.

The two established scalar mesons, $f_0(1500)$ and $f_0(1710)$, are also significantly produced in $J/\psi \to 2\pi^+ 2\pi^-$ with masses of $M_{f_0(1500)} = 1505^{+15}_{-20}$ and $M_{f_0(1710)} = 1740^{+30}_{-25}$, respectively [80]. In addition, the likelihood fit requires a tensor state, $f_2(1950)$, around 2 GeV/c^2 confirming earlier WA91 and WA102 results [106, 158]. Branching fractions determined from $J/\psi \to 2\pi^+ 2\pi^-$ are listed in Table 13. The $f_0(1710)$ scalar state also dominates the reaction $J/\psi \to \gamma K\bar{K}$. Evidence for the $f_0(1500) \to K\bar{K}$ is however insignificant, but included in the partial wave analysis interfering with the $f_0(1710)$. For a description of the 1500 MeV/c^2 mass range, the $f_2'(1525)$ tensor state is required in the analysis [82].

In section 4.1, we have discussed the *flavor-tagging* approach to study the flavor content of mesons in J/ψ decays. Due to the OZI rule, $J/\psi \to \omega X$ couples to the $n\bar{n}$ component of X, while $J/\psi \to \phi X$ couples to $s\bar{s}$. Fig. 13 shows invariant mass distributions of pseudoscalar meson pairs recoiling against ω, ϕ or γ [157]. The K^+K^- mass distribution from ωK^+K^- (b) shows a clear scalar peak at 1710 MeV/c^2 which is not observed in the corresponding spectrum recoiling against the ϕ meson (d). By contrast, the $\pi^+\pi^-$ mass distribution from $\phi\pi^+\pi^-$ (c) indicates an enhancement at $\sim$ 1790 MeV/c^2, which is absent in ϕK^+K^- (d). This observation is puzzling and does not seem to be compatible with a single $f_0(1710)$ state,

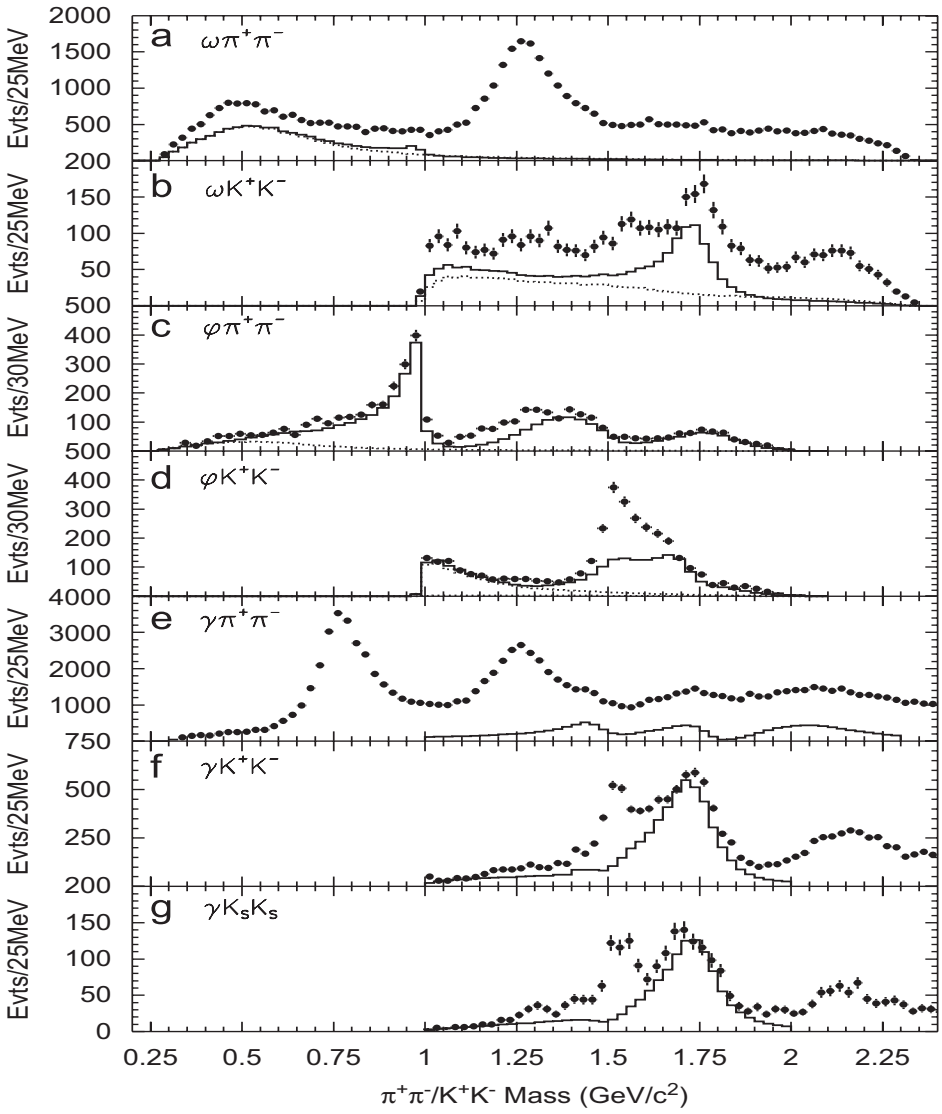

Figure 13: Invariant mass distributions of pseudoscalar meson pairs recoiling against ω, ϕ or γ in J/ψ decays measured at BES II. The dots with error bars are data, the solid histograms are the scalar contributions from PWA, and the dashed lines in (a) through (c) are contributions of $\sigma(485)$ from the fits, while the dashed line in (d) is the $f_0(980)$. Notice that not the full mass spectra are analyzed in (e), (f), and (g). The figure is taken from [157].

which is known to decay dominantly to $K\bar{K}$. The BES collaboration suggested two distinct scalar states around 1.75 GeV/c^2: the known $f_0(1710)$ with ($M \sim 1740$ MeV/c^2, $\Gamma \sim 150$ MeV/c^2) decaying strongly to $K\bar{K}$ and a broad $f_0(1790)$ with ($M \sim 1790$ MeV/c^2, $\Gamma \sim 270$ MeV/c^2) which couples more strongly to $\pi\pi$ [85]. This new state is not confirmed by any other experiment and not listed in the 2008 edition of the "Review of Particle Physics" by the Particle Data Group [6]. The BES collaboration emphasizes that the $\phi f_0(1790)$ signal

Scalar	$\pi^+\pi^-$ [81]	$\pi^\circ\pi^\circ$ [81]	$K\bar{K}$ [82]	$\pi^+\pi^-\pi^+\pi^-$ [80]
$f_0(1500)$	0.67 ± 0.30	0.34 ± 0.15		3.1 ± 1.12
$f_0(1710)$	2.64 ± 0.75	1.33 ± 0.88	$9.62 \pm 0.29_{\,\mathrm{stat}}$	3.1 ± 1.12
$f_0(2100)$				5.1 ± 1.82
$f_2(1270)$	9.14 ± 1.48	4.00 ± 0.59		1.8 ± 0.63
$f_2'(1525)$			$3.42 \pm 0.15_{\,\mathrm{stat}}$	
$f_2(1565)$				3.2 ± 1.12
$f_2(1950)$				5.5 ± 1.92

Table 13: BES results on radiative J/ψ decays. The rates are shown for $J/\psi \to \gamma f_0$ with the subsequent decay of the f_0 to the listed final state. All rates are multiplied by 10^{-4}. The quoted errors are statistical and systematic errors summed in quadrature.

is very close to edge of the available phase space, where the reconstruction efficiency of the ϕ decreases significantly as the momentum of the ϕ decreases. Tails of broad higher-mass states could also interfere with the $f_0(1710)$ generating a structure near the end of the phase space [157]. If both states really exist, it remains a mystery why the $f_0(1710)$ mainly $s\bar{s}$-state is produced recoiling against an ω, and the new $f_0(1790)$ mainly $n\bar{n}$-state is observed recoiling against a ϕ. In fact, it's worth noting that many strong signals due to non-strange states are seen in the $\phi\pi\pi$ data from BES: $f_2(1270)$, $f_0(1370)$, $f_0(1500)$, and $f_0(1790)$. The collaboration makes a strong argument for the existence of a $f_0(1370)$ resonance, which has been doubted previously by several authors. In the analysis, the state interferes with the $f_0(1500)$ and $f_2(1270)$ making it more noticeable, but a determination of its mass and width is challenging for the same reason.

A recent BES observation has increased the scalar puzzle even more. The group observes a state at $M \sim 1812$ MeV/c^2 and $\Gamma \sim 105$ MeV/c^2 in the doubly OZI suppressed process $J/\psi \to \gamma\omega\phi$ [83]. The PWA favors a 0^+ scalar assignment. The state is listed as $X(1835)$ by the PDG, but has not been seen by another experiment. The production ratio should be suppressed by at least an order of magnitude. A value of $\mathcal{B}(J/\psi \to \gamma X) \cdot \mathcal{B}(X \to \omega\phi) = (2.61 \pm 0.27\ (\mathrm{stat}) \pm 0.65\ (\mathrm{syst})) \times 10^{-4}$ is reported. Decay rates for the discussed mesons are listed in Table 13. Moreover, BES reports the ratios of branching fractions into $\pi\pi$ and $K\bar{K}$ for the $f_0(1370)$ [85] and $f_0(1710)$ [86]:

$$\frac{\mathcal{B}(f_0(1370) \to K\bar{K})}{\mathcal{B}(f_0(1370) \to \pi\pi)} \;=\; 0.08 \,\pm\, 0.08 \tag{30}$$

$$\frac{\mathcal{B}(f_0(1710) \to \pi\pi)}{\mathcal{B}(f_0(1710) \to K\bar{K})} \;<\; 0.11\ (@\,95\,\%\ \mathrm{C.L.}) \tag{31}$$

Results on Pseudoscalar and Tensor States

Evidence for the 2^{++} and 0^{-+} glueballs are weak. The BES Collaboration observed signals in radiative J/ψ decays for the $f_J(2220)$, also known as $\xi(2230)$, in a sample of more than

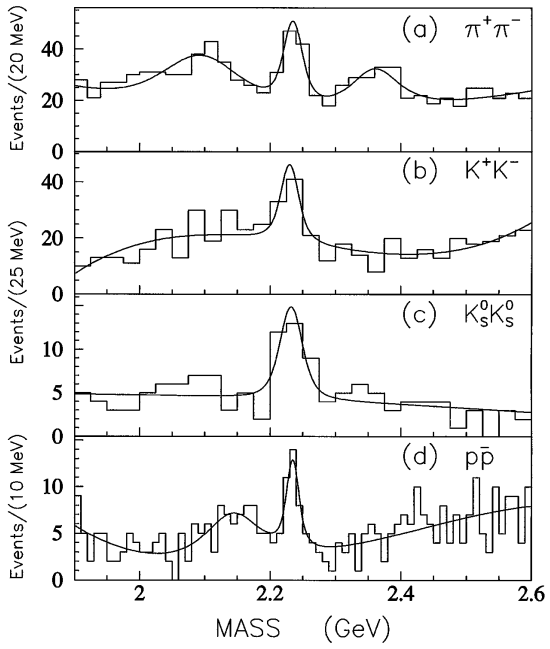

Figure 14: Fitted invariant mass spectra of a) $\pi^+\pi^-$, b) K^+K^-, c) $K^0_SK^0_S$, and d) $p\bar{p}$ from BES suggesting the existence of the $f_J(2220)$. An unbinned maximum-likelihood method was applied using a smooth background plus one or several Breit-Wigners resonances convoluted with Gaussian resolution functions [159].

5×10^6 J/ψ decays in final states including $K\bar{K}$, $\pi^+\pi^-$, and $p\bar{p}$ [159,160]. Fig. 14 shows the fitted invariant mass spectra. However, this signal has not yet been confirmed by the larger data sets from BES II. Visual inspection of the newer invariant mass spectra seem to show no evicence for this state. Given that these data can help resolve this puzzle, it is hoped that BESII or BESIII will be able to say more on the issue. The signal was first observed by the MARK-III Collaboration and published in 1985 in the reactions $J/\psi \to \gamma K^0_S K^0_S$ and $J/\psi \to \gamma K^+K^-$ based on a sample of 5.8×10^6 J/ψ decays [161]. However, limits on the product branching fraction, $\mathcal{B}(J/\psi \to \gamma f_J(2220)) \cdot \mathcal{B}(f_J(2220) \to K^+K^-)$, reported by the DM2 Collaboration were in disagreement with the MARK-III findings [162]. The first indication for a spin-2 particle came from the GAMS Collaboration in 1986. They observed a signal at 2220 MeV/c^2 decaying to $\eta\eta'$ in the $\eta\eta' n$ final state from pion-induced reaction on the proton [163]. This finding was in agreement with the original result from radiative J/ψ decays. Many other experiments carefully searched for the $f_J(2220)$ in proton-antiproton annihilation in-flight, but no evidence was found of this state [164–169]. A high-statistics search in 2000 by the Crystal-Barrel Collaboration also showed no narrow state [170]. If the state really exists, it has a very large branching fraction in radiative J/ψ decays. Future experimental efforts with the BES-III detector may shed some light on the possible existence of this state.

BES also studied $J/\psi \to \gamma\gamma V(\rho, \phi)$ decays with the BES-II detector. A resonance around 1420 MeV/c^2 was observed in the $\gamma\rho$ mass spectrum. The properties of this state were determined to be $M = 1424 \pm 10_{\rm stat} \pm 11_{\rm sys}$ MeV/c^2 and $\Gamma = 101.0 \pm 8.8 \pm 8.8$ MeV/c^2. A branching ratio of $\mathcal{B}(J/\psi \to \gamma X(1424) \to \gamma\gamma\rho) = (1.07 \pm 0.17 \pm 0.11) \times 10^{-4}$ was obtained. A corresponding search for the state decaying into $\gamma\phi$ only resulted in a 95 % CL upper limit of $\mathcal{B}(J/\psi \to \gamma X(1424) \to \gamma\gamma\phi) < 0.82 \times 10^{-4}$. The authors do not draw a definite conclusion

Scalar	Υ(1S)$\rightarrow \gamma$ + meson	$\pi^+\pi^-$	$\pi^\circ\pi^\circ$	K^+K^-	$\pi^+\pi^-\pi^+\pi^-$	$\eta\eta$
$f_0(980)$		< 3				
$f_0(1500)$	< 1.5	< 1.5				< 0.3
$f_0(1710)$			< 0.14	< 0.7		< 0.18
$f_2(1270)$	10.2 ± 0.8 [77]		3.0 ± 0.5			
$f_2'(1525)$	$3.7^{+0.9}_{-0.7}$ [77]					

Table 14: CLEO results on radiative Υ(1S) decays. The rates for the scalar mesons are upper-limit branching fractions at the 90 % confidence level for $\Upsilon \rightarrow \gamma f_0$ with the subsequent decay of the f_0 to the listed final state. All rates are multiplied by 10^{-5}.

and the situation is puzzling. If the $X(1424)$ is identified with the $\eta(1405)$ and considered a glueball candidate, it should decay into $J/\psi \rightarrow \gamma(\gamma\phi)$.

Light Mesons from the CLEO Experiment

Radiative $\Upsilon(1S)$ decays also provide a glue-rich environment for producing exotic states. The CLEO Collaboration has reported on results from $\Upsilon(1S)$ decays to pairs of pseudoscalar mesons [77, 78]. Considering the fact that the quark-photon coupling is proportional to the electric charge and assuming that the quark propagator is roughly proportional to $1/m$ for low-momentum quarks, radiative decays from Υ(1S) should be suppressed by a factor of

$$(q_b/q_c)^2 \cdot (m_c/m_b)^2 \cdot \Gamma_\Upsilon/\Gamma_\psi \approx 0.04 \tag{32}$$

relative to the corresponding J/ψ decay. Table 14 summarizes the results. In particular, the decay rates of $f_0(1500)$ and $f_0(1710)$ to $\pi^\circ\pi^\circ$ are much smaller – by more than an order of magnitude – than predicted based on the scalar-glueball mixing matrix in [35].

The two listed tensor states dominate the di-gluon spectrum in $\Upsilon(1S)$ decays and fair agreement with the naive scaling argument is observed (to the same order of magnitude) for the suppression factor of these states relative to J/ψ decays.

The three-body decays of D-mesons can provide an excellent test of the microscopic structure of scalar mesons. The final state consists of only u and d quarks and antiquarks providing enough energy to cover most of the range of interest to light quark binding. The initial state is relatively simple with little impact on the final state. CLEO published the results of Dalitz-plot analyses for $D^0 \rightarrow \pi^+\pi^-\pi^0$ [88], $D^+ \rightarrow \pi^+\pi^+\pi^-$ [89], $D^0 \rightarrow K^-\pi^+\pi^0$ [91], $D^0 \rightarrow K^0_S\pi^+\pi^-$ [92], $D^0 \rightarrow K^0_S\eta\pi^0$ [93], $D^\pm \rightarrow K^+K^-\pi^\pm$ [94], and $D^0 \rightarrow K^+K^-\pi^0$ [95].

The weak decays of D mesons are expected to be dominated by resonant two-body decays, e.g. [171]. In $D^0 \rightarrow \pi^+\pi^-\pi^0$ decays, there is no evidence observed for any $\pi\pi$ S-wave contribution, only the 3 $\rho(770)\pi$ modes are seen. The $f_0(980)$ meson is observed to be highly-suppressed in the reaction $D^0 \rightarrow f_0(980)\pi^0$ [88]. Though the suppression itself is in good agreement with predictions inserting rescattering effects and considering the $f_0(980)$ as $s\bar{s}$ + a light $q\bar{q}$ pair [171], the calculated ratio $\mathcal{B}(D^+ \rightarrow f_0(980)\pi^+)/\mathcal{B}(D^0 \rightarrow f_0(980)\pi^0)$ of

46.7 is almost an order of magnitude smaller than the experimentally determined lower limit of $> 340\,@\,95\,\%$ confidence level. The Dalitz plot study of $D^+ \to \pi^+\pi^+\pi^-$ [89] finds small contributions from $f_0(1370)$ and $f_0(1500)$ with $2.6 \pm 1.9\,\%$ and $3.4 \pm 1.3\,\%$, respectively. The existence of $f_0(1370)$ is not questioned in the analysis. However, the mass introduced as a free fit parameter is somewhat low: $M = 1260$ MeV/c^2.

The most precise results on $D^0 \to K^0_S\pi^+\pi^-$ come from the CLEO Collaboration. They find a much smaller nonresonant contribution to this reaction than did earlier experiments and attribute the source of this nonresonant component to the broad scalar resonances $K^*_0(1430)$ and $f_0(1370)$ [92]. Some confusion arises from the small $f_0(980)$ contribution to this reaction, which is inconsistent with a large contribution of $f_0(980)$ in $D^0 \to K^0_S K^+K^-$ reported by the ARGUS and BaBar Collaborations. A solution is discussed in a mini-reviw on charm Dalitz plot analyses in the 2008 edition of the PDG [6]. The explanation is a large $a_0(980) \to K^+K^-$ contribution to the reaction $D^0 \to K^0_S K^+K^-$, which is also observed by CLEO in the reaction $D^0 \to K^0_S\eta\pi^0$ [93].

Recently, the existence of the two scalar resonances $f_0(1370)$ and $f_0(1500)$ is also assumed in the CLEO analysis of the reaction $D^0 \to K^+K^-\pi^0$ [95], but not further investigated. The main goal of the analysis is to determine the strong phase difference δ_D between $D^0 \to K^{*-}K^+$ and $D^0 \to K^{*+}K^-$, which is required to extract the Cabibbo-Kobayashi-Maskava (CKM) angle γ.

Scalar Mesons from the B Factories: Belle and BaBar

The $b\bar{b}$ factories also studied decays of D mesons, but more interesting for this review are the results on the three-body charmless decays $B^0 \to K^0\pi^+\pi^-$ [137], $B^+ \to K^+K^+K^-$ and $B^+ \to K^+\pi^+\pi^-$ [138] from the Belle Collaboration as well as $B^0 \to K^+K^-K^0_S$ [] and $B^0 \to \pi^+\pi^-K^0_S$ [135] from BaBar. The Belle Collaboration finds clear signals in the $B^+ \to K^*(892)^0\pi^+$, $B^+ \to \rho(770)^0K^+$, $B^+ \to f_0(980)^0K^+$, and $B^+ \to \phi K^+$ decay channels. It's pointed out in [138] that all the quasi-two-body branching fractions results from Belle and BaBar are in good agreement. The decay mode $B^+ \to f_0(980)^0K^+$ is the first observed example of a B decay to a charmless scalar-pseudoscalar final state. They determine the mass and width of the $f_0(980)$ to be ($M = 976 \pm 4^{+2}_{-3}$, $\Gamma = 61 \pm 9^{+14}_{-8}$) MeV/$c^2$. Fig. 15 shows invariant masses from Belle. A clear signal is visible in the $\pi^+\pi^-$ mass at 980 MeV/c^2 and a broad enhancement in the 1300 MeV/c^2 region denoted as $f_X(1300)$, but no signal is observed for the scalar state, $f_0(1500)$. However, the invariant K^+K^- mass shows a peak around 1500 MeV/c^2 denoted as $f_X(1500)$ by the Belle Collaboration. The latter is best described in the analysis as a scalar resonance with mass and width determined from the fit consistent with the standard $f_0(1500)$ state. An observation of $f_0(1500) \to K^+K^-$, but no signal in the decay to $\pi^+\pi^-$ is inconsistent with the standard $f_0(1500)$, which is expected to couple more strongly to the two-pion decay. The $f_X(1300)$ structure in the $\pi^+\pi^-$ mass is equally well described by a scalar or vector amplitude if approximated by a single resonant state. Higher-statistics data are required to resolve this issue. All these observations are essentially confirmed by BaBar and their conclusion is that the nature of the $f_0(1500)$ remains unclear. An identification as the standard PDG $f_0(1500)$ leads to inconsistencies with the measurement

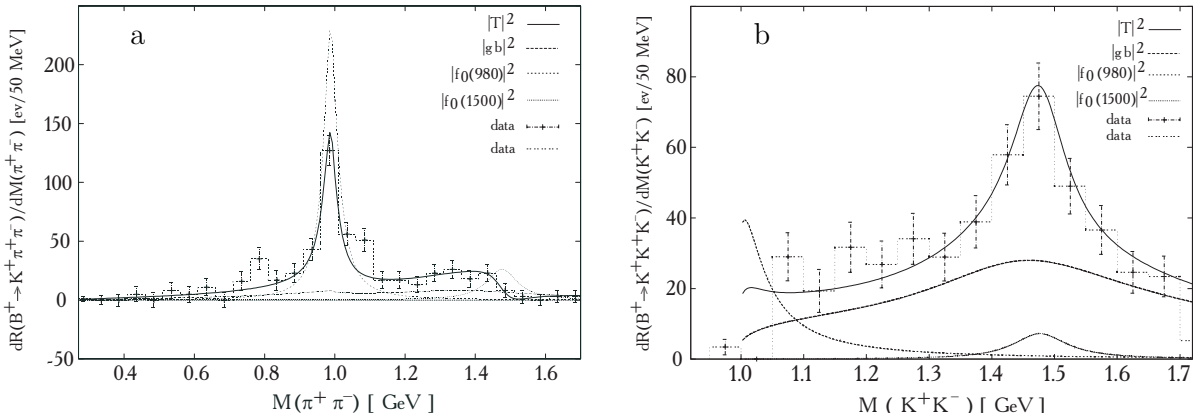

Figure 15: Invariant mass spectra in the decays $B^+ \to K^+\pi^+\pi^-$ and $B^+ \to K^+K^+K^-$ measured by the Belle Collaboration: (a) $\pi^+\pi^-$ and (b) K^+K^-. A clear peak at 980 MeV/c^2 can be seen in the double-pion spectrum and an enhancement around 1400 MeV/c^2. The K^+K^- spectrum is dominated by a peak around 1500 MeV/c^2.

of the $B^0 \to f_0(1500)K^0_S$, $f_0(1500) \to \pi^+\pi^-$ decay [135]. A new scalar resonance could be proposed with a strong coupling to K^+K^- and a weak coupling to $\pi^+\pi^-$. A very similar situation led to the introduction of the $f_0(1790)$ by the BES Collaboration.

Also shown in Fig. 15 is a fit to the data by Minkowski and Ochs providing a possible solution to the puzzle [172]. In their analysis, the remarkable phenomenon of the $f_0(1500)$ signal in $K\bar{K}$, but its apparent absence in $\pi^+\pi^-$, is explained by the constructive and destructive interference with the broad glueball ("red dragon"). They claim that such a behavior would be expected from the near octet flavor composition of the $f_0(1500)$. The data can then be described using both $f_0(980)$ and $f_0(1500)$ with standard properties. No $f_0(1370)$ state is needed in contrast to the analyses performed by Belle and BaBar.

Radiative ϕ Decays from the KLOE Experiment

The KLOE Collaboration reported on radiative ϕ decays into $f_0(980)$ and $a_0(980)$ [98, 98]. As pointed out in [96], these decays have long been recognized as a potential route towards disentangling the nature of these states. The magnitudes of the decay widths are rather sensitive to the fundamental structures of the $f_0(980)$ and $a_0(980)$, and can possibly dis-

Scalar	$\mathcal{B}(\phi \to \gamma +$ meson$)$	Number of Events
$f_0(980) \to \pi^0\pi^0$	$(1.49 \pm 0.07) \times 10^{-4}$ [98]	2438 ± 61 [97]
$f_0(980) \to \pi^+\pi^-$	$(2.1 - 2.4) \times 10^{-4}$ [99]	
$a_0(980) \to \pi^0\eta$	$(7.4 \pm 0.7) \times 10^{-5}$ [98]	802 [98]

Table 15: KLOE results on radiative ϕ decays.

criminate amongst models. According to different interpretations, the $\phi \to a_0\gamma$ branching fraction can range from 10^{-5} for a mostly $q\bar{q}$ and $K\bar{K}$ structure to 10^{-4} for $q\bar{q}q\bar{q}$. The ratio $\mathcal{B}(\phi \to f_0(980)\gamma)/\mathcal{B}(\phi \to a_0(980)\gamma)$ is also highly dependent on the structure of the scalars [96]. The $K\bar{K}$ and $\eta\eta$ thresholds produce sharp cusps in the energy dependence of the resonant amplitude and pose further challenges in the models. Table 15 shows the branching fractions for the decays into two pions and $\pi^0\eta$, respectively. They determined the ratio of the two branching fractions and the ratio of the two couplings to the KK system to be:

$$\frac{\mathcal{B}(\phi \to f_0(980)\gamma)}{\mathcal{B}(\phi \to a_0(980)\gamma)} = 6.1 \pm 0.6 \tag{33}$$

$$\frac{g^2_{f_0KK}}{g^2_{a_0KK}} = 7.0 \pm 0.7 \tag{34}$$

These results are in good agreement with predictions made for four-quark states.

Further Results from Photon-Photon Fusion

Apart from proving the existence of particular states, crucial to establishing the glueball nature of any glueball candidate is an anti-search in two-photon collisions since gluonic states do not couple directly to photons. Results from $\gamma\gamma$ collisions were reported by the LEP collaborations. Fig. 16 (left side) shows three peaks below 2 GeV in the invariant $K^0_SK^0_S$ mass distribution observed by the L3 collaboration [128]. The background is fitted by a second-order polynomial and the three peaks by Breit-Wigner functions. The mass spectrum is dominated by the formation of tensor mesons, the $f'_2(1525)$ and the $f_2(1270)$ interfering with the $a^0_2(1320)$. A clear signal for the $f_J(1710)$ is observed and found to be dominated by the spin-two helicity-two state. No resonance is observed in the 2.2 GeV/c^2 mass region. The $f_0(1500)$ scalar meson is not seen in its decay to $K^0_SK^0_S$ in agreement with central-production data indicating a small $s\bar{s}$ component if this state is interpreted as $q\bar{q}$ meson. Fig. 16 (right side) shows the fitted $\pi^+\pi^-$ spectrum measured by the ALEPH collaboration in $\gamma\gamma$ collisions. Only the $f_2(1270)$ is observed and no signals for the $f_0(1500)$ and $f_J(1710)$. Upper limits for the decay into $\pi^+\pi^-$ have been determined at the 95 %

	Stickiness	Gluiness	Reference
$f_0(1500)$	> 1.4		ALEPH Collaboration [173]
$f_J(1710)$	> 0.3		ALEPH Collaboration [173]
$\eta(1440)$	79 ± 26	41 ± 14	L3 Collaboration [129]
$\eta'(958)$	3.6 ± 0.3	5.2 ± 0.8	
$f_2(2220)$	> 109		CLEO Collaboration [90]

Table 16: Stickiness and gluiness for some of the mesons.

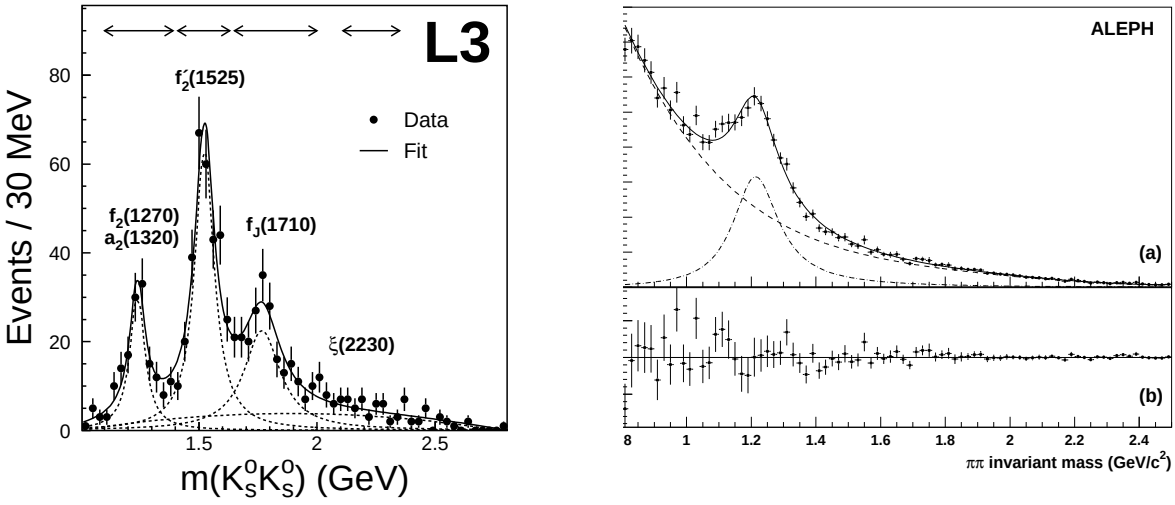

Figure 16: Left: invariant $K_S^0K_S^0$ mass in $\gamma\gamma$ collisions from L3. The solid line corresponds to a maximum-likelihood fit. The arrows represent the $f_2(1270) - a_2^0(1320)$, the $f_2'(1525)$, the $f_J(1710)$, and the $\xi(2230)$ mass regions [128]. Right: invariant $\pi^+\pi^-$ mass distribution from ALEPH. The top plot (a) shows the fit to the data using a Breit-Wigner function for the $f_2(1270)$ (dot-dashed line), a polynomial for the background (dashed line) and the combination of these functions (solid line). The bottom plot (b) shows the data after subtraction of the fitted curves. Only statistical error bars are shown [130].

confidence level:

$$\Gamma(\gamma\gamma \to f_0(1500)) \cdot \mathcal{B}(f_0(1500) \to \pi^+\pi^-) < 0.31 \text{ keV} \quad (35)$$

$$\Gamma(\gamma\gamma \to f_J(1710)) \cdot \mathcal{B}(f_J(1710) \to \pi^+\pi^-) < 0.55 \text{ keV} \quad (36)$$

The CLEO Collaboration has reported on the possible glueball candidate $f_J(2220)$. An upper limit of $\Gamma_{\gamma\gamma}\mathcal{B}(f_J(2220) \to K_S^0K_S^0 \leq 1.1)$ eV at 95 % C.L. was derived from two-photon interactions, $\gamma\gamma \to f_J \to K_S^0K_S^0$, using the CLEO II detector [90]. The same approach for the $f_2'(1525)$ leads to consistent results with PDG values. The CLEO observation is in agreement with the published result from the L3 Collaboration (Fig, 16) of $\Gamma_{\gamma\gamma}\mathcal{B}(f_J \to K_S^0K_S^0 \leq 1.4)$ eV at 95 % C.L. [128]. The non-observation of a signal in the 2.2 GeV/c^2 mass region in two-photon fusion is certainly expected for a true glueball, but the non-existence of this narrow state is also not excluded. Assuming that the BES cross section is correct, the CLEO authors determine a large lower limit for the "stickiness" of > 109 at the 95 % C.L. Further results on stickiness and gluiness are summarized in Table 16.

Two pseudoscalar mesons are reported in the 1400-1500 MeV/c^2 mass region and have been listed as two separate states by the Particle Data Group since ?, the $\eta(1405)$ and $\eta(1475)$. Long time considered only one resonance, the $\eta(1475)$ was first observed in two-photon collisions in 2001 decaying to $K\bar{K}\pi$ by the L3 Collaboration [129]. The reported two-photon partial width is 212 ± 50 (stat.) $\pm$ 23 (sys.) eV. The second η state is neither

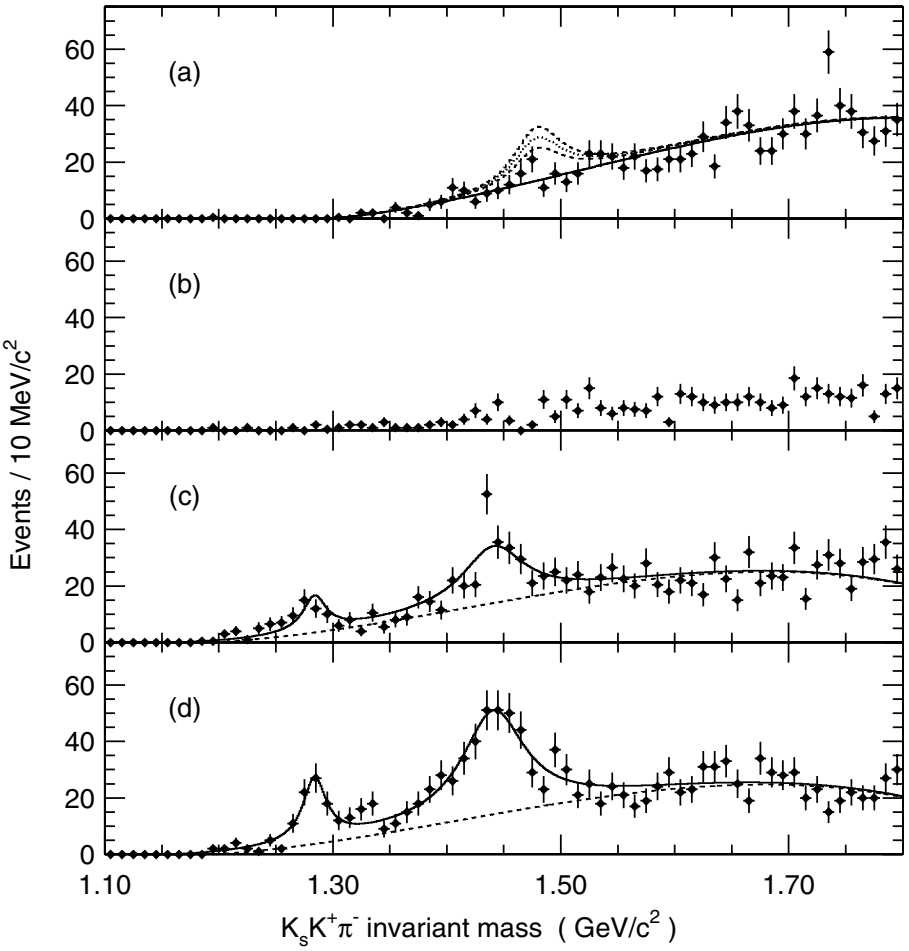

Figure 17: Distributions of the $K^0_S K^{\pm}\pi^{\mp}$ invariant mass for data events detected with (a) $p_\perp \leq 100$ MeV/c, (b) 100 MeV/$c \leq p_\perp \leq 200$ MeV/c, and (c) 200 MeV/$c \leq p_\perp \leq 600$ MeV/c in the untagged mode, and (d) for all $p_\perp$ in the tagged mode. The dashed curves in (a) show the strength of the expected $\eta(1475)$ signal according to the L3 results [129]. The solid curves in (a), (c) and (d) are the results of binned maximum likelihood fits for resonances with a polynomial approximation to the non-interfering combinatorial background.

observed in $K\bar{K}\pi$ nor in $\eta\pi\pi$ by L3, suggesting a large gluonic content of the $\eta(1405)$. In 2005, CLEO published negative results on the search for $\eta(1475) \rightarrow K^0_S K^{\pm}\pi^{\mp}$. The non-observation of any pseudoscalar meson below 1700 MeV/c^2 was based on 5 times more statistics and the results are more than 2 standard deviations inconsistent with the L3 findings. Fig. 17 shows the distributions of the $K^0_S K^{\pm}\pi^{\mp}$ invariant mass for different ranges of $p_\perp$. Signals due to pseudoscalar mesons are expected in (a). The authors observe two statistically significant enhancements in the $\eta(1475)$ mass region (Fig. 17 (c)). However, the enhancements have large transverse momentum which rules them out as being due to pseudoscalar resonances. The observation is consistent with the production of axial-vector

CLEO	$\eta(1295)$	$\eta(1405)$	$\eta(1475)$	L3 on $\eta(1475)$
Mass in [MeV/c^2]	1294	1410	1481	-
Upper limit at 90 % CL [eV]	14	24	89	$212 \pm 50 \pm 23$

Table 17: Upper limits on the two-photon partial widths of pseudoscalar resonances from CLEO: $\Gamma_{\gamma\gamma}(\eta)\mathcal{B}(K\bar{K}\pi)$. For comparison, the L3 result is also given.

mesons. Table 17 summarizes CLEO upper limits on the two-photon partial widths of pseudoscalar states. All these are consistent with the glueball and the radial excitation hypotheses of the $\eta(1295)$, $\eta(1405)$, and $\eta(1475)$. Unfortunately with no state observed, it is difficult to come to a conclusion about the nature of the pseudoscalar resonances. Only two ground-state axial vector mesons were reported in this mass range consistent with quark model expectations [125].

Evidence for $\eta(1295)$ *using* $\pi^- p$ *Reactions: The E852 Experiment*

The $\eta(1295)$ is the lowest-mass pseudoscalar meson above the η' and thus, often interpreted as the first radial excitation of the η meson. It is also degenerate in mass with the $\pi(1300)$ suggesting ideal mixing. The PDG has listed the $\eta(1295)$ meson in the summary table [6]. Although the resonance has not been observed in proton-antiproton annihilation, $\gamma\gamma$ collisions, central production, and J/ψ decays, evidence seems to be solid in pion-induced reactions. It was first observed in a PWA analysis of the $\eta\pi\pi$ system [174] and later confirmed by other experiments, e.g. [175–179]. A small $\eta(1295)$ signal at 1255 MeV/c^2 was found in the analysis of $\bar{p}p \to \eta\pi^+\pi^-\pi^+\pi^-$ [180], but the peak was later explained by an insufficient simulation of trigger conditions in the Monte Carlo. In particular, the E852 experiment is probably the only experiment with clear signals for the $\eta(1295)$, the $\eta(1405)$ and the $\eta(1475)$.

The E852 Collaboration performed a partial-wave analysis of the $\eta\pi^+\pi^-$ system produced in the reaction $\pi^- p \to \eta\pi^+\pi^- n$ at 18 GeV based on 9082 events in the $1205 \leq M(\eta\pi^+\pi^-) \leq 1535$ MeV/c^2 [178]. Since the $J^{PC} = 0^{-+}$ states often have a $a_0(980)\pi$ decay mode and $a_0(980)$ couples to both $\eta\pi$ and $K\bar{K}$ final states, a comparison of resonances produced in $\eta\pi^+\pi^-$ and $K\bar{K}\pi$ can help identify states. Fig. 18 shows the fitted intensity distributions for the 0^{-+} wave. A clear enhancement is observed around 1300 MeV/c^2 in panel (a), which is identified with the $\eta(1295) \to a_0(980)\pi$. The distribution in (b) shows a double-peak structure indicating contributions from $\eta(1295)$ and $\eta(1440)$. It's pointed out in the publication that the dominant higher-mass peak is somewhat inconsistent with previous

	Mass [GeV/c^2]	Width [GeV/c^2]	$\mathcal{B}(\eta \to a_0\pi)/\ \mathcal{B}(\eta \to \sigma\eta)$
$\eta(1295)$	1.282 ± 0.005	0.066 ± 0.013	0.48 ± 0.22
$\eta(1440)$	1.404 ± 0.006	0.080 ± 0.021	0.15 ± 0.04

Table 18: Properties of the $J^{PC} = 0^{-+}$ states from E852 [178].

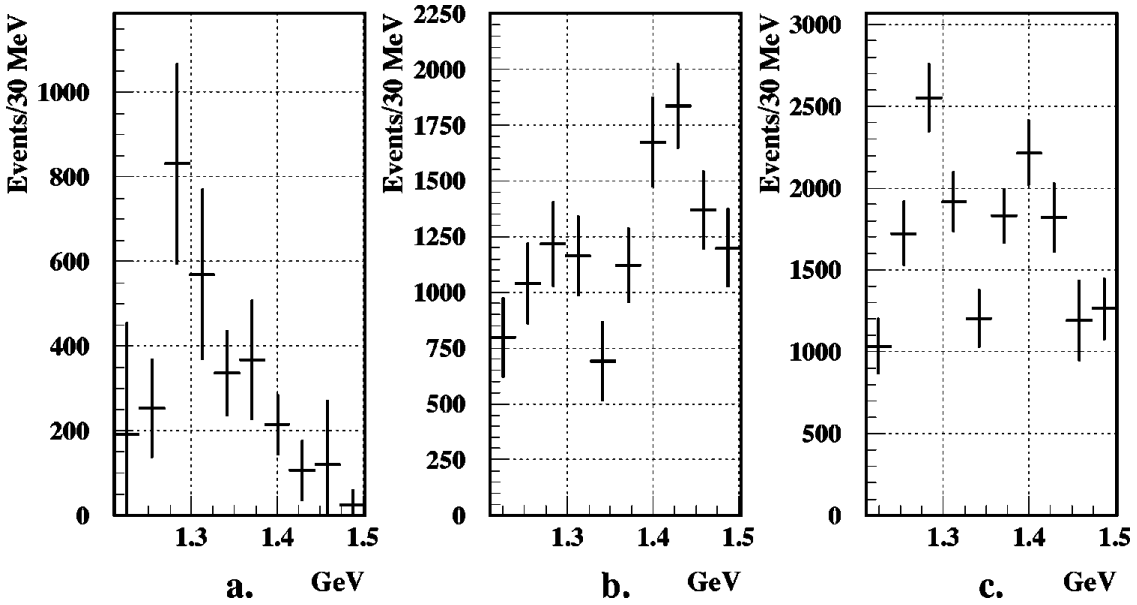

Figure 18: Fitted intensity distributions from E852 for the 0^{-+} wave [178]: (a) $a_0\pi$ intensity, (b) $\eta(\pi\pi)_S$ intensity, and (c) total 0^{-+} intensity. A sharp peak at about 1300 MeV/c^2 is visible in (a), consistent with the assumption of $\eta(1295) \to a_0(980)\pi$.

analyses [175,176], which do not see it as dominant. The result of the incoherent sum of the two modes is shown in Fig. 18 (c). In summary, the authors find that the lower-mass region is dominated by the $\eta(1295)$, accounting for about 80 % of the signal. The dominance has a significant influence on the $f_1(1285)$ branching fractions. The properties of the pseudoscalars states are summarized in Table 18.

In a later analysis, E852 looked at the reaction $\pi^- p \to K\bar{K}\pi p$ [179]. In the $K\bar{K}\pi$ final state, they observed two partial wave, KK^* and $a_0\pi$, both of which coupled to 0^{-+} quantum numbers. Figure 19 shows the results of the partial wave analysis of this channel. There is clear evidence for two pseudoscalar states above 1.4 GeV as well as the $f_1(1485)$ state. The lower mass 0^{-+} state, $\eta(1405)$, couples to both $a_0\pi$ and KK^*, while the higher mass state, $\eta(1475)$, couples mostly to KK^*.

5 Gluonic Excitations

5.1 *The Pseudoscalar Mesons*

Within the pseudoscalar sector, the ground states are the well established $\eta(548)$ and $\eta\prime(958)$. Only radial excitations of these states are expected in the framework of the quark model. Beyond the simple quark model, a nonet of hybrid pseudoscalar mesons is expected in the 1.8 to 2.2 GeV/c^2 mass region, and a glueball is expected in the $\sim$ 2 GeV/c^2 region. Table 8

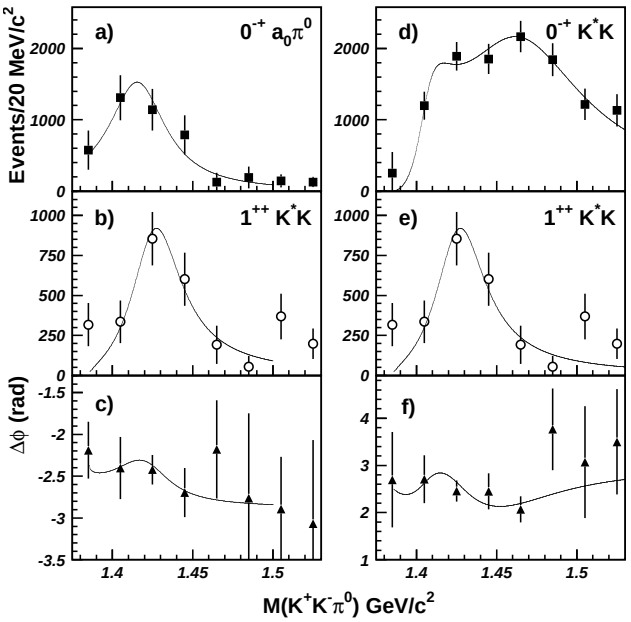

Figure 19: The intensity observed in the $K\bar{K}\pi$ final state from E852 [179]. (a) shows the 0^{-+} intensity in the $a_0(980)\pi$ partial wave, (b) and (e) show the 1^{++} intensity in the K^*K partial wave, (d) shows the 0^{-+} intensity in the K^*K partial wave, and (e) and (f) shows the phase differences between (a) and (b) and between (d) and (e) respectively.

shows the current known pseudoscalar states. The $\eta(1295)$ and the $\eta(1405)$ are often considered as the radial excitations. The $\eta(1760)$ is often taken as the partner of the $\pi(1800)$ which leaves the $\eta(1475)$ as the odd state out. The higher mass $\eta(2225)$ has mass that is not inconsistent with a glueball interpretation, but the single measurement of this state needs confirmation, and more of its decay modes need to be measured.

In the initial studies of radiative J/ψ decays, a great deal of excitement was raised over the very large cross section for a pseudoscalar state known as the ι [181], [182], [183]. The apparently large production of this state, now known as the $\eta(1405)$, led to speculation that this was a glueball, or at least a state with sizable glueball content. Later analysis by MARK III [154] indicated that there are actually two pseudoscalar states in this mass region. This splitting was later confirmed by the OBELIX collaboration [45].

While the two pseudoscalar states near 1400 are listed by the pdg [6], there has been some speculation by Klempt [5] that they are in fact a single state with a node in the wave function. There is also some speculation [5] that the $\eta(1295)$ may not exist. In its clearest observations, it is always seen in conjunction with the $f_1(1285)$ and it could possibly be explained as feed through from the 1^{++} state.

Under this latter interpretation, the $\eta(1405)$ and $\eta(1475)$ become the radial excitations of the ground state pseudoscalar mesons. This is consistent with the observations in $\bar{p}p$ annihilation, where the $\eta(1405)$ is strongly produced.

However, independent of the scenarios, one is no closer to identifying the pseudoscalar

glueball. A good discussion of the history of this and the current state of these two states can be found in the PDG mini-review [184] on this topic. There is hope that new data from BESIII will be able to help clarify the situation.

5.2 *The Tensor Mesons*

Within the quark model, there are two quark configurations which yield 2^{++} quantum numbers, the $^3\mathrm{P}_2$ ($L = 1, S = 1, J = 2$) and the $^3\mathrm{F}_2$ ($L = 3, S = 1, J = 2$) nonets. Members of the former are the well established isoscalar states $f_2(1270)$ and $f_2\,'(1525)$, while the latter is expected in mass similar to the 4^{++} states of the same orbital angular momentum. These are observed near 2 GeV/c^2. For both of these nonets, radial excitations are also expected.

Evidence for a tensor glueball is essentially non-existent. Below 2 GeV/c^2, only one further resonance is listed in the Meson Summary Table, the $f_2(1950)$. Four additional reported resonances require confirmation. For this reason, none of the reported isoscalars above the $f_2'(1525)$ can be definitely assigned to one of the nonets $2^3\mathrm{P}_2$, $3^3\mathrm{P}_2$, or $1^3\mathrm{F}_2$, and the identification of a glueball as a resonance that has no place in the $q\bar{q}$ nonets is premature. The latest mini-review published by the Particle Data Group in 2004 considers evidence for the $f_2(1565)$ observed in $p\bar{p}$ annihilation at rest as more solid. It could be a member of the $2^3\mathrm{P}_2$ nonet and is perhaps the same state as the $f_2(1640)$, seen in its decay to $\omega\omega$ and 4π.

Above 2 GeV/c^2, the BES Collaboration has reported on the $f_J(2220)$, likely $J = 2$, and has considered it a glueball candidate since it is produced strongly in radiative J/ψ decays and seems to be non-existent in $\gamma\gamma$ collisions. However, careful searches by other experiments could not confirm this resonance. It has neither been observed in radiative Υ decays, nor in formation in $p\bar{p}$ annihilation into K^+K^-, K_SK_S, $\phi\phi$, $\eta\eta$, or $\pi\pi$. The evidence is thus very weak and more data is needed to clarify the situation. BES-III can possibly shed some light on this, but a confirmation in $p\bar{p}$ would certainly be desirable.

Moving beyond the the quark-model picture, a nonet of hybrid states is expected in the 1.8 to 2.2 GeV/c^2 mass region, and a 2^{++} glueball is expected in the 2 GeV/c^2 mass region. Needless to say, the tensors are expected to be an extremely busy sector, and this is clearly born out by the large number of states in the PDG (see Table 7).

5.3 *The Scalar Sector*

The $J^{PC} = 0^{++}$ ($L = 1,\ S = 1$) scalar sector is without doubt the most complex one and the interpretation of the states' nature and nonet assignments are still very controversial. In particular, the number of observed $I = 0$ isosinglet states with masses below 1.9 GeV/c^2 is under debate. According to the PDG mini-review on non-$q\bar{q}$ candidates [6], five isoscalar resonances are well established: the very broad $f_0(600)$ or so-called σ state, the $f_0(980)$, the broad $f_0(1370)$, and the rather narrow $f_0(1500)$ and $f_0(1710)$ resonances. Naive arguments without chiral symmetry constraints and the close proximity of states in other J^{PC} nonets suggest that the $f_0(600)$, $f_0(980)$, and $a_0(980)$ are members of the same nonet. The missing $I = 1/2$ state – usually called $K_0^*(800)$ or κ – is not listed by the Particle Data Group in its

latest 2008 edition. The nature of this nonet is not necessarily $q\bar{q}$. Very often, $f_0(980)$ and $a_0(980)$ are interpreted as multi-quark states or $K\bar{K}$ molecules [185, 186].

Using the same naive arguments, the $a_0(1450)$, $K^*(1430)$, and two states out of the $I = 0$ group, $f_0(1370)$, $f_0(1500)$, and $f_0(1710)$, would form an SU(3) flavor nonet. These nonet assignments however pose some serious challenges. While almost all models agree on the $K^*(1430)$ to be the quark model $s\bar{u}$ or $s\bar{d}$ state, the situation is very ambiguous for the isoscalar resonances. The most striking observation is that one f_0 state appears supernumerary, thus leaving a non-$q\bar{q}$ (most likely) glueball candidate. Both the $f_0(1370)$ and $f_0(1500)$ decay mostly into pions. In fact, all analyses agree that the 4π decay mode accounts for at least half of the $f_0(1500)$ decay width and dominates the $f_0(1370)$ decay pointing to a mostly $n\bar{n}$ content of these states. On the other hand, the LEP experiments indicate that the $f_0(1500)$ is essentially absent in $\gamma\gamma \to K\bar{K}$ (L3 Collaboration [128]) and $\gamma\gamma \to \pi^+\pi^-$ (ALEPH Collaboration [130]). If the state were of $q\bar{q}$ nature, the extremely small upper limit for the branching fraction into $\pi^+\pi^-$ (35) would suggest a mainly $s\bar{s}$ content. This contradiction emphasizes the non-$q\bar{q}$ nature of the $f_0(1500)$ resonance. On the other hand, the observed decays into $\pi\pi$, $\eta\eta$, $\eta\eta'$, and $K\bar{K}$ are not in agreement with predictions for a pure glueball. For this reason, a large variety of mixing scenarios of the pure glueball with the nearby $n\bar{n}$ and $s\bar{s}$ isoscalar mesons has been described. These are discussed in section 5.4.

Challenges in the interpretation of the scalar sector involve both experimental and theoretical efforts. The following key questions account for the major differences in the models on scalar mesons and need to be addressed in the future:

- What is the nature of the $f_0(980)$ and $a_0(980)$? Do they have mainly a quarkonium structure or are these additional non-$q\bar{q}$ states? Though very often interpreted as a $K\bar{K}$ molecule, the decay $\phi \to \gamma f_0\ (a_0) \to \gamma K\bar{K}$ is kinematically suppressed and has not been observed, yet. Data from DAPHNE [97, 98] on $\phi \to \eta\pi^0\gamma$ and $\phi \to \pi^0\pi^0\gamma$ favor these states to be four-quark ($q^2\bar{q}^2$) states [187, 188]. In a more sophisticated picture [187], the two mesons are mostly $(qq)_{\bar{3}}(\bar{q}\bar{q})_3$ in S-wave near the center, but further out they rearrange as $(q\bar{q})(q\bar{q})$ and finally as meson-meson states. A Dalitz plot analysis of $D_S^+ \to \pi^-\pi^+\pi^+$ by the E791 Collaboration finds a dominant contribution from $f_0(980)\pi^+$ pointing to a large $s\bar{s}$ component in the wave function [189]. The charm meson decay $D_S^+ \to \pi^-\pi^+\pi^+$ is Cabibbo-favored, but has no strange meson in the final state.

- Is the $f_0(1370)$ a true $q\bar{q}$ resonance or of different nature, e.g. generated by $\rho\rho$ molecular dynamics as suggested in [5]. The latter is supported by the huge $\Gamma_{\rho\rho}$, but very small $\Gamma_{\eta\eta}$ and $\Gamma_{\sigma\sigma}$ partial widths observed in central production (Table 11). However, these results completely disagree with Crystal-Barrel results on the decay width of this state (Table 9). The experimental situation is unclear. The Particle Data Group has however accepted the $f_0(1370)$ as an established resonance.
  In the *red dragon* interpretation [190], the $f_0(1370)$ is also not considered a genuine resonance, but part of the broad background amplitude, which itself is associated with

the expected glueball. In contrast, a recent *study in depth of* $f_0(1370)$ [191] shows a highly significant improvement of χ^2 with the state included as resonance in fits to the five primary sets of data requiring its existence. These sets include Crystal-Barrel data on $p\bar{p} \to 3\pi^0$ at rest, data on $p\bar{p} \to \pi^0\pi^0\eta$, BES-II data on $J/\psi \to \phi\pi^+\pi^-$, and the CERN-Munich data for $\pi\pi$ elastic scattering.

- Though the $f_0(1500)$ cannot be accommodated easily in $q\bar{q}$ nonets and exhibits reduced $\gamma\gamma$ couplings – all signatures expected for glueballs –, data on $J/\psi \to \gamma f_0(1500)$ is still statistically limited. More data from the BES-III Experiment is certainly required to show its enhanced production in gluon-rich radiative J/ψ decays.

- Are the two resonances listed in Table 6, $f_0(1710)$ and $f_0(1790)$, distinct states? Experimental evidence is claimed only by the BES Collaboration and has not been confirmed by others. The Particle Data Group does not list the $f_0(1790)$ as resonance and also does not include it in averages, fits, limits, etc.

Other pictures have emerged for the assignment of scalar mesons to SU(3) flavor nonets based on different approaches to the questions above. Minkowski and Ochs have classified the isoscalar resonances $f_0(980)$ and $f_0(1500)$ together with $a_0(980)$ and $K_0^*(1430)$ as members of the 0^{++} nonet [190]. They claim a mixing of the isoscalar states, which is similar to that of the pseudoscalar η and η'. In this scenario, the $(\eta',\ f_0(980))$ pair forms a parity doublet, which is approximately degenerate in mass. Moreover, the $f_0(600)$ and $f_0(1370)$ are interpreted as different signals of the same broad resonance, which is associated with the lowest-lying 0^{++} glueball. Very similar nonet assignments are discussed in a quark model which is based on short-range instanton effects [192], also not considering the $f_0(1370)$ as $q\bar{q}$ resonance.

Moreover, the Gatchina group performed a K-matrix analysis of the isoscalar 0^{++} waves in the invariant mass range 280-1900 MeV/c^2 based on a large variety of different data sets including data from GAMS, BNL on $\pi^- p$, Crystal Barrel, and CERN-Munich on $\pi^+\pi^- \to \pi^+\pi^-$. The ground-state $q\bar{q}$ scalar nonet is suggested to consist of $a_0(980)$, $f_0(1300)$ and $f_0(980)$, whereas $a_0(1450)$, $f_0(1760)$ and $f_0(1500)$ form the nonet of the first radial excitation [193].

If we adopt the point of view of the Particle Data Group, then five isoscalar resonances are well established: $f_0(600)$, $f_0(980)$, $f_0(1370)$, $f_0(1500)$, and $f_0(1710)$. The following section discusses possible mixing scenarios of the $J^{PC} = 0^{++}$ $q\bar{q}$ nonet with the lowest-mass 0^{++} glueball resulting in the three established $I = 0$ resonances above 1 GeV/c^2.

5.4 *Mixing in the scalar sector*

There have been many authors who have considered that the $f_0(1370)$, the $f_0(1500)$ and the $f_0(1710)$ are the physical manifestations of the underlying 0^{++} quarkonium nonet and the lowest mass glueball. It is generally assumed that the three bare states mix to yield the three physical states. Inputs to such calculations include the masses of the physical states as well as their decay rates into pairs of pseudoscalar mesons. The masses of the bare states

and the mixing of the physical states then result. In addition to the choice of physical states, there appears to also be some dependence on whether one assumes the bare glueball is more or less massive than the mostly $s\bar{s}$ state.

In the literature, the mixing is typically written in terms of equation 37, where the physical states, $f_{1,2,3}$ are identified with the $f_0(1370)$, $f_0(1500)$ and $f_0(1710)$ respectively, and the bare states are parameterized in terms of the ideally mixed $q\bar{q}$ states.

$$\begin{array}{rcl} n\bar{n} & = & \frac{1}{\sqrt{2}}\left(u\bar{u}+d\bar{d}\right) \\ s\bar{s} & & \end{array}$$

. However, it is also useful to look at these in terms of the SU(3) symmetric states as well

$$\begin{aligned} \mid 1> &= \frac{1}{\sqrt{3}}\left(u\bar{u}+d\bar{d}+s\bar{s}\right) \\ \mid 8> &= \frac{1}{\sqrt{6}}\left(u\bar{u}+d\bar{d}-2s\bar{s}\right) \end{aligned}$$

$$\left(\begin{array}{c} \mid f_1> \\ \mid f_2> \\ \mid f_3> \end{array}\right) = \left(\begin{array}{ccc} M_{1n} & M_{1s} & M_{1g} \\ M_{2n} & M_{2s} & M_{2g} \\ M_{3n} & M_{3s} & M_{3g} \end{array}\right) \cdot \left(\begin{array}{c} \mid n\bar{n}> \\ \mid s\bar{s}> \\ \mid G> \end{array}\right) \tag{37}$$

There is also some model dependence included in the analysis.

Broadly speaking, the results divide into two categories. The first in which the bare glueball comes out lighter than the $s\bar{s}$ state, and the second in which the bare glueball comes out heavier than the $s\bar{s}$ state. We summarize these by first looking that the case where the bare glueball is lighter. One of the earliest of these came from Close and Amsler [8,9]. They allowed for the rate of $s\bar{s}$ quark production from the vacuum to be different from the u and d quarks. They also allowed for the bare glueball to have a different coupling to $s\bar{s}$ than from $u\bar{u}$ and $d\bar{d}$. However, in their work, the resulting couplings were generally consistent with the flavor-blind assumption. Based mostly on results from the Crystal Barrel experiment, they found a mixing as given equation 38.

$$\begin{array}{lcl} \left(\begin{array}{c} \mid f_0(1370)> \\ \mid f_0(1500)> \\ \mid f_0(1710)> \end{array}\right) & = & \left(\begin{array}{ccc} -0.91 & -0.07 & 0.40 \\ -0.41 & 0.35 & -0.84 \\ 0.09 & 0.93 & 0.36 \end{array}\right) \cdot \left(\begin{array}{c} \mid n\bar{n}> \\ \mid s\bar{s}> \\ \mid G> \end{array}\right) \\ \left(\begin{array}{c} \mid f_0(1370)> \\ \mid f_0(1500)> \\ \mid f_0(1710)> \end{array}\right) & = & \left(\begin{array}{ccc} -0.78 & -0.47 & 0.40 \\ -0.13 & -0.52 & -0.84 \\ 0.61 & -0.71 & 0.36 \end{array}\right) \cdot \left(\begin{array}{c} \mid 1> \\ \mid 8> \\ \mid G> \end{array}\right) \end{array} \tag{38}$$

Close and colleagues [16] later extended this by including additional data and found a mixing

scheme as given in equation 39.

$$\begin{array}{ccc} | f_0(1370)> & & \\ | f_0(1500)> & = & \\ | f_0(1710)> & & \end{array} \begin{pmatrix} 0.86 & 0.13 & -0.50 \\ 0.43 & -0.61 & -0.61 \\ 0.22 & 0.76 & 0.60 \end{pmatrix} \cdot \begin{array}{c} | n\bar{n}> \\ | s\bar{s}> \\ | G> \end{array}$$

$$\begin{array}{ccc} | f_0(1370)> & & \\ | f_0(1500)> & = & \\ | f_0(1710)> & & \end{array} \begin{pmatrix} 0.78 & 0.39 & -0.50 \\ 0.00 & 0.75 & 0.61 \\ 0.62 & -0.49 & 0.60 \end{pmatrix} \cdot \begin{array}{c} | 1> \\ | 8> \\ | G> \end{array} \tag{39}$$

Giacosa [194] looked at mixing in an effective chiral approach. They took the couplings to be flavor blind, and carried out their analysis both with and without a direct decay of the glueball. In the case without direct decay, the decays proceed via the $q\bar{q}$ content of the states. For the case of the mass of the bare glueball lighter than the $s\bar{s}$ state, they found the solution in equation 40 for the case without a direct glueball decay and that in equation 41 for the case with a direct glueball decay.

$$\begin{array}{ccc} | f_0(1370)> & & \\ | f_0(1500)> & = & \\ | f_0(1710)> & & \end{array} \begin{pmatrix} 0.86 & 0.24 & 0.45 \\ -0.45 & -0.06 & 0.89 \\ -0.24 & 0.97 & -0.06 \end{pmatrix} \cdot \begin{array}{c} | n\bar{n}> \\ | s\bar{s}> \\ | G> \end{array}$$

$$\begin{array}{ccc} | f_0(1370)> & & \\ | f_0(1500)> & = & \\ | f_0(1710)> & & \end{array} \begin{pmatrix} 0.84 & 0.30 & 0.45 \\ -0.40 & -0.21 & 0.89 \\ 0.36 & -0.93 & -0.06 \end{pmatrix} \cdot \begin{array}{c} | 1> \\ | 8> \\ | G> \end{array} \tag{40}$$

$$\begin{array}{ccc} | f_0(1370)> & & \\ | f_0(1500)> & = & \\ | f_0(1710)> & & \end{array} \begin{pmatrix} 0.79 & 0.26 & 0.56 \\ -0.58 & 0.02 & 0.81 \\ -0.20 & 0.97 & -0.16 \end{pmatrix} \cdot \begin{array}{c} | n\bar{n}> \\ | s\bar{s}> \\ | G> \end{array}$$

$$\begin{array}{ccc} | f_0(1370)> & & \\ | f_0(1500)> & = & \\ | f_0(1710)> & & \end{array} \begin{pmatrix} 0.80 & 0.24 & 0.56 \\ 0.46 & -0.35 & 0.81 \\ 0.40 & -0.91 & -0.16 \end{pmatrix} \cdot \begin{array}{c} | 1> \\ | 8> \\ | G> \end{array} \tag{41}$$

The common features of these mixing schemes are that the $f_0(1710)$ has a very large $s\bar{s}$ component, while the largest part of the glueball tends to be on the $f_0(1500)$, it is generally split over at least two of the three states. One also sees that the $f_0(1370)$ has the largest SU(3) singlet component.

The other situation is that in which the bare glueball comes out heavier than the bare $s\bar{s}$ state. The first of these was carried out by Weingarten and Lee [17]. They computed both the masses of the bare states as well as information on the decay of these states on the lattice. In their model, they had a decay rate that favored heavier quarks, thus enhancing

the coupling to the $s\bar{s}$ states. They found the mixing scheme as in equation 42.

$$\begin{array}{lcl} \mid f_0(1370)> & & \\ \mid f_0(1500)> & = & \left(\begin{array}{ccc} 0.819 & 0.290 & -0.495 \\ -0.399 & 0.908 & -0.128 \\ 0.413 & 0.302 & 0.859 \end{array} \right) \cdot \begin{array}{l} \mid n\bar{n}> \\ \mid s\bar{s}> \\ \mid G> \end{array} \\ \mid f_0(1710)> & & \\ \mid f_0(1370)> & & \\ \mid f_0(1500)> & = & \left(\begin{array}{ccc} 0.836 & 0.236 & -0.495 \\ 0.198 & -0.972 & 0.128 \\ 0.512 & -0.008 & 0.859 \end{array} \right) \cdot \begin{array}{l} \mid 1> \\ \mid 8> \\ \mid G> \end{array} \\ \mid f_0(1710)> & & \end{array} \tag{42}$$

Giacosa [194] also have two solutions in which the bare glueball mass is heavier than the $s\bar{s}$ mass. For the case of no direct glueball decay, the mixing is given in equation 43, while for the case of the direct glueball decay included, the nixing is given in equation 44.

$$\begin{array}{lcl} \mid f_0(1370)> & & \\ \mid f_0(1500)> & = & \left(\begin{array}{ccc} 0.81 & 0.19 & 0.54 \\ -0.49 & 0.72 & 0.49 \\ -0.30 & 0.67 & -0.68 \end{array} \right) \cdot \begin{array}{l} \mid n\bar{n}> \\ \mid s\bar{s}> \\ \mid G> \end{array} \\ \mid f_0(1710)> & & \\ \mid f_0(1370)> & & \\ \mid f_0(1500)> & = & \left(\begin{array}{ccc} 0.77 & 0.31 & 0.54 \\ 0.02 & -0.87 & 0.49 \\ 0.14 & -0.72 & -0.68 \end{array} \right) \cdot \begin{array}{l} \mid 1> \\ \mid 8> \\ \mid G> \end{array} \\ \mid f_0(1710)> & & \end{array} \tag{43}$$

$$\begin{array}{lcl} \mid f_0(1370)> & & \\ \mid f_0(1500)> & = & \left(\begin{array}{ccc} 0.82 & 0.57 & -0.07 \\ -0.57 & 0.82 & 0.00 \\ -0.06 & 0.04 & -0.99 \end{array} \right) \cdot \begin{array}{l} \mid n\bar{n}> \\ \mid s\bar{s}> \\ \mid G> \end{array} \\ \mid f_0(1710)> & & \\ \mid f_0(1370)> & & \\ \mid f_0(1500)> & = & \left(\begin{array}{ccc} 1.00 & 0.01 & -0.07 \\ 0.01 & -1.00 & 0.00 \\ -0.03 & -0.07 & -0.99 \end{array} \right) \cdot \begin{array}{l} \mid 1> \\ \mid 8> \\ \mid G> \end{array} \\ \mid f_0(1710)> & & \end{array} \tag{44}$$

Finally, Cheng [195] used lattice calculations for the mass of the a_0 the scalar glueball to set the starting values for their fit to the exiting data. They also limited the input data on decay rates. In particular, they did not use the strong coupling of the $f_0(1500)$ to $\eta\eta\prime$ due to the complications of the threshold opening. They find the mixing scheme as given in equation 45.

$$\begin{array}{lcl} \mid f_0(1370)> & & \\ \mid f_0(1500)> & = & \left(\begin{array}{ccc} 0.78 & 0.51 & -0.36 \\ -0.54 & 0.84 & 0.03 \\ 0.32 & 0.18 & 0.93 \end{array} \right) \cdot \begin{array}{l} \mid n\bar{n}> \\ \mid s\bar{s}> \\ \mid G> \end{array} \\ \mid f_0(1710)> & & \\ \mid f_0(1370)> & & \\ \mid f_0(1500)> & = & \left(\begin{array}{ccc} 0.93 & 0.03 & -0.36 \\ 0.04 & -0.99 & 0.03 \\ 0.37 & 0.04 & 0.93 \end{array} \right) \cdot \begin{array}{l} \mid 1> \\ \mid 8> \\ \mid G> \end{array} \\ \mid f_0(1710)> & & \end{array} \tag{45}$$

A common feature of these latter mixing schemes is that the glueball component ends up mostly in the highest mass state ($f_0(1710)$), while the $f_0(1500)$ comes out being mostly an SU(3) octet and the $f_0(1370)$ is mostly an SU(3) singlet state.

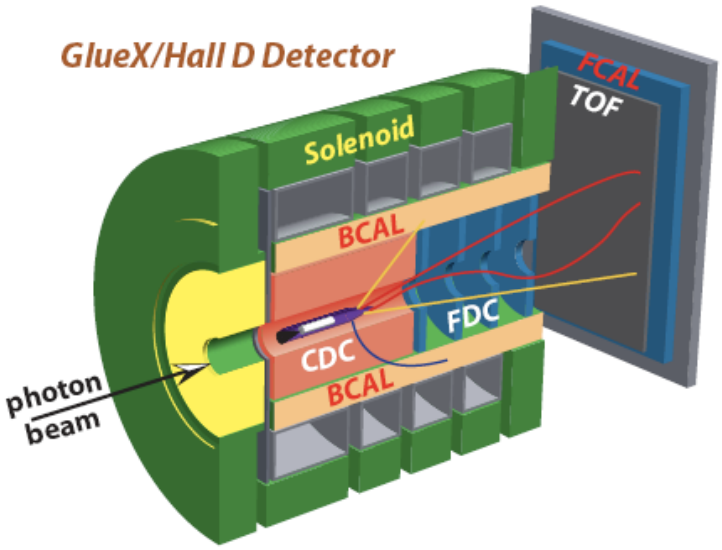

Figure 20: Layout of the GlueX Experiment at Jefferson Laboratory

6 Planned Experiments

The GlueX Experiment at Jefferson Laboratory

The GlueX experiment is part of the Jefferson Lab 12-GeV upgrade—and energy doubling upgrade of the CEBAF accelerator. GlueX will be housed in a new photon-only experimental building (Hall D). Electrons of energy 12 GeV will impinge in thin diamond target and via coherent bremsstrahlung, produce a linearly-polarized, $8.4 - 9.0$ GeV photon beam that interacts in the experimental target.

The main physics program of GlueX will be to search for light-quark hybrid mesons and to map out the spectrum of the exotic-quantum-number states. In order to do this, it will be necessary to reconstruct final states with several charged particles and photons. The GlueX experiment has been designed to have nearly full solid angle coverage for these particles with sufficient energy and momentum resolution to exclusively identify the desired final states.

The base-line detector is shown in 20. The detectors are in a 2.2 T solenoidal magnet which was originally used for the LASS experiment at SLAC. The all solenoidal design is well matched to the 9 GeV photon energy and the final states with 4-6 particles.

The 12 GeV upgrade received U.S. Department of Energy approval and construction is expected to commence in 2009. First beam on target GlueX is expected in 2014.

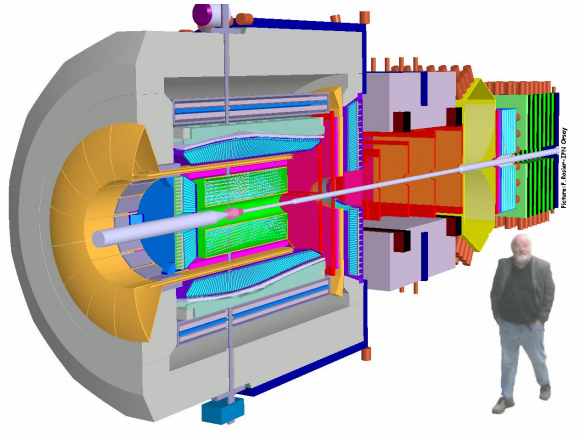

Figure 21: Layout of the PANDA experiment at GSI

The PANDA Experiment at GSI

The PANDA research program will be conducted at the Facility for Antiproton and Ion Research (FAIR), localized near Frankfurt in Germany. The heart of the new facility is a super-conducting synchrotron double-ring facility with a circumference of about 1,100 meters. A system of cooler-storage rings for effective beam cooling at high energies and various experimental halls will be connected to the facility.

At the new FAIR facility, antiproton beams will allow high-precision hadron physics in the upcoming years. A dedicated high-energy storage ring, HESR, will deliver antiproton beams in the momentum range between 1.5 and 15 GeV/c with unprecedented beam qualities. The energy range has been chosen to allow detailed studies of hadronic systems up to charmonium states. The physics will be done with the PANDA multipurpose detector located inside the HESR. Fig. 21 shows the general layout of the detector. The PANDA collaboration consists of $\sim$ 400 physicists from 48 institutions worldwide.

The general-purpose detector PANDA allows the detection and identification of neutral and charged particles over the relevant angular and energy range. The inner part of the detector can be modified for the needs of individual physics programs. To achieve the physics aims, the detector needs to cover the full solid angle. Good particle identification and excellent energy and angular resolution for charged particles and photons is provided by the following components:

BES III

The BESIII experiment at BEPCII in Beijing started operation in summer of 2008. It will ultimately accumulate data samples on the order of 10×10^9 J/ψ, 3×10^9 $\psi(2S)$ and 30 million $D\bar{D}$ per year of running year. Such large data sets will make it possible to study hadron spectroscopy in the decays of the charmonium states and the charmed mesons. Of particular interest for glueball searches is the fact that $J\Psi$ decays have always been viewed

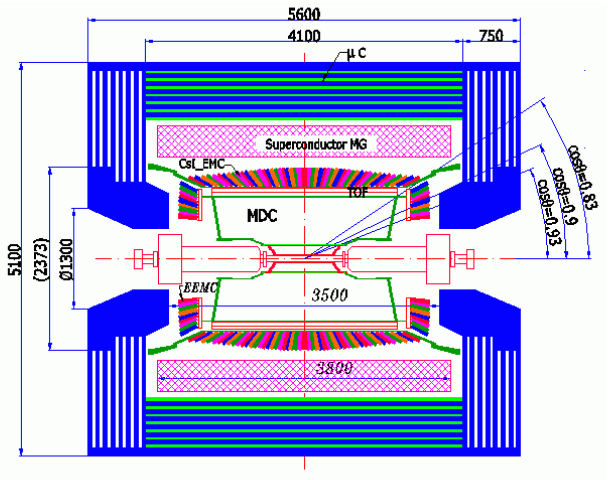

Figure 22: Layout of the BES III Experiment at BEPCII.

as one of the best places to look for these states.

The BESIII detector is shown schematically in Figure 22. In capability, it will be very similar to the CLEO-c detector–being able to accurately reconstruct both charged particles and photons.

7 Summary

To be written

References

[1] F E Close. Gluonic hadrons. *Reports on Progress in Physics*, 51(6):833–882, 1988.

[2] Claude Amsler. Proton antiproton annihilation and meson spectroscopy with the Crystal Barrel. *Rev. Mod. Phys.*, 70:1293–1340, 1998.

[3] Stephen Godfrey and Jim Napolitano. Light-meson spectroscopy. *Rev. Mod. Phys.*, 71:1411–1462, 1999.

[4] C. Amsler and N. A. Tornqvist. Mesons beyond the naive quark model. *Phys. Rept.*, 389:61–117, 2004.

[5] Eberhard Klempt and Alexander Zaitsev. Glueballs, Hybrids, Multiquarks. Experimental facts versus QCD inspired concepts. *Phys. Rept.*, 454:1–202, 2007.

[6] C. Amsler et al. Review of particle physics. *Phys. Lett.*, B667:1, 2008.

[7] Amsler, C., De-Grand, T. and Krusche, B. Review of Particle Physics. *J. Phys.*, G33:165, 2006.

[8] Claude Amsler and Frank E. Close. Evidence for a scalar glueball. *Phys. Lett.*, B353:385–390, 1995.

[9] Claude Amsler and Frank E. Close. Is $f_0(1500)$ a scalar glueball? *Phys. Rev.*, D53:295–311, 1996.

[10] A. Chodos, R. L. Jaffe, K. Johnson, C. B. Thorn, and V. F. Weisskopf. New extended model of hadrons. *Phys. Rev. D*, 9(12):3471–3495, 1974.

[11] R. L. Jaffe and K. Johnson. Unconventional States of Confined Quarks and Gluons. *Phys. Lett.*, B60:201, 1976.

[12] Michael S. Chanowitz. RESONANCES IN PHOTON-PHOTON SCATTERING. Presented at 6th Int. Workshop on Photon-Photon Collisions, Lake Tahoe, CA, Sep 10-13, 1984.

[13] Mariaelena Boglione and M. R. Pennington. Unquenching the scalar glueball. *Phys. Rev. Lett.*, 79:1998–2001, 1997.

[14] M. R. Pennington, T. Mori, S. Uehara, and Y. Watanabe. Amplitude Analysis of High Statistics Results on $\gamma\gamma \to \pi^+\pi^-$ and the Two Photon Width of Isoscalar States. *Eur. Phys. J.*, C56:1–16, 2008.

[15] Mesut Bahadir Cakir and Glennys R. Farrar. Radiative decay of vector quarkonium: Constraints on glueballs and light gluinos. *Phys. Rev.*, D50:3268–3278, 1994.

[16] Frank E. Close, Glennys R. Farrar, and Zhen-ping Li. Determining the gluonic content of isoscalar mesons. *Phys. Rev.*, D55:5749–5766, 1997.

[17] Weon-Jong Lee and D. Weingarten. Scalar quarkonium masses and mixing with the lightest scalar glueball. *Phys. Rev.*, D61:014015, 2000.

[18] Nathan Isgur and Jack E. Paton. A Flux Tube Model for Hadrons. *Phys. Lett.*, B124:247, 1983.

[19] Nathan Isgur and Jack E. Paton. A Flux Tube Model for Hadrons in QCD. *Phys. Rev.*, D31:2910, 1985.

[20] Masaharu Iwasaki, Shin-Ichi Nawa, Takayoshi Sanada, and Fujio Takagi. Flux tube model for glueballs. *Phys. Rev. D*, 68(7):074007, Oct 2003.

[21] Colin J. Morningstar and Mike J. Peardon. Efficient glueball simulations on anisotropic lattices. *Phys. Rev.*, D56:4043–4061, 1997.

[22] Ludvig Faddeev, Antti J. Niemi, and Ulrich Wiedner. Glueballs, closed fluxtubes and $\eta(1440)$. *Phys. Rev.*, D70:114033, 2004.

[23] Y. Koma, H. Suganuma, and H. Toki. Flux-tube ring and glueball properties in the dual ginzburg-landau theory. *Phys. Rev. D*, 60(7):074024, Sep 1999.

[24] V. A. Novikov, Mikhail A. Shifman, A. I. Vainshtein, and Valentin I. Zakharov. In a Search for Scalar Gluonium. *Nucl. Phys.*, B165:67, 1980.

[25] Leonard S. Kisslinger and Mikkel B. Johnson. Scalar mesons, glueballs, instantons and the glueball/sigma. *Phys. Lett.*, B523:127–134, 2001.

[26] S. Narison. QCD tests of the puzzling scalar mesons. *Phys. Rev.*, D73:114024, 2006.

[27] Adam P. Szczepaniak and Eric S. Swanson. The low lying glueball spectrum. *Phys. Lett.*, B577:61–66, 2003.

[28] Urs M. Heller. SU(3) lattice gauge theory in the fundamental adjoint plane and scaling along the Wilson axis. *Phys. Lett.*, B362:123–127, 1995.

[29] Christopher Michael and M. Teper. The Glueball Spectrum and Scaling in SU(3) Lattice Gauge Theory. *Phys. Lett.*, B206:299, 1988.

[30] C. Michael and M. Teper. The Glueball Spectrum in SU(3). *Nucl. Phys.*, B314:347, 1989.

[31] G. S. Bali et al. A Comprehensive lattice study of SU(3) glueballs. *Phys. Lett.*, B309:378–384, 1993.

[32] Y. Chen et al. Glueball spectrum and matrix elements on anisotropic lattices. *Phys. Rev.*, D73:014516, 2006.

[33] J. Sexton, A. Vaccarino, and D. Weingarten. Numerical Evidence for the Observation of a Scalar Glueball. *Phys. Rev. Lett.*, 75:4563–4566, 1995.

[34] Don Weingarten. Scalar quarkonium and the scalar glueball. *Nucl. Phys. Proc. Suppl.*, 53:232–235, 1997.

[35] Frank E. Close and Andrew Kirk. Scalar glueball $q\bar{q}$ mixing above 1 GeV and implications for lattice QCD. *Eur. Phys. J.*, C21:531–543, 2001.

[36] F. Giacosa, T. Gutsche, and Amand Faessler. A covariant constituent quark-gluon model for the glueball-quarkonia content of scalar-isoscalar mesons. *Phys. Rev.*, C71:025202, 2005.

[37] Colin J. Morningstar and Mike J. Peardon. The Glueball spectrum from an anisotropic lattice study. *Phys. Rev.*, D60:034509, 1999.

[38] A. Hart and M. Teper. On the glueball spectrum in O(a)-improved lattice QCD. *Phys. Rev.*, D65:034502, 2002.

[39] Craig McNeile. Hard hadron spectroscopy. *PoS*, LATTICE2007:019, 2007.

[40] E. B. Gregory, A. C. Irving, C. C. McNeile, S. Miller, and Z. Sroczynski. Scalar glueball and meson spectroscopy in unquenched lattice QCD with improved staggered quarks. *PoS*, LAT2005:027, 2006.

[41] F. E. Close. QUARKS IN HADRONS AND NUCLEI. *Prog. Part. Nucl. Phys.*, 20:1–19, 1988.

[42] A. Abele et al. Test of $N\bar{N}$ potential models: Isospin relations in $\bar{p}d$ annihilations at rest and the search for quasinuclear bound states. *Eur. Phys. J.*, C17:583–592, 2000.

[43] A. Adamo et al. First physics results from OBELIX. *Sov. J. Nucl. Phys.*, 55:1732–1742, 1992.

[44] P. Salvini et al. $\bar{p}p$ annihilation into four charged pions at rest and in flight. *Eur. Phys. J.*, C35:21–33, 2004.

[45] A. Bertin et al. E/ι decays to $K\bar{K}\pi$ in $\bar{p}p$ annihilation at rest. *Phys. Lett.*, B361:187–198, 1995.

[46] A. Bertin et al. Measurement of the $\eta(1440) \to K^{\pm}K^{0}_{L}\pi^{\mp}$ production rates from $\bar{p}p$ annihilation at rest at three different hydrogen target densities. *Phys. Lett.*, B385:493–499, 1996.

[47] C. Cicalo et al. Evidence for two pseudoscalar states in the 1.4 to 1.5 GeV mass region. *Phys. Lett.*, B462:453–461, 1999.

[48] F. Nichitiu et al. Study of the $K^+K^-\pi^+\pi^-\pi^0$ final state in anti-proton annihilation at rest in gaseous hydrogen at NTP with the OBELIX spectrometer. *Phys. Lett.*, B545:261–271, 2002.

[49] A. Bertin et al. Study of the isovector scalar mesons in the channel $\bar{p}p \to K^{\pm}K^0_S\pi^{\mp}$ at rest with initial angular momentum state selection. *Phys. Lett.*, B434:180–188, 1998.

[50] M. Bargiotti et al. Coupled channel analysis of $\pi^+\pi^-\pi^0$, $K^+K^-\pi^0$ and $K^{\pm}K^0_S\pi^{\mp}$ from $\bar{p}p$ annihilation at rest in hydrogen targets at three densities. *Eur. Phys. J.*, C26:371–388, 2003.

[51] E. Aker et al. The Crystal Barrel spectrometer at LEAR. *Nucl. Instrum. Meth.*, A321:69–108, 1992.

[52] C. Amsler et al. Coupled channel analysis of $\bar{p}p$ annihilation into $\pi^0\pi^0\pi^0$, $\pi^0\eta\eta$ and $\pi^0\pi^0\eta$. *Phys. Lett.*, B355:425–432, 1995.

[53] C. Amsler et al. High statistics study of $f_0(1500)$ decay into $\pi^0\pi^0$. *Phys. Lett.*, B342:433–439, 1995.

[54] C. Amsler et al. Proton-antiproton annihilation into $\eta\eta\pi$: Observation of a scalar resonance decaying into $\eta\eta$. *Phys. Lett.*, B291:347–354, 1992.

[55] C. Amsler et al. High statistics study of $f_0(1500)$ decay into $\eta\eta$. *Phys. Lett.*, B353:571–577, 1995.

[56] C. Amsler et al. $\eta\eta'$ threshold enhancement in $\bar{p}p$ annihilations into $\pi^0\eta\eta'$ at rest. *Phys. Lett.*, B340:259–263, 1994.

[57] C. Amsler et al. Protonium annihilation into $K^0_LK^0_S\pi^0$ and $K^0_LK^0_S\eta$. *Phys. Lett.*, B319:373–380, 1993.

[58] A. Abele et al. Antiproton-proton annihilation at rest into $K^+K^-\pi^0$. *Phys. Lett.*, B468:178–188, 1999.

[59] A. Abele et al. Observation of $f_0(1500)$ decay into K_LK_L. *Phys. Lett.*, B385:425–432, 1996.

[60] A. Abele et al. Study of the $\pi^0\pi^0\eta'$ final state in $\bar{p}p$ annihilation at rest. *Phys. Lett.*, B404:179–186, 1997.

[61] C. Amsler et al. E decay to $\eta\pi\pi$ in $\bar{p}p$ annihilation at rest. *Phys. Lett.*, B358:389–398, 1995.

[62] A. Abele et al. Study of $\bar{p}p \to \eta\pi^0\pi^0\pi^0$ at rest. *Nucl. Phys.*, B514:45–59, 1998.

[63] C. Amsler et al. Observation of a scalar resonance decaying to $\pi^+\pi^-\pi^0\pi^0$ in $\bar{p}p$ annihilation at rest. *Phys. Lett.*, B322:431–440, 1994.

[64] A. Abele et al. A Study of $f_0(1500)$ decays into $4\pi^0$ in $\bar{p}p \to 5\pi^0$ at rest. *Phys. Lett.*, B380:453–460, 1996.

[65] A. Abele et al. Study of f_0 decays into four neutral pions. *Eur. Phys. J.*, C19:667–675, 2001.

[66] A. Abele et al. 4π decays of scalar and vector mesons. *Eur. Phys. J.*, C21:261–269, 2001.

[67] A. Abele et al. High-mass ρ-meson states from $\bar{p}d$ annihilation at rest into $\pi^-\pi^0\pi^0 p_{spectator}$. *Phys. Lett.*, B391:191–196, 1997.

[68] A. Abele et al. $\bar{p}d$ annihilation at rest into $\pi^+\pi^-\pi^- p_{spectator}$. *Phys. Lett.*, B450:275–280, 1999.

[69] C. Amsler et al. Antiproton-proton annihilation at rest into $\omega\pi^0\pi^0$. *Phys. Lett.*, B311:362–370, 1993.

[70] C. Amsler et al. Study of antiproton annihilation on neutrons into $\omega\pi^-\pi^0$. *Nucl. Phys.*, A740:130–146, 2004.

[71] C. Amsler et al. Study of $K\bar{K}$ resonances in $\bar{p}p \to K^+K^-\pi^0$ at 900 MeV/c and 1640 MeV/c. *Phys. Lett.*, B639:165–171, 2006.

[72] A. Abele et al. Observation of resonances in the reaction $\bar{p}p \to \pi^0\eta\eta$ at 1.94 GeV/c. *Eur. Phys. J.*, C8:67–79, 1999.

[73] J. Adomeit et al. Evidence for two isospin zero $J^{PC} = 2^{-+}$ mesons at 1645 MeV and 1875 MeV. *Z. Phys.*, C71:227–238, 1996.

[74] A. Abele et al. $\bar{p}p$ annihilation into $\omega\pi^0$, $\omega\eta$ and $\omega\eta'$ at 600 MeV, 1200 MeV and 1940 MeV/c. *Eur. Phys. J.*, C12:429–439, 2000.

[75] C. Amsler et al. Proton-antiproton annihilation at 900 MeV/c into $\pi^0\pi^0\pi^0$, $\pi^0\pi^0\eta$ and $\pi^0\eta\eta$. *Eur. Phys. J.*, C23:29–41, 2002.

[76] S. Ahmad et al. The ASTERIX Spectrometer at LEAR. *Nucl. Instrum. Meth.*, A286:76, 1990.

[77] S. B. Athar et al. Radiative decays of the $\Upsilon(1S)$ to a pair of charged hadrons. *Phys. Rev.*, D73:032001, 2006.

[78] D. Besson et al. Radiative Decays of the $\Upsilon(1S)$ to $\gamma\pi^0\pi^0$, and $\gamma\eta\eta$ and $\gamma\pi^0\eta$. *Phys. Rev.*, D75:072001, 2007.

[79] J. Z. Bai et al. The BES upgrade. *Nucl. Instrum. Meth.*, A458:627–637, 2001.

[80] J. Z. Bai et al. Partial Wave Analysis of $J/\psi \to \gamma\pi^+\pi^-\pi^+\pi^-$. *Phys. Lett. B*, 472:207, 2000.

[81] M. Ablikim et al. Partial Wave Analysis of $J/\psi \to \gamma\pi^+\pi^-$ and $\gamma\pi^0\pi^0$. *Phys. Lett. B*, 642:441, 2006.

[82] J. Z. Bai et al. Partial Wave Analysis of $J/\psi \to \gamma K^+K^-$ and $\gamma K^0_S K^0_S$. *Phys. Rev. D*, 68:052003, 2003.

[83] M. Ablikim et al. Observation of a near-threshold enhancement in the $\omega\phi$ mass spectrum from the doubly OZI suppressed decay $J/\psi \to \gamma\omega\phi$. *Phys. Rev. Lett.*, 96:162002, 2006.

[84] M. Ablikim et al. The σ pole in $J/\psi \to \omega\pi^+\pi^-$. *Phys. Lett. B*, 598:149, 2004.

[85] M. Ablikim et al. Resonances in $J/\psi \to \phi\pi^+\pi^-$ and ϕK^+K^-. *Phys. Lett. B*, 607:243, 2005.

[86] M. Ablikim et al. Study of $J/\psi \to \omega K^+K^-$. *Phys. Lett. B*, 603:138, 2004.

[87] S. E. Kopp. The CLEO III Detector. *Nucl. Instrum. Meth.*, A384:61–66, 1996.

[88] D. Cronin-Hennessy et al. Searches for CP violation and $\pi\pi$ S-wave in the Dalitz- plot of $D^0 \to \pi^+\pi^-\pi^0$. *Phys. Rev.*, D72:031102, 2005.

[89] G. Bonvicini et al. Dalitz plot analysis of the $D^+ \to \pi^-\pi^+\pi^+$ decay. *Phys. Rev.*, D76:012001, 2007.

[90] K. Benslama et al. Anti-search for the glueball candidate $f_J(2220)$ in two-photon interactions. *Phys. Rev.*, D66:077101, 2002.

[91] S. Kopp et al. Dalitz analysis of the decay $D^0 \to K^-\pi^+\pi^0$. *Phys. Rev.*, D63:092001, 2001.

[92] H. Muramatsu et al. Dalitz analysis of $D^0 \to K^0_S\pi^+\pi^-$. *Phys. Rev. Lett.*, 89:251802, 2002.

[93] P. Rubin et al. First observation and Dalitz analysis of the $D^0 \to K^0_S\eta\pi^0$ decay. *Phys. Rev. Lett.*, 93:111801, 2004.

[94] P. Rubin et al. Search for CP Violation in the Dalitz-Plot Analysis of $D^\pm \to K^+K^-\pi^\pm$. *Phys. Rev.*, D78:072003, 2008.

[95] C. Cawlfield et al. Measurement of interfering $K^{*+}K^-$ and $K^{*-}K^+$ amplitudes in the decay $D^0 \to K^+K^-\pi^0$. *Phys. Rev.*, D74:031108, 2006.

[96] Frank E. Close and Andrew Kirk. Large isospin mixing in ϕ radiative decay and the spatial size of the $f_0(980) - a_0(980)$ meson. *Phys. Lett.*, B515:13–16, 2001.

[97] A. Aloisio *et al.* Study of the decay $\phi \to \pi^0\pi^0\gamma$ with the KLOE detector. *Phys. Lett.*, B537:21, 2002.

[98] A. Aloisio *et al.* Study of the decay $\phi \to \eta\pi^0\gamma$ with the KLOE detector. *Phys. Lett.*, B536:209, 2002.

[99] F. Ambrosino et al. Study of the decay $\phi \to f_0(980)\gamma \to \pi^+\pi^-\gamma$ with the KLOE detector. *Phys. Lett.*, B634:148–154, 2006.

[100] D. Robson. A Basic Guide for the Glueball Spotter. *Nucl. Phys.*, B130:328, 1977.

[101] A. Kirk. A glueball $q\bar{q}$ filter in central production. 1999.

[102] T. A. Armstrong et al. Study of the centrally produced $\pi\pi$ and $K\bar{K}$ systems at 85 GeV/c and 300 GeV/c. *Z. Phys.*, C51:351–364, 1991.

[103] F. Binon et al. Hodoscope Multi-Photon Spectrometer Gams-2000. *Nucl. Instrum. Meth.*, A248:86, 1986.

[104] D. Alde et al. Acquisition System for the Hodoscope Spectrometer Gams-4000. *Nucl. Instrum. Meth.*, A240:343, 1985.

[105] S. Abatzis et al. A further study of the centrally produced $\pi^+\pi^-$ and $\pi^+\pi^-\pi^+\pi^-$ channels in pp interactions at 300 and 450 GeV/c. *Phys. Lett.*, B353:589–594, 1995.

[106] D. Barberis et al. A study of the centrally produced $\pi^+\pi^-\pi^+\pi^-$ channel in pp interactions at 450 GeV/c. *Phys. Lett.*, B413:217–224, 1997.

[107] D. Barberis et al. A spin analysis of the 4π channels produced in central pp interactions at 450 GeV/c. *Phys. Lett.*, B471:440–448, 2000.

[108] D. Barberis et al. A study of the $f_0(1370)$, $f_0(1500)$, $f_0(2000)$ and $f_2(1950)$ observed in the centrally produced 4π final states. *Phys. Lett.*, B474:423–426, 2000.

[109] D. Barberis et al. A partial wave analysis of the centrally produced $\pi^0\pi^0$ system in pp interactions at 450 GeV/c. *Phys. Lett.*, B453:325–332, 1999.

[110] D. Barberis et al. A partial wave analysis of the centrally produced $\pi^+\pi^-$ system in pp interactions at 450 GeV/c. *Phys. Lett.*, B453:316–324, 1999.

[111] D. Barberis et al. A partial wave analysis of the centrally produced K^+K^- and $K^0_SK^0_S$ systems in pp interactions at 450 GeV/c and new information on the spin of the $f_J(1710)$. *Phys. Lett.*, B453:305–315, 1999.

[112] D. Barberis et al. A coupled channel analysis of the centrally produced K^+K^- and $\pi^+\pi^-$ final states in pp interactions at 450 GeV/c. *Phys. Lett.*, B462:462–470, 1999.

[113] D. Barberis et al. A study of the $\eta\eta'$ and $\eta'\eta'$ channels produced in central pp interactions at 450 GeV/c. *Phys. Lett.*, B471:429–434, 2000.

[114] D. Barberis et al. A study of the $\eta\eta$ channel produced in central pp interactions at 450 GeV/c. *Phys. Lett.*, B479:59–66, 2000.

[115] D. Barberis et al. A study of the centrally produced $\phi\phi$ system in pp interactions at 450 GeV/c. *Phys. Lett.*, B432:436–442, 1998.

[116] D. Barberis et al. A study of the $\omega\omega$ channel produced in central pp interactions at 450 GeV/c. *Phys. Lett.*, B484:198–204, 2000.

[117] D. Barberis et al. A study of the centrally produced $K^*(892)\bar{K}^*(892)$ and $\phi\omega$ systems in pp interactions at 450 GeV/c. *Phys. Lett.*, B436:204–210, 1998.

[118] D. Barberis et al. A study of the centrally produced $\pi^0\pi^0\pi^0$ channel in pp interactions at 450 GeV/c. *Phys. Lett.*, B507:14–18, 2001.

[119] D. Barberis et al. A study of the centrally produced $\pi^+\pi^-\pi^0$ channel in pp interactions at 450 GeV/c. *Phys. Lett.*, B422:399–404, 1998.

[120] D. Barberis et al. A study of the centrally produced $\eta\pi^0$ and $\eta\pi^-$ systems in pp interactions at 450 GeV/c. *Phys. Lett.*, B488:225–233, 2000.

[121] D. Barberis et al. A study of the $\eta\pi^+\pi^-$ channel produced in central pp interactions at 450 GeV/c. *Phys. Lett.*, B471:435–439, 2000.

[122] D. Barberis et al. A study of the $K\bar{K}\pi$ channel produced centrally in pp interactions at 450 GeV/c. *Phys. Lett.*, B413:225–231, 1997.

[123] S. Cooper. Meson Production in Two-Photon Collisions. *Ann. Rev. Nucl. Part. Sci.*, 38:705–749, 1988.

[124] Chen-Ning Yang. Selection Rules for the Dematerialization of a Particle into Two Photons. *Phys. Rev.*, 77:242–245, 1950.

[125] R. Ahohe et al. The search for $\eta(1440) \to K^0_S K^\pm \pi^\mp$ in two-photon fusion at CLEO. *Phys. Rev.*, D71:072001, 2005.

[126] D. Decamp et al. ALEPH: A Detector for Electron-Positron Annihilations at LEP. *Nucl. Instrum. Meth.*, A294:121–178, 1990.

[127] The Construction of the L3 Experiment. *Nucl. Instrum. Meth.*, A289:35–102, 1990.

[128] M. Acciarri et al. $K^0_S K^0_S$ final state in two-photon collisions and implications for glueballs. *Phys. Lett.*, B501:173–182, 2001.

[129] M. Acciarri et al. Light resonances in $K^0_S K^{\pm}\pi^{\mp}$ and $\eta\pi^+\pi^-$ final states in $\gamma\gamma$ collisions at LEP. *Phys. Lett.*, B501:1–11, 2001.

[130] R. Barate et al. Search for the glueball candidates $f_0(1500)$ and $f_J(1710)$ in $\gamma\gamma$ collisions. *Phys. Lett.*, B472:189–199, 2000.

[131] D. Aston et al. The Strange Meson Resonances Observed in the Reaction $K^- p \to \bar{K}^0\pi^+\pi^- n$ at 11 GeV/c. *Nucl. Phys.*, B292:693, 1987.

[132] S. I. Bityukov et al. Observation of resonance with mass M = 1814 MeV, decaying into $\pi^-\eta\eta$. *Phys. Lett.*, B268:137–141, 1991.

[133] S. Teige et al. Properties of the $a_0(980)$ meson. *Phys. Rev.*, D59:012001, 1999.

[134] B. Aubert et al. The BaBar Detector. *Nucl. Instrum. Meth.*, A479:1–116, 2002.

[135] B. Aubert et al. Measurements of neutral B decay branching fractions to $K^0_S\pi^+\pi^-$ final states and the charge asymmetry of $B^0 \to K^{*+}\pi^-$. *Phys. Rev.*, D73:031101, 2006.

[136] T. Iijima and E. Prebys. Commissioning and first results from BELLE. *Nucl. Instrum. Meth.*, A446:75–83, 2000.

[137] A. Garmash et al. Dalitz analysis of three-body charmless $B^0 \to K^0\pi^+\pi^-$ decay. *Phys. Rev.*, D75:012006, 2007.

[138] A. Garmash et al. Dalitz analysis of the three-body charmless decays $B^+ \to K^+\pi^+\pi^-$ and $B^+ \to K^+K^+K^-$. *Phys. Rev.*, D71:092003, 2005.

[139] W. M. Yao *et al.* Review of particle physics. *J. Phys.*, G33:1, 2006.

[140] S. Spanier and N. A. Tornqvist. Scalar mesons. *Eur. Phys. J.*, C15:437, 2000.

[141] S. Spanier and N. A. Tornqvist. Note on scalar mesons. *J. of Phys.*, G33:546, 2006.

[142] C. Amsler and A. Masoni. The $\eta(1405)$, $\eta(1475)$, $f_1(1420)$ and $f_1(1510)$. *Phys. Lett.*, B592:549, 2004.

[143] C. Amsler. Non-$q\bar{q}$ Mesons. *Eur. Phys. J.*, C15:682, 2000.

[144] S. Devons et al. Observations of $\bar{p}p \to 3\pi^0$, $2\pi^0\eta$ at Rest. *Phys. Lett.*, B47:271, 1973.

[145] L. Gray, T. Kalogeropoulos, A. Nandy, J. Roy, and S. Zenone. Evidence for a $\pi\pi$ Isoscalar Resonance Degenerate with the f' Produced in $\bar{p}n$ Annihilations at Rest. *Phys. Rev.*, D27:307–310, 1983.

[146] F. G. Binon et al. G(1590): A Scalar Meson Decaying Into Two η Mesons. *Nuovo Cim.*, A78:313, 1983.

[147] F. G. Binon et al. Study of $\pi^- p \to \eta' \eta n$ in a Search for Glueballs. *Nuovo Cim.*, A80:363, 1984.

[148] M. Gaspero. Evidence for the dominance of an $I^G\ J^{PC} = 0^+\ 0^{++}$ resonance in $\bar{p}n \to 2\pi^+ 3\pi^-$ annihilation at rest. *Nucl. Phys.*, A562:407–445, 1993.

[149] M. Strohmeier-Presicek, T. Gutsche, Amand Faessler, and R. Vinh Mau. 4π decay modes of the $f_0(1500)$ resonance. *Phys. Lett.*, B438:21–26, 1998.

[150] C. Edwards et al. Observation of an $\eta\eta$ Resonance in J/ψ Radiative Decays. *Phys. Rev. Lett.*, 48:458, 1982.

[151] Donald E. Groom et al. Review of Particle Physics. *Eur. Phys. J.*, C15:1–878, 2000.

[152] D. Aston et al. A STUDY OF THE K0(S) K0(S) SYSTEM IN THE REACTION K- p → K0(S) K0(S) LAMBDA AT 11-GeV/c. *Nucl. Phys.*, B301:525, 1988.

[153] J. Reinnarth. Exotische Mesonen im Endzustand $2\pi^+ 2\pi^- \eta$ in der Antiproton-Proton-Vernichtung in Ruhe. *Ph.D. Thesis, University of Bonn*, 2003.

[154] Z. Bai et al. Partial wave analysis of $J/\psi \to \gamma K^0_S K^\pm \pi^\mp$. *Phys. Rev. Lett.*, 65:2507–2510, 1990.

[155] C. Amsler et al. Production and decay of $\eta'(958)$ and $\eta(1440)$ in $\bar{p}p$ annihilation at rest. *Eur. Phys. J.*, C33:23–30, 2004.

[156] A. Kirk. Resonance production in central pp collisions at the CERN Omega spectrometer. *Phys. Lett.*, B489:29–37, 2000.

[157] Chang-Zheng Yuan. Hadron Spectroscopy from BES and CLEO-c. *AIP Conf. Proc.*, 814:65–77, 2006.

[158] F. Antinori et al. A Further study of the centrally produced $\pi^+\pi^-$ and $\pi^+\pi^-\pi^+\pi^-$ channels in pp interactions at 300 and 450 GeV/c. *Phys. Lett.*, B353:589–594, 1995.

[159] J. Z. Bai et al. Studies of $\xi(2230)$ in J/ψ radiative decays. *Phys. Rev. Lett.*, 76:3502–3505, 1996.

[160] J. Z. Bai et al. Experimental study of J/ψ radiative decay to $\pi^0\pi^0$. *Phys. Rev. Lett.*, 81:1179–1182, 1998.

[161] R. M. Baltrusaitis et al. Observation of a Narrow $K\bar{K}$ State in J/ψ Radiative Decays. *Phys. Rev. Lett.*, 56:107, 1986.

[162] J. E. Augustin et al. Radiative Decay of J/ψ into $\gamma\pi^+\pi^-$. *Z. Phys.*, C36:369–376, 1987.

[163] D. Alde et al. 2.22 GeV $\eta\eta'$ Structure Observed in 38 GeV/c and 100 GeV/c $\pi^- p$ Collisions. *Phys. Lett.*, B177:120, 1986.

[164] A. Hasan and D. V. Bugg. A search for the $\xi(2235)$ in $\bar{p}p \to \pi^-\pi^+$. *Phys. Lett.*, B388:376–379, 1996.

[165] G. Bardin et al. Search for a Narrow Resonance about the $\xi(2230)$ in the Formation Channel $\bar{p}p \to K^+K^-$. *Phys. Lett.*, B195:292, 1987.

[166] J. Sculli, J. H. Christenson, G. A. Kreiter, P. Nemethy, and P. Yamin. Limits on $\xi(2.2)$ Formation in $\bar{p}p \to K^+K^-$. *Phys. Rev. Lett.*, 58:1715–1718, 1987.

[167] C. Evangelista et al. Measurement of the $\bar{p}p \to K_S K_S$ reaction from 0.6 GeV/c to 1.9 GeV/c. *Phys. Rev.*, D56:3803–3810, 1997.

[168] C. Evangelista et al. Study of the reaction $\bar{p}p \to \phi\phi$ from 1.1 GeV/c to 2.0 GeV/c. *Phys. Rev.*, D57:5370–5381, 1998.

[169] A. Buzzo et al. Search for narrow $\bar{p}p$ resonances in the reaction $\bar{p}p \to \bar{p}p\pi^+\pi^-$. *Z. Phys.*, C76:475–478, 1997.

[170] K. K. Seth. A high resolution search for the tensor glueball. *Nucl. Phys.*, A663:600–605, 2000.

[171] F. Buccella, Maurizio Lusignoli, and A. Pugliese. Charm non-leptonic decays and final state interactions. *Phys. Lett.*, B379:249–256, 1996.

[172] Peter Minkowski and Wolfgang Ochs. B decays into light scalar particles and glueball. *Eur. Phys. J.*, C39:71–86, 2005.

[173] R. W. L. Jones. Search for the glueball candidates $f_0(1500)$ and $f_J(1710)$ in $\gamma\gamma$ collisions in ALEPH. Prepared for PHOTON 2000: International Workshop on Structure and Interactions of the Photon (Including 13th International Workshop on Photon-Photon Collisions), Ambleside, Lake District, England, 26-31 Aug 2000.

[174] N. R. Stanton et al. Evidence for Axial Vector and Pseudoscalar Resonances Near 1.275 GeV in $\eta\pi^+\pi^-$. *Phys. Rev. Lett.*, 42:346–349, 1979.

[175] A. Ando et al. Evidence for two Pseudoscalar Resonances of $\eta\pi^+\pi^-$ System in the $D(1285)$ and E/ι Regions. *Phys. Rev. Lett.*, 57:1296, 1986.

[176] S. Fukui et al. Study on the $\eta\pi^+\pi^-$ system in the $\pi^- p$ charge exchange reaction at 8.95 GeV/c. *Phys. Lett.*, B267:293–298, 1991.

[177] D. Alde et al. Partial-wave analysis of the $\eta\pi^0\pi^0$ system produced in $\pi^- p$ charge exchange collisions at 100 GeV/c. *Phys. Atom. Nucl.*, 60:386–390, 1997.

[178] J. J. Manak et al. Partial-wave analysis of the $\eta\pi^+\pi^-$ system produced in the reaction $\pi^- p \to \eta\pi^+\pi^- n$ at 18 GeV/c. *Phys. Rev.*, D62:012003, 2000.

[179] G. S. Adams et al. Observation of pseudoscalar and axial vector resonances in $\pi^- p \to K^+K^-\pi^0 n$ at 18 GeV. *Phys. Lett.*, B516:264–272, 2001.

[180] A. V. Anisovich et al. Resonances in $\bar{p}p \to \eta\pi^+\pi^-\pi^+\pi^-$ at rest. *Nucl. Phys.*, A690:567–594, 2001.

[181] C. Edwards et al. Observation of a Pseudoscalar State at 1440 MeV in J/ψ Radiative Decays. *Phys. Rev. Lett.*, 49:259, 1982.

[182] J. E. Augustin et al. Radiative Decay of J/ψ into $\eta(1430)$ and Nearby States. *Phys. Rev.*, D42:10–19, 1990.

[183] D. L. Scharre et al. Observation of the Radiative Transition $\psi \to \gamma E(1420)$. *Phys. Lett.*, B97:329, 1980.

[184] C. Amsler and A. Masoni. Review of Particle Physics. *J. Phys.*, G33:591, 2006.

[185] John D. Weinstein and Nathan Isgur. $K\bar{K}$ Molecules. *Phys. Rev.*, D41:2236, 1990.

[186] M. P. Locher, V. E. Markushin, and H. Q. Zheng. Structure of $f_0(980)$ from a coupled channel analysis of S-wave $\pi\pi$ scattering. *Eur. Phys. J.*, C4:317–326, 1998.

[187] Frank E. Close and Nils A. Tornqvist. Scalar mesons above and below 1 GeV. *J. Phys.*, G28:R249–R267, 2002.

[188] N. N. Achasov, A. V. Kiselev, and G. N. Shestakov. Theory of Scalars. *Nucl. Phys. B, Proc. Suppl. 181-182*, 2008:169–174, 2008.

[189] E. M. Aitala et al. Study of the $D_s^+ \to \pi^-\pi^+\pi^+$ decay and measurement of f_0 masses and widths. *Phys. Rev. Lett.*, 86:765–769, 2001.

[190] Peter Minkowski and Wolfgang Ochs. Identification of the glueballs and the scalar meson nonet of lowest mass. *Eur. Phys. J.*, C9:283–312, 1999.

[191] D. V. Bugg. A Study in Depth of $f_0(1370)$. *Eur. Phys. J.*, C52:55–74, 2007.

[192] E. Klempt, B. C. Metsch, C. R. Munz, and H. R. Petry. Scalar mesons in a relativistic quark model with instanton induced forces. *Phys. Lett.*, B361:160–166, 1995.

[193] V. V. Anisovich and A. V. Sarantsev. K-matrix analysis of the $(I\,J^{PC} = 0\,0^{++})$-wave in the mass region below 1900 MeV. *Eur. Phys. J.*, A16:229–258, 2003.

[194] F. Giacosa, Th. Gutsche, V. E. Lyubovitskij, and Amand Faessler. Scalar nonet quarkonia and the scalar glueball: Mixing and decays in an effective chiral approach. *Phys. Rev.*, D72:094006, 2005.

[195] Hai-Yang Cheng, Chun-Khiang Chua, and Keh-Fei Liu. Scalar glueball, scalar quarkonia, and their mixing. *Phys. Rev.*, D74:094005, 2006.